UNIVERSITY OF OKLAHOMA

GRADUATE COLLEGE

THEORETICAL AND EXPERIMENTAL ANALYSIS OF DOWNWARD LIQUID-GAS FLOW IN VERTICAL TUBULARS

A THESIS

SUBMITTED TO THE GRADUATE FACULTY

In partial fulfillment of the requirements for the

Degree of

MASTER OF SCIENCE

By

OLUCHI CHIZOROM OSUAGWU

Norman, Oklahoma

2024

Downloaded from SHAREOK. Persistent Handle URL: https://hdl.handle.net/11244/341309

THEORETICAL AND EXPERIMENTAL ANALYSIS OF DOWNWARD LIQUID-GAS FLOW IN VERTICAL TUBULARS

A THESIS APPROVED FOR THE

MEWBOURNE SCHOOL OF PETROLEUM AND GEOLOGICAL ENGINEERING

BY THE COMMITTEE CONSISTING OF

Dr. Hamid Karami, Chair

Dr. Deepak Devegowda

Dr. Rouzbeh Moghanloo

© Copyright by OLUCHI CHIZOROM OSUAGWU 2024
All Rights Reserved.

ACKNOWLEDGEMENT

I am deeply grateful to my advisor, Dr. Karami, for the invaluable opportunity to work alongside him on this Master's journey. His unwavering support, encouragement, and understanding have guided me not only in my academic and research endeavors but throughout my overall experience at the University of Oklahoma. I am sincerely thankful for his mentorship and for fostering an environment that allowed me to explore, learn, and grow.

I extend my heartfelt thanks to Dr. Deepak and Dr. Rouzbeh for serving as integral members of my committee. Their insights, commitment, and valuable contributions have significantly enhanced my research and have been instrumental in shaping the quality of this work. I am deeply appreciative of their dedication and support.

My gratitude also goes to Jeff McCaskill and Eric Powell for their assistance with laboratory equipment and their expert guidance at the Well Construction and Technology Center (WCTC). Their technical knowledge and willingness to assist were invaluable in successfully completing my experiments. Special thanks to my colleagues Camilo Mateus and Orkhan Khankishiyev, whose guidance and assistance were crucial in running experiments; their generosity in sharing their expertise made a lasting impact on my work.

I would also like to express my appreciation to my friend Michael Gyaabeng for always being ready to lend a hand whenever I encounter challenges with handling equipment. His support has been a steady and valued presence throughout this journey. Additionally, I am immensely grateful to the dedicated administrative team at the Mewbourne School of Petroleum and Geological Engineering: Sonya Grant, Francey Freeman and most especially, Katie Shapiro. Their diligent support helped me navigate numerous challenges, providing me with the stability and resources needed to persevere.

My deepest thanks go to my partner, Clinton Akalazu whose constant encouragement and steadfast support and love have been instrumental in my personal development and career pursuits. His presence has made an indelible difference in my life during this chapter and in general.

I am thankful as well to friends, Chinedu Nwosu and Kayode Sanni, whose assistance has been a source of strength throughout my academic journey. To all my friends, thank you for your unwavering support, kindness, and care—your encouragement has meant the world to me.

Finally, to my family—Mr. and Mrs. David Osuagwu, Obinna, Chidinma, Prisca, Ikemba, Ezinne, and Nnadozie—your unconditional love, faith, and encouragement have been the pillars that keep me grounded and motivated. This accomplishment would not have been possible without you. Above all, I thank God for His grace, love, and mercy that have sustained me every step of the way.

TABLE OF CONTENT

ACKNOWLEDGEMENT iv
TABLE OF CONTENT vi
LIST OF FIGURES ix
LIST OF TABLES xiii
ABSTRACT xiv
Chapter 1 . INTRODUCTION 1
1.1. Significance of Study 4
1.2. Research Hypothesis 5
1.3. Research Objectives 6
1.4. Research Scope 6
1.5. Research Outline 7
Chapter 2 . LITERATURE REVIEW 9
2.1. Vertical Downward Liquid-Gas Flow Applications 9
2.2. Basic principles of two-phase flow 11
2.2.1. Flow patterns in two-phase flow 12
2.2.2. Review of two-phase flow parameters 14
2.3. Review of Experimental Studies on Downward Gas-Liquid Flow 16
2.4. Review of Empirical Correlations on Gas-Liquid Flow Prediction 19
2.4.1. Void Fraction Prediction 19
2.4.2. Flow Pattern Identification 22
2.4.3. Pressure Gradient Prediction 22
2.5. Machine Learning Applications in Vertical Downward Multiphase Flow 24
2.6. Summary of Reviewed Literatures 25
Chapter 3 . DATA ANALYSIS AND MACHINE LEARNING MODEL DEVELOPMENT 27
3.1. Data Analysis 27
3.2. Dimensional Analysis 29
3.3. Machine Learning Model Development 29
3.3.1. Data preprocessing 30
3.3.2. Model Selection and Development 33
3.3.3. Model Evaluation 35
3.4. Overview of Model Results 37

3.4.1. Overview of Void Fraction Result 37
3.4.2. Overview of Flow Pattern Result 42
Chapter 4 . EXPERIMENTAL METHODOLOGY 45
4.1. Experimental Setup 45
4.2. Measurement and Control Systems 49
4.2.1. Pressure measurements 49
4.2.2. Gas and liquid flow control 50
4.2.3. Quick-closing valves (QCVs) 51
4.2.4. Data acquisition and control 52
4.2.5. Video recording 53
4.2.6. Test Procedure 54
4.3. Data Analysis 56
4.4. Test Matrix 60
Chapter 5 . RESULT AND DISCUSSION 61
5.1. Experimental Results 61
5.1.1. Flow Observations 61
5.1.2. Void Fraction and Flow Pattern Analysis 65
5.1.3. Pressure Gradient and Flow Pattern Analysis 68
5.1.4. Test Repeatability 70
5.2. Physical Model Evaluation 71
5.2.1. Void Fraction Prediction 72
5.2.2. Pressure Gradient Predictions 76
5.3. Machine Learning Model Evaluation 80
5.3.1. Void Fraction Prediction Based on CatBoost Model 80
5.3.2. Flow Pattern Prediction based on LGBM Model 81
5.3.3. Pressure Gradient Prediction 82
5.4. Relative Error Comparison Across All Models 83
5.4.1. Void Fraction Relative Error 83
5.4.2. Pressure Gradient Relative Error 87
5.5. Summary of Result 91
Chapter 6 . CONCLUSION AND RECOMMENDATION 93
6.1. Conclusions on Downward Flow Data-Based Modeling 93
6.2. Conclusions on Experimental Observations 93
6.3. Conclusions on Model Performances 94

6.3.1. Void Fraction Prediction 94
6.3.2. Pressure Gradient Prediction 95
6.3.3. Flow Pattern Observation and Prediction 95
6.3.4. Potential of Machine Learning in Two-Phase Flow Modeling 95
6.4. Recommendations 95
NOMENCLATURE 97
REFERENCE 99
APPENDIX A . Experimental Error Analysis 109

LIST OF FIGURES

Figure 1.1. Multiphase flow in vertical pipes (modified from (Bar-Neir, 2014)) 2

Figure 1.2 Multiphase flow in horizontal pipes (modified from (Usama Kadri, 2009)) 2

Figure 2.1. Flow patterns observed in co-current downward vertical two-phase flow in a 50.8 mm pipe (Qiao et al., 2023) 12

Figure 2.2 Flow pattern map for classification of vertical downward two-phase flow (from Bouyahiaoui et al. (2008)) 15

Figure 3.1. (a) v_{Sg} vs. void fraction (b) v_{SL} vs. void fraction 28

Figure 3.2. Flow pattern map for varying v_{SL} and v_{Sg} values 28

Figure 3.3. Original and logarithmic transformation of the v_{Sg} data 30

Figure 3.4. Original and logarithmic transformation of the v_{SL} data 31

Figure 3.5. Class Distribution of Flow Pattern 32

Figure 3.6. Feature Importance Plot for Void Fraction 35

Figure 3.7. Feature Importance Plot for Flow Pattern 35

Figure 3.8. Void Fraction Prediction Errors of Various Models (Dimensional Parameters) 38

Figure 3.9. Void Fraction Prediction Errors of Various Models (Dimensionless Parameters) 39

Figure 3.10. Coefficient of Determination (R^2) Results for Various Models (Dimensional Parameters) 39

Figure 3.11. Coefficient of Determination (R^2) Results for Various Models (Dimensionless Parameters) 39

Figure 3.12. Cross Validation Result for CB Model (Dimensional Parameters)..... 40

Figure 3.13. Cross Validation Result for CB Model (Dimensionless Parameters) 40

Figure 3.14. Actual Void Fraction vs Predicted Void Fraction by CB model (Dimensional Parameters) 41

Figure 3.15. Actual Void Fraction vs Predicted Void Fraction by CB model (Dimensionless Parameters) 41

Figure 3.16. Confusion Matrix for LGBM Flow Pattern Prediction (Dimensional Parameters) . 43

Figure 3.17. Confusion Matrix for LGBM Flow Pattern Prediction (Dimensionless Parameters) 43

Figure 3.18. Predicted Flow Pattern Map 44

Figure 4.1. Vertical Flow Loop Overview Image 46

Figure 4.2. An Illustration of the Facility Schematic 46

Figure 4.3. Fluid Mixing at Tee 47

Figure 4.4. Pump Driven by an Electric Motor 47

Figure 4.5. Variable Frequency Drive 48

Figure 4.6. Air Compressor 48

Figure 4.7. Differential Pressure Sensor 50

Figure 4.8. A Picture of the Quick-Closing Valve 51

Figure 4.9. Data Acquisition System 52

Figure 4.10. LabVIEW Program during a Test 53

Figure 4.11. LabVIEW Block Diagram 53

Figure 4.12. Sight Glass, Video Section 54

Figure 4.13. Error Margin between Target and Measured v_{sg} 59

Figure 5.1. Vertical Downward Two-phase Flow Behavior at v_{SL} = 0.26 ft/sec 63

Figure 5.2. Vertical Downward Two-phase Flow Behavior at v_{SL} = 0.07 ft/s 64

Figure 5.3. Vertical Downward Two-phase Flow Behavior at v_{SL} = 1 ft/s 64
Figure 5.4. Void Fraction Experimental Analysis 66
Figure 5.5. Void Fraction vs GLR 67
Figure 5.6. void fraction vs. no-slip void faction 68
Figure 5.7. Pressure Gradient Experimental Analysis 69
Figure 5.8. Pressure Gradient Region Separation 70
Figure 5.9. Void Fraction Repeatability Plot 70
Figure 5.10. Pressure Gradient Repeatability Plot 71
Figure 5.11. Experimental Results vs. Olga Predictions (Void Fraction) 73
Figure 5.12. Experimental vs Gregory (Void Fraction) 74
Figure 5.13. Experimental vs Ansari (Void Fraction) 75
Figure 5.14. Experimental vs TUFFP (Void Fraction) 76
Figure 5.15. Experimental vs OLGA (Pressure Gradient) 77
Figure 5.16. Experimental vs Gregory (Pressure Gradient) 78
Figure 5.17. Experimental vs Ansari (Pressure Gradient) 78
Figure 5.18. Experimental vs TUFFP (Pressure Gradient) 79
Figure 5.19. Experimental vs CatBoost (Void Fraction) 81
Figure 5.20. Experimental vs LGBM (Flow Pattern) 81
Figure 5.21. Actual vs Predicted Pressure Gradient 83
Figure 5.22. Void Fraction Relative Error Comparison 84
Figure 5.23. Void Fraction Relative Error Comparison (CatBoost) 85
Figure 5.24. Void Fraction Relative Error Comparison (OLGA) 85
Figure 5.25. Void Fraction Relative Error Comparison (TUFFP) 86

Figure 5.26. Pressure Gradient Relative Error Comparison for the Physical Models 88

Figure 5.27. Pressure Gradient Relative Error Comparison (OLGA and TUFFP)..... 89

Figure 5.28. Pressure Gradient Relative Error Comparison (OLGA and TUFFP, v_{SL} = 0.07ft/sec) 90

Figure 5.29. Pressure Gradient Relative Error Comparison (OLGA and TUFFP, v_{SL} = 0.33 ft/sec) 90

Figure 5.30. Pressure Gradient Relative Error Comparison (OLGA and TUFFP, v_{SL} = 1.0 ft/sec) 90

Figure A.1. Void Fraction Experimental Error Plot 110

Figure A.2. Pressure Gradient Experimental Error Plot 110

LIST OF TABLES

Table 2-1. Overview of Experimental Studies or Gas-Liquid flow 18

Table 3-1 Summary of Flow Pattern Results for Various Models Using Dimensional Parameters 42

Table 3-2 Summary of Flow Pattern Results for Various Models Using Dimensionless Parameters 42

Table 4-1. Tested Fluid Properties 47

Table 4-2. Test Matrix 60

Table 5-2. Overview of Models Performance 82

Table 5-3 Void Fraction Error Summary Table 87

Table 5-4 Pressure Gradient Error Analysis Summary Table 91

Table A-1 Measuring Equipment Uncertainty 109

ABSTRACT

Vertical downward two-phase flow is a critical phenomenon in various industrial applications, hydrocarbon injection wells, chemical reactors, and nuclear cooling systems. The accurate prediction of flow patterns, void fractions, and pressure gradients is vital for optimizing operational efficiency in such flows. This study focuses on the theoretical and experimental analysis of vertical downward liquid-gas flow in tubular systems.

Firstly, a machine learning model was developed to predict flow pattern and void fraction using data from 11 published works on vertical downward two-phase flow. Data points, including superficial gas and liquid velocities (v_{Sg} and v_{SL}), void fractions and flow pattern were gathered from various studies to build a robust training set. Dimensionless features like Reynolds and Weber numbers of both liquid and gas phases were utilized, along with several machine learning models. CatBoost and LightGBM emerged as the best-performing algorithms for void fraction and flow pattern prediction, respectively. This model served as a foundation for later comparisons with experimental observations, highlighting the potential for machine learning applications.

An experimental setup was designed, consisting of a 25-ft vertical flow loop equipped with differential pressure sensors and a camera to capture flow behavior with a test matrix of 15 v_{Sg} and 5 v_{SL} values. The experiments were conducted using water and air as the liquid and gas phases to investigate the downward flow dynamics. Images were analyzed to observe flow patterns, along with void fractions and pressure gradients at different flow conditions. The experimental observations revealed distinct flow pattern transitions, including slug, churn, and annular flow, as gas velocity increased. Void fraction was found to increase non-uniformly with rising v_{Sg}, while

pressure gradients generally decreased with increasing v_{Sg}, moving from gravity dominated to friction dominated regions. Higher v_{SL} values influenced the flow patterns by expanding the slug and churn flow regions and delaying transitions to annular flow.

The performances of established physical models (OLGA, Gregory, Ansari, and TUFFP) were compared with experimental data. The machine learning models developed, LightGBM and CatBoost, showed improved accuracy in predicting flow patterns and void fractions over traditional models. The results showed that the CatBoost model slightly outperformed traditional models in predicting void fraction, with an average error of 1.28% compared to OLGA's 1.49%. Pressure gradient predictions were more challenging, with OLGA performing best at 82.49% relative error. Flow pattern observations aided in validating machine learning predictions. LGBM performed well in predicting the flow patterns of experimental data.

This study concludes that machine learning models provide a robust alternative to traditional mechanistic models in predicting complex multiphase flow behaviors. The work contributes to the broader understanding of vertical downward multiphase flow and offers practical recommendations for improving flow prediction models in industrial applications.

Chapter 1

INTRODUCTION

The concept of two-phase fluid flow in vertical systems has remained a relevant concept in the past decades. It has various applications across different fields associated with petroleum, nuclear, chemical, and petrochemical industries (Bouyahiaoui et al., 2018). For example, absorption, distillation, and extraction operations in chemical reactors commonly involve two-phase flow systems. The flow regime affects the contact between the liquid and gas phases, which determines the efficiency of these processes. (Madhumitha et al., 2023; Qian et al., 2019). Similarly, in the petroleum industry, during oil and gas extraction, understanding the behavior of gas-liquid mixtures in vertical pipes is critical for designing risers and downcomers, ensuring efficient fluid transport and operational stability (Gosline, 1936). Additionally, a good understanding of this flow is essential for improving and validating mechanical and thermal hydraulic flow models, as well as computational fluid dynamics (CFD) codes. Reliable multiphase flow data is necessary for both industrial applications and advanced research, Szalinski et al., (2010), hence, studying two-phase fluid flow is crucial.

Two-phase flow can be described as a multiphase flow with simultaneous flow of two of the several phases (solid, liquid or gas). Two-phase flow can be solid-liquid flow, liquid-liquid flow, gas-solid flow, or gas-liquid flow. This type of multiphase flow can be seen in both vertical and horizontal configurations, each exhibiting distinct flow patterns and parameters. Typical examples of these flow pattern configurations can be seen in Figure 1.1 and Figure 1.2, representing vertical and horizontal flow patterns, respectively.

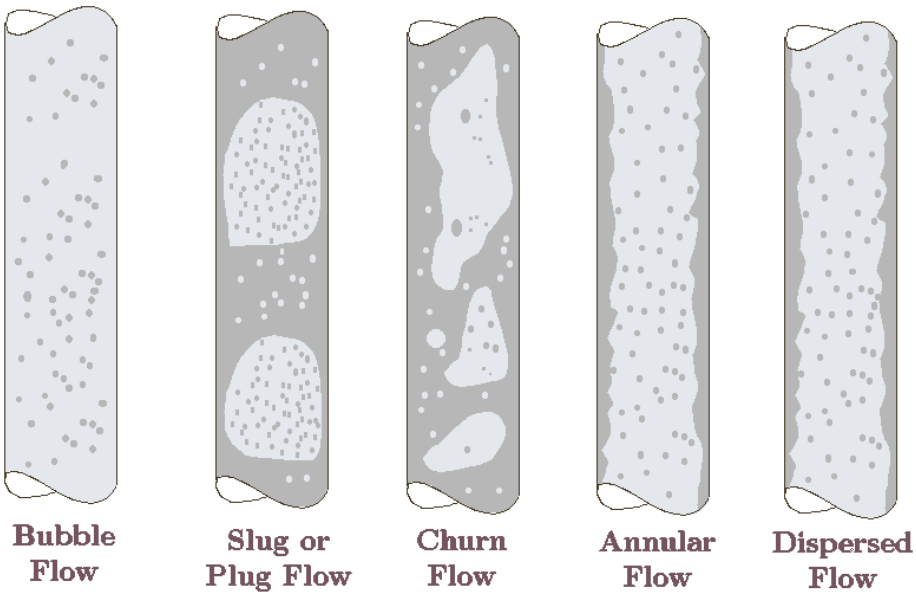


***Figure 1.1. Multiphase flow in vertical pipes (modified from** (Bar-Neir, 2014))*

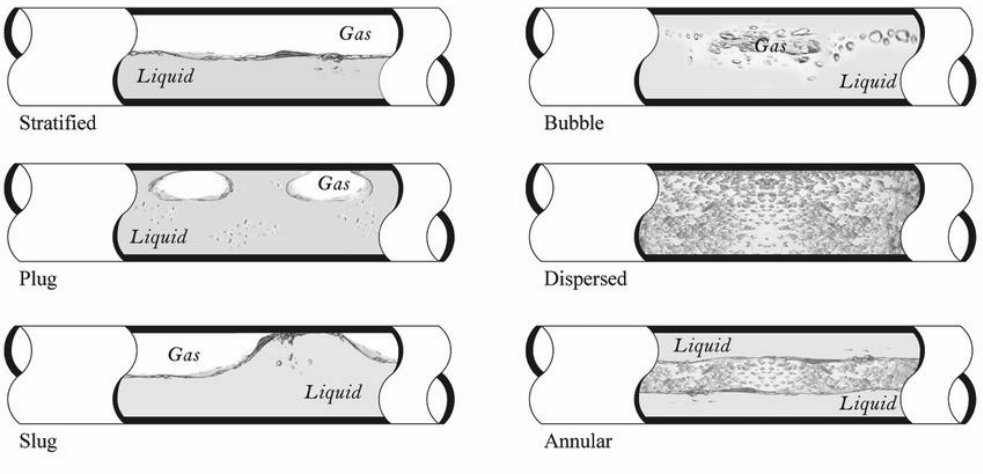


***Figure 1.2 Multiphase flow in horizontal pipes (modified from** (Usama Kadri, 2009))*

In vertical configuration, multiphase flow can be in upward or downward motion. While these two vertical systems share similarities, they also demonstrate unique behaviors due to influences such as surface tension, gravity, buoyancy, and liquid inertia forces (Lokanathan & Hibiki, 2016). In these flow systems, two key characteristics have been subjects matter in various research works, including the flow pattern and the void fraction. Flow pattern is the gas-liquid interfacial geometric form that arises in two-phase flow, as a result of the balance between gravity

and inertia forces. A good understanding of flow pattern helps in the accurate calculation of thermal and hydraulic design parameters, including the pressure drops and heat transfer coefficients (Cheng et al., 2008).

Void fraction is defined as the portion of the two-phase column that is occupied by the gas phase. In research on two-phase flow, it is one of the most important quantities. It is required for the computation of numerous other parameters, including two-phase mixture densities, viscosities, the velocities of the phases, pressure-drop, etc. (Xue et al., 2016). The interaction of buoyancy, gravity, inertia, and surface tension forces governs the void fraction. (Shi et al., 2021).

The determination of these parameters (flow pattern and void fraction) has largely relied on experimental and empirical correlation methods for two-phase systems. Xue et al. (2016) studied void fraction in gas-liquid two-phase flow in vertically downward pipes using an experimental loop. After considering 39 correlations for calculating void fraction against the experimental data, it was revealed that current prediction methods need improvement, particularly for small void fractions. Likewise, Shi et al. (2021), proposed a new model based on the drift flux approach for predicting void fraction while considering flow patterns to address errors by previous correlations. They attempted to handle low superficial liquid velocities, as they fell outside their intended scope. Majority of research works focus on two-phase flow in horizontal and vertically-upward tubes, and very few of them consider gas–liquid two-phase flows in vertically-downward pipes (Xue et al., 2016). It can also be pointed out that most correlations are constrained to certain void fraction ranges, making them less robust.

This thesis investigates the dynamics of downward liquid-gas flow in vertical tubular systems theoretically and experimentally. The focus is on determining the void fraction, flow pattern, and pressure drop to enhance the understanding of multiphase flow dynamics and optimize

industrial applications involving downward two-phase flow. It attempts to enhance accuracy and create a more robust application by applying machine learning approaches.

1.1. Significance of Study

The significance of this study lies in its potential to advance the understanding of liquid-gas flow in vertical downward tubular systems. This research contributes to the field in several keyways:

1. The investigation into how variations in superficial gas and liquid velocities affect flow pattern transitions provides valuable knowledge for controlling and predicting flow regimes. This understanding is essential for designing systems such as risers and downcomers, and tubulars encountered in the transportation and production systems. Effective control of flow patterns not only ensures stability and efficiency of extraction processes but also mitigates risks associated with phenomena like slugging, which can severely disrupt production operations.
2. Other industries, such as chemical processing and geothermal energy systems also rely on the principles of multiphase downward flow to optimize fluid transport and enhance heat transfer efficiency. In these contexts, understanding how variations in liquid and gas rates influence flow pattern transition is crucial. This study explores the suitability of machine learning to model these complex dynamics, potentially leading to models capable of predicting flow behavior across varying operating conditions. This, in turn, enables more precise control mechanisms, ensuring cost-effective and reliable operations.
3. The use of machine learning in this study provides an innovative approach to capturing the complex dynamics between superficial velocities, void fractions, and flow patterns. This

has practical implications for industries like petroleum and chemical processing where real-time monitoring and prediction of flow behavior are critical for operational decision-making. By validating machine learning models against experimental and physical modeling results, this research strengthens the theoretical framework. It also ensures that the findings can be applied to enhance the design and operation of systems dealing with multiphase downward flow in real-world conditions.

1.2. Research Hypothesis

Below are the research hypotheses developed for this study:

1. Increased superficial gas velocity (v_{Sg}) with decreased superficial liquid velocity (v_{SL}) in vertical downward pipes leads to flow pattern transition from slug to annular flow.
2. The variability and regime transitions of two-phase flow in vertical downward pipes can be attributed to the intricate relationships between gravity and inertia forces in liquid and gas phases, suggesting a nonlinear dependence suitable for machine learning modeling.
3. Dimensionless parameters improve machine learning models' accuracy when compared to models that only use dimensional characteristics.
4. Machine learning models (specifically LGBM and CatBoost) perform well in predicting flow patterns and void fraction in downward vertical tubulars using a comprehensive dataset.
5. The insights gained from this study can lead to optimized design and operational strategies for liquid-gas flow systems in various industrial applications.

1.3. Research Objectives

The primary objective of this research is to investigate the dynamics of downward liquid-gas flow in vertical tubular systems theoretically and experimentally. This objective is achieved through the following targets:

1. Review literature to understand the dynamics of downward liquid-gas flow in vertical tubulars.
2. Develop machine learning models using both dimensional and dimensionless parameters from literature data to predict flow patterns and void fractions.
3. Conduct experiments and data analysis to observe flow pattern transitions, void fraction, and pressure gradient changes as functions of v_{Sg} and v_{SL}.
4. Apply the developed models to predict flow patterns and void fractions based on experimental data.
5. Compare the experimental result with the machine learning model and common two-phase flow physical models.
6. Analyze the study findings to propose practical guidelines and strategies for improving efficiency in industrial applications.

1.4. Research Scope

The objective of this work is to investigate the theoretical dynamics of downward liquid-gas flow in vertical tubulars. For this purpose, experimental research is conducted, and machine learning techniques are employed in predicting and evaluating the outcome of the downward two-phase flow dynamics.

The experiments are carried out in a 25-ft (7.6-m) long and 2-in. (0.0508-m) inner diameter vertical flow loop, designed to flow downward. Air and water are used for the gas and liquid phases, respectively. Five superficial liquid velocities are tested, 0.07, 0.26, 0.33, 0.6 and 1.0 ft/s. Superficial gas velocities are tested in the range 3.5 to 49.8 ft/s, to encompass slug, churn and annular flows. The data acquired and examined for each test include liquid holdup (converted to void fraction for consistent analysis), pressure drop, and visual recordings of flow pattern transitions.

In addition to the experimental work, machine learning models are developed using literature data that spans a wider range of conditions, including v_{Sg} values from 0.03 to 275.6 ft/s and v_{SL} values from 0.1 to 23 ft/s, with small to large diameter tubulars and fluids such as air-water, air-viscous liquid, and CO2. These models are trained to predict flow patterns and void fractions, with the performance of the best model tested on the experimental dataset. This approach allows for a comprehensive comparison between the experimental results and machine learning predictions, in addition to other physical models.

1.5. Research Outline

This thesis includes 6 main chapters. It is structured in the following key chapters below:

Chapter 1 Introduction: This chapter introduces the background and significance of the study. It outlines the research objectives, hypotheses, and the scope of the study.

Chapter 2 Literature Review: This chapter reviews existing literature on liquid-gas flow dynamics in vertical downward tubular systems, limitations on conventional methods, and recent studies on modern methods. It includes theoretical foundations, empirical studies, and the application of machine learning in this field.

Chapter 3 Data Analysis and Machine Learning Model Development: This chapter introduces and analyzes data collected from 9 sources in the literature. Machine learning models are developed to predict the void fraction and flow patterns using both dimensional and dimensionless parameters. It describes the process of data collection and preprocessing, details the selection of various machine learning models, and evaluates the models.

Chapter 4 Experimental Methodology: This chapter provides an overview of the experimental design. It describes the experimental facility, the data acquisition process, the key parameters measured during the experiments, and the test matrix.

Chapter 5 Results and Discussion: This chapter presents and interprets the results from the experiments and model evaluations. It includes a comparative analysis of machine learning and some commonly used physical models against the experimental data, discussing flow pattern transitions, void fractions and pressure gradients.

Chapter 6 Conclusion and Recommendations: The concluding chapter summarizes the study's conclusions, highlighting the significance of the findings. It provides practical recommendations for industrial applications and suggests areas for future research.

Chapter 2

LITERATURE REVIEW

The study of vertical liquid-gas flow dynamics is essential for various industrial applications, including heat exchangers, injection wells, refrigeration cycles with refrigerant phase changes, chemical distillation towers, nuclear reactors, and CO2 sequestration systems. Understanding the intricate behaviors of two-phase flows, where liquid and gas phases interact within a confined space, is crucial for optimizing system performance and ensuring operational efficiency. This chapter provides a comprehensive review of the existing literature on liquid-gas flow dynamics. It begins with an overview of liquid-gas flow dynamics, highlighting the key physical phenomena and forces involved. Then, empirical correlations used for predicting flow behavior are examined. These correlations, derived from extensive experimental data, provide valuable tools for estimating flow parameters, such as, void fraction, flow pattern and pressure gradient. Various applications of machine learning techniques for more accurate prediction of these parameters are then investigated, focusing on downward liquid-gas flow. This literature review aims to better understand the current state of knowledge in downward liquid-gas flow and identify gaps in existing research.

2.1. Vertical Downward Liquid-Gas Flow Applications

Vertical downward two-phase flow plays a critical role in various industrial domains, particularly in the petroleum and chemical industries. In the petroleum industry, vertical downward flow is integral to the operation of multiphase flow reactors such as trickle bed reactors, which are

employed in essential processes like hydrogenation and hydrodesulfurization (Bouyahiaoui et al., 2008). Additionally, these reactors are crucial in processes such as biological treatment of wastewater and electrochemical treatment in the chemical industry, where understanding two-phase flow dynamics is necessary for optimizing process efficiency and ensuring operational safety.

Beyond petroleum, two-phase flow can be observed in carbon capture, utilization, and storage (CCUS) systems where vertical downward two-phase flow plays a vital role in absorption columns. Here, the liquid absorbent, such as amine solutions, flows downward while contacting the upward-flowing gas containing CO2. This counter-current flow arrangement enhances mass transfer, improving CO2 absorption efficiency. Furthermore, in various CCUS processes, heat exchangers often employ vertical downward two-phase flow to manage cooling or heating of process streams (Schmid et al., 2022). This flow pattern significantly enhances heat transfer efficiency in these units, making it an essential component of many CCUS technologies.

Two-phase flow is also a common phenomenon in the nuclear energy sector, where it is observed in several key engineering applications (Qiao et al., 2017). For example, in nuclear reactors, the occurrence of a Loss of Coolant Accident (LOCA) can lead to transient downward two-phase flow conditions. In such scenarios, knowledge of the flow regime, hydrodynamics, and heat transfer characteristics is crucial for reactor safety. The downward flow of coolant in the event of a LOCA, often resulting from a break or cut in the coolant pipe, causes a flow reversal and downward two-phase flow out of the reactor (Martin, 1976).

In advanced reactor designs, vertical downward two-phase flow is further emphasized in passive safety systems, such as the passive containment cooling system utilized in the AP1000 reactor (Yang et al., 2018). In these systems, the gas-water mixture flows downward along the

containment walls, a process that requires a thorough understanding of the flow characteristics for effective containment cooling. Many gravity-driven safety systems in nuclear plants also rely on downward two-phase flow, highlighting the importance of mastering the flow dynamics for ensuring the functionality of these passive safety mechanisms.

Beyond the nuclear sector, vertical downward two-phase flow is prevalent in various industrial apparatuses. For instance, certain boiler designs incorporate tubular channels with downward flow to optimize heat exchange processes. Safety analysis for small leak accidents in light water reactors (LWR) also necessitates precise knowledge of downward two-phase flow phenomena, as these dynamics influence the reactor's safety response (USUI & SATO, 1989). Additionally, heat exchangers with U-shaped tubes, often examined for very high-temperature gas-cooled reactors (VHTR), further demonstrate the relevance of vertical downward flow in ensuring efficient cooling (USUI & SATO, 1989)

The significance of downward two-phase flow extends to offshore platforms as well, particularly in the downcomers from manifolds, where understanding flow behavior is crucial for the reliable operation of gas-liquid systems in offshore environments. Whether in reactors, boilers, or pipelines, a clear understanding of the downward two-phase flow is essential for the design and operation of these systems, ensuring both safety and efficiency.

2.2. Basic principles of two-phase flow

This section discusses the basic concepts of two-phase liquid-gas flow in downward vertical pipes. The flow patterns and the main characteristics of this type of flow will be introduced and evaluated here.

2.2.1. Flow patterns in two-phase flow

Certain flow patterns are observed for downward two-phase gas-liquid flow within a system. Some of these flow patterns can be seen in Figure 2.1 from Qiao et al. (2023).

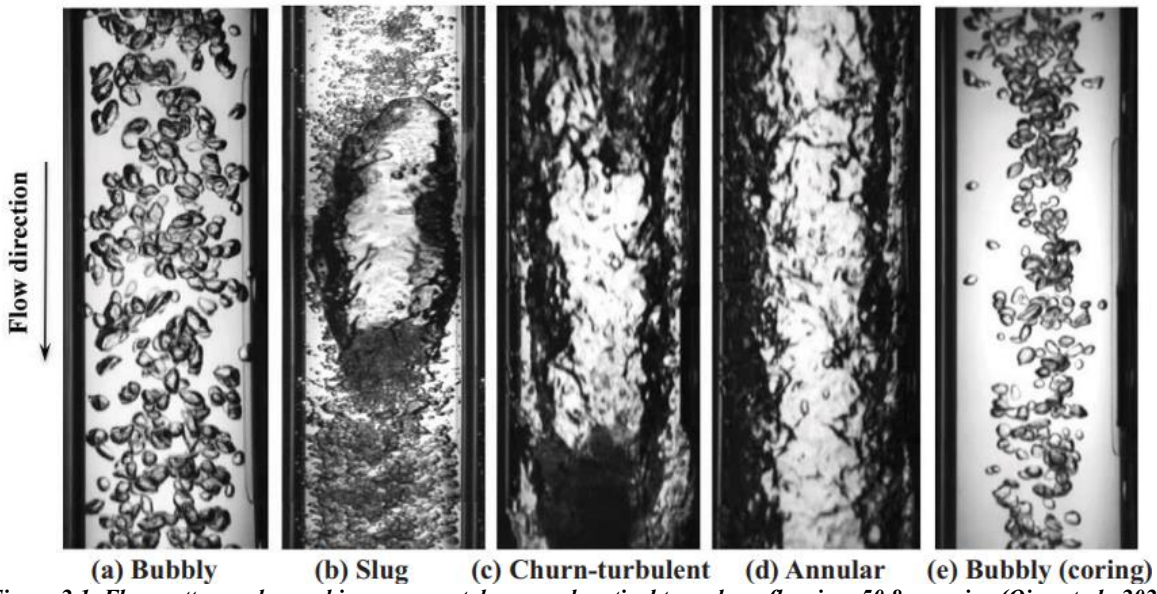


Figure 2.1. Flow patterns observed in co-current downward vertical two-phase flow in a 50.8 mm pipe (Qiao et al., 2023)

In bubbly flow, gas bubbles are usually observed to be dispersed in the liquid, flowing along a tube. Schmid et al. (2022) observed that the bubbles are significantly smaller than the tube diameter, often spherical, with varying sizes and shapes. They move with the liquid at nearly the same speed, showing minimal slippage, except at very low mass rates. This flow pattern occurs at low vapor qualities and can appear even before the liquid reaches saturation, during subcooled boiling (Troniewski & Selsak, 1987). However, there are slight differences in bubbly downward flow. As the liquid velocity increases, bubbles start to concentrate at the pipe center, known as the 'coring phenomenon'. This is caused by the combined effects of the lift force and wall repulsion force in vertical downward flow, where the lift force pushes bubbles towards the center due to the relative velocity difference between phases (Qiao et al., 2023).

In slug flow, increasing vapor fractions cause bubbles to merge into larger bullet-shaped "Taylor Bubbles" nearly the size of the tube's diameter. These bubbles have a hemispherical front and a fluctuating tail, with liquid slugs containing small bubbles separating them. A liquid film typically wets the tube's perimeter and may flow in the opposite direction in upward flow due to gravity. While both the bullet-shaped bubbles and liquid slugs occur alternatively in the pipe, the bubbles are more distorted and have off-centered noses in the vertical downward flow. The difference in the slug shape can be explained by the phase interactions. The buoyance force accelerates the Taylor bubble in vertical upward flow but decelerates it in vertical downward flow. Therefore, the film-bubble interaction is more significant in downward flow, making the bubble more distorted (Qiao et al., 2023).

Churn flow is characterized by a chaotic mix of phases, developing as liquid slugs become unstable and collapse. The liquid's flow direction oscillates between up and down, but it has a net upward movement. In the transition from slug to churn flow, the vapor concentration in the liquid slug peaks, and the turbulent wake from one Taylor bubble affects the next one. The transition to churn flow is marked by the disappearance of sustained liquid slugs, reducing their frequency to zero (Kawaji, 2017; Montoya et al., 2016; Tengesdal et al., 1999).

Annular flow in vertical downward two-phase systems shares similarities with its upward counterpart, characterized by a continuous gas core in the center of the pipe, droplet entrainment within the gas core and a continuous wavy liquid film along the pipe wall. However, in downward flow, annular flow can be further classified into two distinct subcategories:

- Falling Film Flow: This occurs when there is insufficient liquid to completely fill the test section. The liquid forms a thin film that flows down the pipe wall under the influence of gravity.

- Annular Drop Flow: This regime closely resembles the annular flow observed in upward systems. It forms at high gas flow rates, where the gas core carries entrained liquid droplets while a wavy liquid film coats the pipe wall.

The primary difference between these subcategories lies in the liquid distribution and the mechanism of liquid transport. In falling film flow, gravity plays a more dominant role in liquid movement, while in annular drop flow, the high-velocity gas core significantly influences liquid entrainment and transport. Understanding these distinctions is crucial for accurately predicting flow behavior and designing efficient systems for various industrial applications involving vertical downward two-phase flow (Qiao et al., 2017).

2.2.2. Review of two-phase flow parameters

In this section selected key flow parameters are discussed with focus on how they affect or influence downward two-phase flow. Liquid superficial velocity *(v_{SL})* is the volumetric flow rate of liquid ($\dot{Q}_l$) divided by the pipe cross-sectional area (A). The liquid's velocity would have if it were the sole phase flowing in the pipe. It can be expressed as seen in Equation 2-1. Likewise, gas superficial velocity *(v_{Sg})* refers to the velocity of the gas phase ($\dot{Q}_g$) assuming it is the only fluid flowing in the pipe. It is defined as the volumetric flow rate of the gas phase divided by the pipe cross sectional area, as shown in Equation 2-2.

$$v_{SL} = \frac{\dot{Q}_l}{A} \qquad \text{Equation 2-1}$$

$$v_{Sg} = \frac{\dot{Q}_g}{A} \qquad \text{Equation 2-2}$$

Superficial liquid and gas velocities, among other factors, can be used to classify various flow patterns (bubble, slug, churn, annular, etc.) for any given multiphase flow system (Ishii et al., 2004; Zhao et al., 2013). This classification is generally done using what is called the flow pattern map as seen in Figure 2.2.

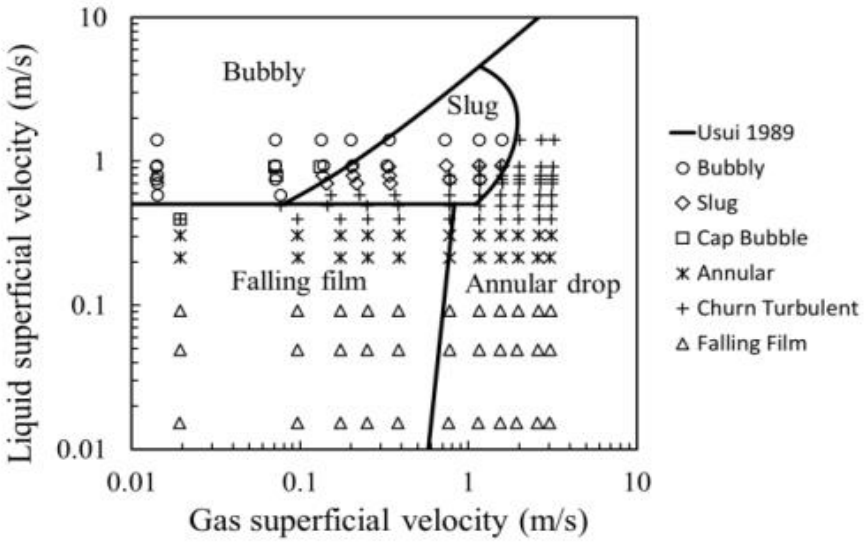


Figure 2.2 Flow pattern map for classification of vertical downward two-phase flow (from Bouyahiaoui et al. (2008))

Void fraction is another key two-phase flow parameter, described as the fraction of the pipe cross-sectional area occupied by the gas phase. It is mathematically defined in equation 2-3. The void fraction is a crucial parameter for gas-liquid two-phase flow, impacting the mixture density, velocity, viscosity, heat transfer, and pressure gradient.

$$\alpha = \frac{\dot{A}_g}{\dot{A}} = \frac{\dot{A}_g}{\dot{A}_l + \dot{A}_g} \qquad \text{Equation 22-3}$$

Dimensionless parameters have traditionally been used as key contributors to characterize fluid dynamics, including single-phase and multiphase flows. They positively influence the understanding and classification of flow behavior. Two of the important dimensionless parameters are Reynolds number and Weber number.

Reynolds number (R_e) is defined as the ratio of inertial to viscous force scales, often utilized to determine whether the flow is laminar or turbulent**.** It uses the fluid's velocity, density, viscosity, and a particular length scale (like diameter) to distinguish between laminar and turbulent flow. Equations 2-4 and 2-5 show the definitions used for the superficial gas and liquid Reynolds numbers in two-phase flow.

$$R_{e_{sg}} = \frac{\rho_g v_{Sg} d}{\mu_g}$$ Equation 22-4

$$R_{e_{SL}} = \frac{\rho_L v_{SL} d}{\mu_L}$$ Equation 2-5

Where ρ_g and ρ_L are densities of gas and liquid, respectively, v_{Sg} and v_{SL} are the superficial gas and liquid velocities, d is the inner pipe diameter, and μ_g and μ_L are the viscosities of gas and liquid phases, respectively.

Weber number (W_e) represents a measure of inertial forces compared to interfacial forces. This parameter is useful in analyzing the formation of droplets and bubbles. If the surface tension of the fluid decreases, bubbles/droplets will become smaller because of higher momentum transfer between the phases. Equations 2-6 and 2-7 show the definitions used for the superficial gas and liquid Weber numbers, where σ is the liquid-gas surface tension.

$$W_{e_{sg}} = \frac{\rho_g {V_{sg}}^2 d}{\sigma}$$ Equation 2-6

$$W_{e_{SL}} = \frac{\rho_L {V_{SL}}^2 d}{\sigma}$$ Equation 2-7

Multiphase flow research has primarily concentrated on horizontal and vertical upward pipe flows, ignoring the intricacies of vertical downward pipe flows, influenced by buoyancy, gravity, and inertial forces (Shi et al., 2021). It is critical to bridge these gaps to progress void fraction measurement and modeling. This can eventually contribute to the development of safer and more effective two-phase flow systems.

2.3. Review of Experimental Studies on Downward Gas-Liquid Flow

The experimental studies on downward gas-liquid flow primarily focus on air-water systems, with some studies exploring CO2 or viscous liquids. Flow regime transitions are a central area of investigation, with studies such as those by Barnea et al. (1982) and Usui & Sato (1989)

mapping transitions between bubbly, slug, churn, and annular flow patterns. These transitions differ from those observed in upward flow, due to the opposing influences of gravity and flow direction.

Kendoush & Al-Khatab (1994) and Wang et al. (2018) find that at higher liquid velocities, bubbles tend to migrate toward the center of the pipe, a phenomenon known as coring. This contrasts with upward flow, where bubbles typically move toward the pipe walls.

Studies by Zhao et al. (2013) and Xue et al. (2016) show that pressure drop is generally lower in downward flow compared to upward flow under similar conditions. The gravity-assisted motion of the liquid phase reduces frictional resistance, leading to lower pressure losses.

Interfacial structures in downward flow, particularly in large-diameter pipes is observed by Li et al. (2018) and Shi et al. (2021). They observe that these structures differ significantly from those found in smaller pipes, due to scale effects. Such variations have implications for flow regime transitions and the overall behavior of two-phase flow in larger industrial systems.

Troniewski & Selsak (1987) explore how increased liquid viscosity influences flow patterns and pressure drops, demonstrating that higher viscosity shifts flow regime transitions and increases frictional pressure losses.

Table 2.1 provides an overview of various research studies focused on fluid dynamics in pipes. These experiments span a wide range of superficial liquid and gas velocities and are conducted in pipes with diameters ranging from 15 mm (about 0.59 in) to 203.2 mm (about 8 in). They offer insights into the behaviors of different fluid combinations, including CO2, air-water mixtures, and air-viscous liquids.

Table 2-1. Overview of Experimental Studies or Gas-Liquid flow

Researchers	v_{SL} ***(m/s)***	v_{Sg} ***Range (m/s)***	***Pipe ID (mm)***	***Fluids Tested***
(Hammer et al., 2021)	0.15 – 2.77	0.6 – 2.77	44	CO2
(Shi et al., 2021)	0.089 – 0.885	0.354 – 70.771	20	Air-Water
(Z. Li et al., 2018)	0.02 - 3	0.1 – 1.75	203.2	Air-Water
(Xue et al., 2016)	0.14 – 1.7	0.274 – 1.709	25	Air-Water
(Zhao et al., 2013)	0.3 – 0.4	0.1 – 3.88	200	Air-Water
(Bouyahiaoui et al., 2018)	0 – 3.27	0.015 – 1.4	34	Air-Water
(Wang et al., 2018)	0.1 – 1.5	0.05 - 3	203.2	Air-Water
(Kendoush & Ai-Khatab, 1994)	0.5 – 1.8	0 – 0.75	38	Air-Water
(Barnea et al., 1982)	0.1 – 1.7	0.01 - 15	25	Air-Water
(Troniewski & Selsak, 1987)	0.003 – 1.1	0.01 - 38	15	Air- Viscous Liquid
(Chalgeri & Jeong, 2019)	0.2 – 3.5	0.02 - 7	2.35	Air-Water
(Yamaguchi & Yamazaki, 1984)	-0.2 to -1.3	-3.6 to -84	25	Air-Water
(Usui & Sato, 1989)	-0.06 to -1.1	-0.024 to -17.0	16	Air-Water
(Ishii, 1977)	-1 to -8	-0.3 to -10	25.4	Air-Water
(Lee et al., 2008)	-0.6 to -7	-0.01 to -26	25.4	Air-Water

Despite the valuable insights these studies provide, they also present certain limitations. Most experiments focus on near-ambient conditions with air-water systems, leaving gaps in the understanding of high-pressure, high-temperature scenarios relevant in many industrial applications. Furthermore, while some studies utilize large-diameter pipes, the majority focus on smaller diameters, raising questions about the scalability of their results to larger, industrial-scale systems. Only a few studies examine the effects of fluids other than air and water, underscoring the need for further research into systems involving more diverse fluids, such as oils or refrigerants.

Another limitation lies in the influence of inlet conditions on flow development, which could affect the interpretation of results in practical applications. Moreover, older studies may be

constrained by the measurement techniques available at the time, potentially affecting the accuracy and resolution of the collected data.

While these experimental studies advance the understanding of downward gas-liquid flow, there is still a need for further research to address these limitations. Expanding experimental conditions to include more varied fluid properties, pipe sizes, and industrial operating conditions enhances the applicability of these findings to real-world systems.

2.4. Review of Empirical Correlations on Gas-Liquid Flow Prediction

2.4.1. Void Fraction Prediction

Predicting void fraction in downward gas-liquid flow presents unique challenges due to the opposing effects of gravity and flow direction. While many general two-phase flow correlations exist, only a few have been specifically developed or validated for downward flow conditions. The empirical correlations or models used for the prediction of void fraction can be classified into homogeneous-model-based correlations, slip-ratio-model-based correlations, and drift-flux-model-based correlations (Xue et al., 2016).

Homogeneous models, also known as gas volumetric flow fraction models, assume that the two-phase flow in pipes is a homogenous mixture of liquid and gas flowing at the same velocity. They usually predict void fraction considering the no-slip gas–liquid volumetric flow rate ratio, β, as seen in equations 2-8 and 2-9.

$$\alpha = f(\beta) \qquad \text{Equation 2-8}$$

$$\beta = \frac{Q_G}{Q_G + Q_L} \qquad \text{Equation 2-9}$$

Where α is the void fraction, Q_G is the gas flow rate, and Q_L is the liquid flow rate.

An example of this kind of model is described by Yamaguchi & Yamazaki (1984b), who researched the void percentage of gas-water two-phase flow in vertical downward pipes (25 mm ID) using quick-closing valves. According to their findings, the void fraction rises as the volumetric gas flow increases. The association was tested with 560 data points, and the model's percentage error was ± 20%. The following empirical association was presented:

$$\frac{\alpha_g}{(1-\alpha_g)(1-K\alpha_g)} = \frac{\beta}{1-\beta} \quad \text{Equation 2-10}$$

For $\beta \leq 0.2$, $K = 2 - 0.4/\beta$ Equation 2-11

For $\beta \geq 0.2$, $K = -0.25 + 1.25/\beta$ Equation 2-12

Where α_g is void fraction, and β is the gas volumetric flow fraction, defined by Equation 2-9.

The second type, slip-ratio-model-based correlations assumes that the gas and liquid phases travel separately at different velocities, with one phase uniformly dispersed into the other (Xue et al., 2016). The slip-ratio (S_p) is defined as the ratio of the gas phase velocity to the liquid phase velocity, as shown in Eq. 2-13. The void fraction is calculated by using Eq. 2-14 and 2-15. The slip-ratio is a function of gas mass fraction and physical properties of the two phases.

$$S_p = \frac{u_G}{u_L} \quad \text{Equation 2-13}$$

$$\alpha = \frac{1}{1+\left(\frac{1-x}{x}\right)^p \left(\frac{\rho_G}{\rho_L}\right)^q S_p} \quad \text{Equation 2-14}$$

$$x = (Q_G \cdot \rho_G)/(Q_L \cdot \rho_L + Q_G \cdot \rho_G) \quad \text{Equation 2-15}$$

Where u_G and u_L are velocities of gas and liquid phases, respectively, α is the void fraction, x is gas mass fraction of the two-phase flow, p and q are indexes used in correlations for the calculation of slip ratio, and Q_G and Q_L are gas and liquid flow rates, respectively.

The third type, drift-flux model, as described by Xue et al. (2016), utilizes certain parameters known as the distribution parameter (C_0) and the drift velocity (U_{gm}) in the calculation of the void fraction, as shown in Eq. 2-16.

$$\langle\langle u_G \rangle\rangle = \frac{\langle J_G \rangle}{\langle \alpha \rangle} = C_0 \langle J_m \rangle + \langle\langle U_{gm} \rangle\rangle \quad \text{Equation 2-16}$$

While the distribution parameter depends on pressure, channel geometry, and flow rates, the drift velocity depends on the two parameters seen in equations 2-17 and 2-18.

$$\prod_1 = \left(\frac{g\sigma(\rho_L - \rho_G}{{\rho_L}^2}\right)^{0.25} \quad \text{Equation 2-17}$$

$$\prod_2 = \left(\frac{g d_h(\rho_L - \rho_G}{\rho_L}\right)^{0.5} \quad \text{Equation 2-18}$$

Where $\langle\ \rangle$ and $\langle\langle\ \rangle\rangle$ notations represent average area and void fraction-weighted mean values, respectively, and $\prod_1$ and $\prod_2$ are combined parameters in m/s.

In another study, Shi et al. (2021) develop a new void fraction prediction correlation based on drift flux model for gas–liquid two-phase flow within a vertical downward pipe with a 20 mm inner diameter using quick-closing valves. They address the gap of flow pattern consideration in older correlations. The average relative error and average absolute error for the new correlation are -2.80% and 6.49%, respectively, compared to the ranges of −21.65-8.65% for the average relative errors and 8.57-23.17% for the average absolute errors of the existing correlations. Their developed correlation is shown in Equation 2-19.

$$\alpha_g = \frac{v_{sg}}{\left[1+0.16\left(1-\frac{\rho_g v_{sg}}{\rho_g v_{sg}+\rho_L v_{sl}}\right)\right]\left((v_{sg}+v_{sL})-C\left(g\sigma\left(\frac{\rho_L-\rho_g}{{\rho_L}^2}\right)\right)\right)^{0.25}} \quad \text{Equation 2--19}$$

Where α_g is the void fraction of gas-liquid flow and C is a flow pattern coefficient.

2.4.2. Flow Pattern Identification

The determination of flow patterns generally relies on observational efforts. However, less observatory methods are currently utilized in the identification of flow patterns. These recent methods cut across correlations and neural networks. They are proven effective to a high degree in the identification of flow patterns for different systems (Qiao et al., 2017).

In a study conducted by Lee et al. (2008)**,** a method was developed for instantaneous identification of two-phase downward flow patterns using preprocessed impedance signals of the cross-sectional void fraction. The self-organized neural networks were tested with experimental data for upward and downward flows in pipes of 25.4- and 50.8-mm diameters. From their experiment, they observe that downward flow patterns show a dependency on pipe diameter.

Li et al. (2018) published a similar work on the identification of flow patterns. By considering larger 203.2 mm pipe diameters, the authors leveraged probability density function (PDF) and cumulative probability density function (CPDF) of void fraction signals for self-organized neural network (SONN). The self-organized neural network (SONN) is applied to identify flow patterns for both downward and horizontal flows. They observed that despite satisfactory results for flow pattern maps of 101.6 mm and higher pipe sizes, the model demonstrates poor performance for lower pipe diameter sizes, limiting it to only larger pipes.

2.4.3. Pressure Gradient Prediction

According to Yao et al. (2018), the four main components of gas-liquid two-phase flow pressure gradient are hydrostatic, frictional, local and acceleration-based. Initial developed correlations for calculating the frictional pressure drop are divided into two categories. The first group were developed using the separated flow model approach, first introduced by Lockhart and

Martinelli. The second group were developed using the homogenous flow model, as previously discussed.

Autee et al. (2015) worked with small diameter tubes orientated horizontally, vertically and at two downward inclinations of 30° and 60°. To calculate the pressure gradient in macro and mini-microchannels, they compared their two-phase pressure gradient observations with other existing correlations. They noticed that the two-phase pressure gradient in small diameter tubes cannot be accurately predicted by the current correlations. They proposed a new correlation by incorporating additional parameters, such as Reynolds, Froude, and Bond numbers into Chisholm's (1967) correlation, taking into account their significant effects.

In a similar approach, Yao et al. (2018) carried out several experiments involving frictional pressure gradient determination on four tubes with inner diameters of 15, 25, 40, and 65 mm. By investigating the prediction performance of 19 correlations leveraging 978 experimental data points, they proposed a new correlation by modifying that of Chisholm (1967). Equation 2-20 shows the original correlation, which has better prediction accuracy for horizontal and vertically upward pipes but not for vertically downward pipes. Yao's modification, Equation 2-21 includes the consideration of buoyancy induced pressure gradient, to improve the accuracy for vertical downward pipes.

$$\left(\frac{dP}{dL}\right) tp, f = \left(\frac{dP}{dL}\right) g + \left(\frac{dP}{dL}\right) l + C\sqrt{\left(\frac{dP}{dL}\right) g * \left(\frac{dP}{dL}\right) l} \qquad \text{Equation 2-19}$$

$$\left(\frac{dP}{dL}\right) tp, f = \left(\frac{dP}{dL}\right) g + \left(\frac{dP}{dL}\right) l + C\sqrt{\left(\frac{dP}{dL}\right) g * \left(\frac{dP}{dL}\right) l} + \left(\frac{dP}{dL}\right) b \qquad \text{Equation 2-20}$$

Where $(dP/dL)_{tp}$ is the total two-phase frictional pressure gradient, $(dP/dL)_g$ is the gas-only pressure gradient, $(dP/dL)_l$ is the liquid-only pressure gradient, and $(dP/dL)_b$ is the frictional pressure gradient induced by buoyancy.

2.5. Machine Learning Applications in Vertical Downward Multiphase Flow

Machine learning techniques have been increasingly employed in gas-liquid flow prediction, addressing the limitations of traditional empirical correlations and mechanistic models. According to Kanin et al. (2018), empirical correlations are often limited to their respective data-fitting ranges, while mechanistic models rely heavily on empirically based closure relations, which can restrict their applicability. Although research focusing specifically on vertical downward two-phase flow is still developing, the few available studies have demonstrated the potential of machine learning in improving flow predictions in this field.

Schmid et al., (2022) shows machine learning techniques used to analyze a substantial amount of flow pattern data (431 for upward flow and 123 for downward flow) recorded under different conditions in tubes. A pre-trained frame- and flow-regime-classifier is employed to classify the flow regimes, demonstrating the ability of machine learning to process complex flow pattern data. The performance of the machine learning model is significant because it identifies discrepancies between the observed flow pattern transitions and existing flow pattern maps. These differences lead to the development of new flow transition lines for both vertical upward and downward flow, suggesting that machine learning can detect patterns and make classifications that deviate from traditional models.

In a study conducted by Zhong et al., (2021) a novel feature extraction method is proposed using non-stationary conductivity probe signals for flow regime identification in vertical downward two-phase flow. The study develops two discriminative network models: the probabilistic neural network (PNN) and the nonlinear support vector machine (SVM). These models are designed to address classification challenges using small sample sets. The results

indicate that the nonlinear SVM achieves an identification accuracy of 90.47%, outperforming the PNN method, which achieves 83.33% accuracy. The study highlights the effectiveness of nonlinear SVM in handling small sample sizes and nonlinear classification problems. However, the accuracy of the flow regime identification, particularly near transitional boundaries between flow regimes, remains an area for improvement and requires further investigation.

These studies emphasize the growing role of machine learning in overcoming the limitations of traditional models, offering more robust and widely applicable solutions for predicting complex gas-liquid flow dynamics. The ability of machine learning algorithms to handle large datasets and capture non-linear relationships makes them a valuable tool in both academic research and industrial applications.

2.6. Summary of Reviewed Literatures

The study of multiphase flow has shown its relevance and its various applications across different fields associated with chemical, petroleum, nuclear and other industries. Various methods are engaged in modeling, experimentation and studying downward multiphase flow. One of the key major areas is the laboratory experiments unraveling possible flow patterns and their characteristics. However, this method is usually constrained to specific sizes and materials of study, which may not be applicable in varying cases.

To provide less observative methods for studying multiphase flow characteristics, various correlations have been proposed. However, these correlations have limiting assumptions and have been built for specific use cases. Similarly, machine learning models and neural networks commonly leverage advanced algorithms, some of which might be complex with little interpretability, while availability of data continues to be a major issue.

Additionally, it is seen through the reviewed literature that most of the studies focus on horizontal or upward vertical multiphase flow, compared to downward flow. With the growth of carbon capture and sequestration and other injection wells, applications of downward flow increase. As a result, the need for accurate and robust studies in this regard increases. This growing need makes this subject area requiring more studies and solutions to fill up these gaps.

Chapter 3

DATA ANALYSIS AND MACHINE LEARNING MODEL DEVELOPMENT

Machine learning (ML), a branch of artificial intelligence, has proven to be highly proficient at finding patterns and insights in large complex datasets. Beyond the constraints of traditional methods, machine learning has interesting possibilities to enhance our comprehension and predictive abilities for downward liquid-gas flow. By using large datasets from tests and operational data, machine learning models may be trained to predict flow patterns and optimize operating conditions.

The development of ML models addresses the complex dynamics of vertical downward two-phase flow. This chapter elaborates on the data analysis and model development process undertaken to predict void fraction and flow pattern in vertical downward two-phase flow (Osuagwu and Karami, 2024). The ML models were trained using a wide range of data to predict void fractions and flow patterns. The experimental data collected later in this study was used against the developed models for validation purposes.

3.1. Data Analysis

As documented in Osuagwu and Karami (2024), a comprehensive dataset was compiled from 11 published studies on downward liquid-gas flow in vertical pipes, totaling over 1,500 data points. These data points span through v_{SL} and v_{Sg}, with ranges of 0.003 to 3.5 m/s (0.01-11.5 ft/s) and 0.01 to 70 m/s (0.03-229.7 ft/s), respectively. Table 2.1 references all these studies, providing a robust foundation for model development. An initial assessment of the dataset confirms a

comprehensive range, providing a solid foundation for further analysis. To explore the relationships between different variables, scatter plots are generated, revealing key trends and associations. Figures 3.1 and 3.2 offer detailed visualizations of the relationships between void fraction, v_{SL}, and v_{Sg}. These visualizations highlight significant trends, such as the increase in void fraction with rising v_{Sg} and the decrease in void fraction with rising v_{SL}. The flow pattern transitions are also clear from bubbly to slug to churn to annular, with increasing v_{Sg} values.

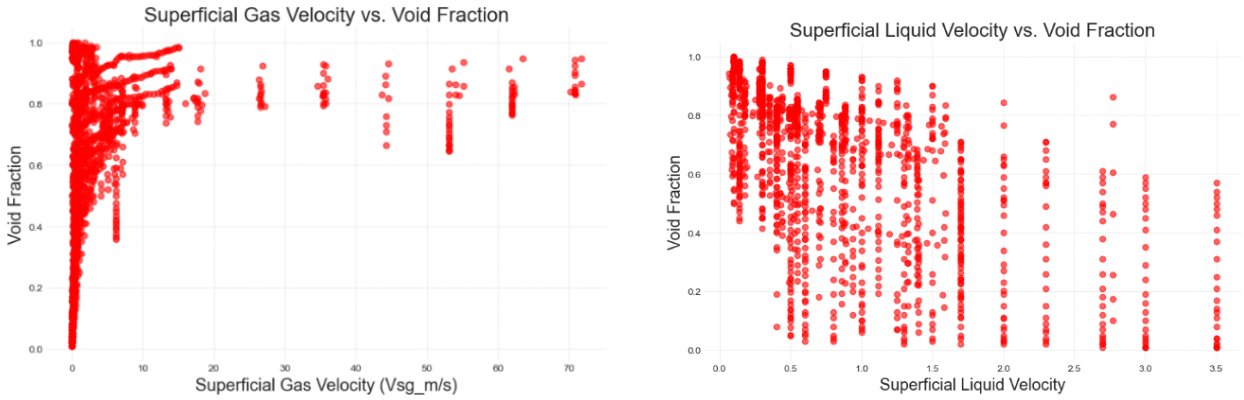


Figure 3.1. (a) v_{Sg} vs. void fraction (b) v_{SL} vs. void fraction

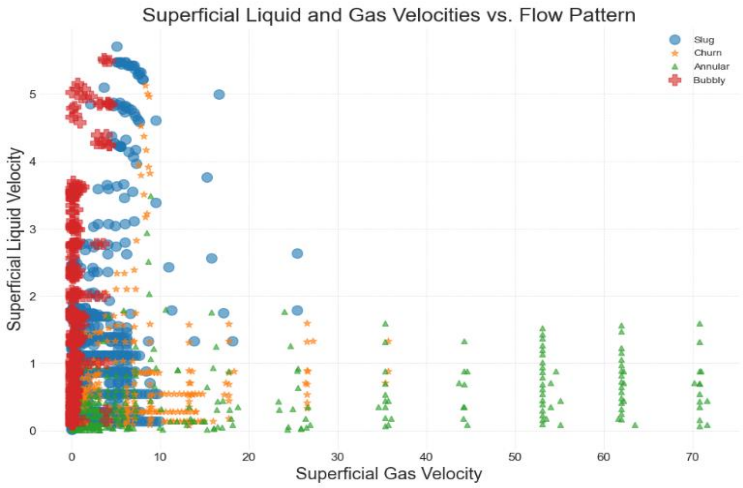


Figure 3.2. Flow pattern map for varying v_{SL} and v_{Sg} values

These plots highlight the importance of v_{Sg} and v_{SL} in predicting flow patterns of vertical downward two-phase flow systems. Higher gas velocities lead to gas-dominant regimes, whereas

higher liquid velocities decrease the void fraction and lead to more liquid-heavy flows. These insights have practical applications in various industries, where managing gas-liquid interactions in pipelines, reactors, or other process equipment is key to ensuring efficiency and stability in operations. The collection of data from several papers highlights the importance of cross-study comparisons in spotting discrepancies and patterns. This is especially crucial because of the various experimental setups or methods used in these studies.

3.2. Dimensional Analysis

This study extends the analysis by utilizing both dimensional (v_{SL}, v_{Sg}) and dimensionless numbers (no-slip liquid holdup, Reynolds, and Weber numbers) as features in predictive modeling. The dimensionless numbers are products of dimensional analysis, a basic method for normalizing the intricate interactions of physical forces. It uses the Buckingham π theorem to determine which dimensionless numbers best capture the system's behavior. This analysis aims to non-dimensionalize the flow parameters and generate results that may be used to various operating circumstances and scales (Ojeda, 2023). Variables like the pipe diameter, velocities, viscosities, surface tension, and densities of the two phases must be considered when applying the Buckingham π theorem. At this study, the dimensionless values used to describe the flow behavior were identified as the superficial Reynolds and Weber numbers of the two phases. In addition, the no-slip void fraction was used as a fifth dimensionless number in the forecasts.

3.3. Machine Learning Model Development

The predicted model of this study was developed using various machine learning techniques. The objective was to model the complex dynamics of vertical downward two-phase

flow and accurately forecast key flow properties such as void fraction and flow pattern. The process begins with meticulous data preprocessing, followed by the development, training, and validation of the models. By leveraging the diverse dataset compiled from multiple studies referenced in Table 2.1, we bridge the gap between theoretical predictions and practical observations, with a particular focus on ensuring robustness across different flow patterns.

3.3.1. Data preprocessing

In preparation for model development, the dataset is organized into two primary subsets, each serving distinct predictive goals: one focused on void fraction and the other on flow pattern prediction. The void fraction subset contains 1,413 data points, while the flow pattern subset comprises 1,642 observations. The predictive goal of each subset is achieved in two ways: first using the dimensional parameters, v_{SL} and v_{Sg} (ft/sec) as input features and secondly, using dimensionless parameters (no-slip liquid holdup, superficial Reynolds, and Weber numbers for both phases) as input features. The input features for the models are carefully chosen to include the critical parameters in characterizing the flow dynamics of vertical downward two-phase flow.

Figures 3.3 and 3.4 provide more visualizations to show that the data exhibit a skewed distribution. To address this issue and ensure a more uniform distribution, logarithmic transformations were applied to the data.

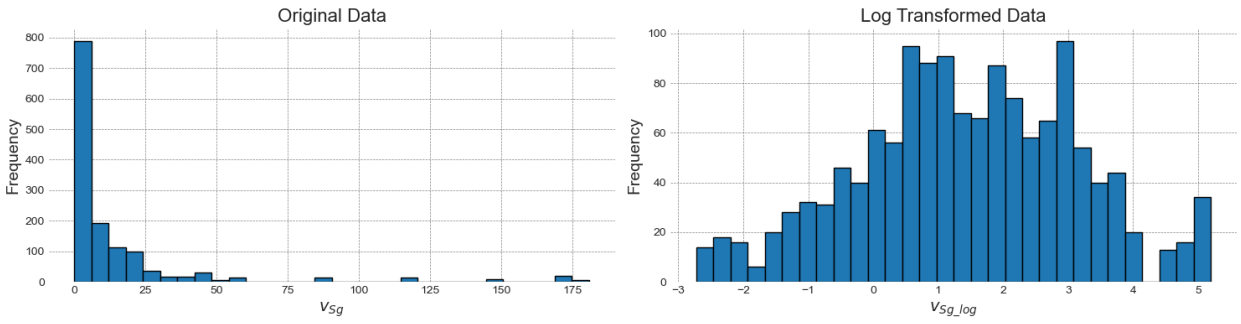


Figure 3.3. Original and logarithmic transformation of the v_{Sg} data

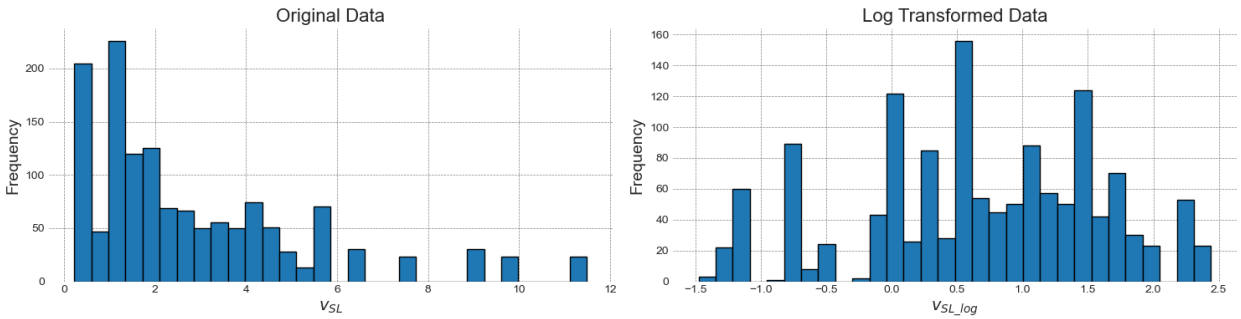


Figure 3.4. Original and logarithmic transformation of the v_{SL} data

In addition, the flow pattern target variable presents an imbalance across different classes, as shown in Figure 3.5. There are more data points with a slug flow pattern, and fewer with churn flow. This can potentially bias the predictive models. To mitigate this, random oversampling was applied to balance the representation of each class in the dataset. Random oversampling is a method used to balance the distribution of classes in a dataset by randomly duplicating samples from the minority class. This process increases the number of instances in the underrepresented class to match or approach the number of instances in the majority class (Chawla et al., 2002).

The categorical labels for flow patterns are then converted into a binary matrix through one-hot encoding, a crucial step for feeding the data into classification algorithms. One-hot encoding is a technique used to convert categorical variables into a form that can be provided to machine learning algorithms. It creates binary columns for each category in the original data and assigns a 1 or 0 to each column to indicate the presence or absence of that category (Potdar et al., 2017).

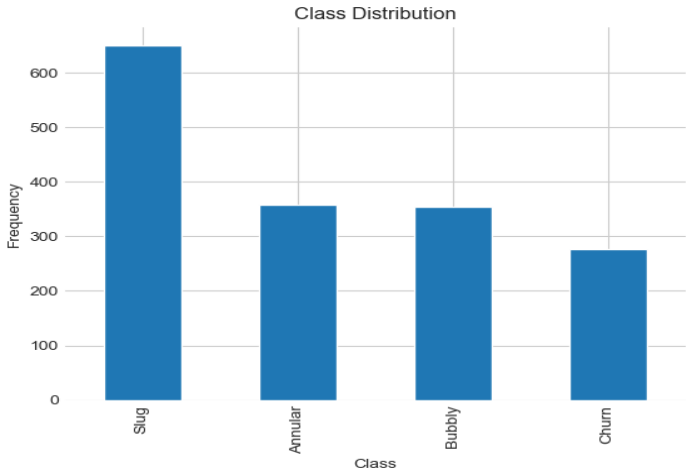


Figure 3.5. Class Distribution of Flow Pattern

For model training and evaluation, the dataset is divided into training and testing sets, with 80% allocated for training and 20% for testing. The split is performed in a stratified manner to ensure that the distribution of phase pair observations is consistent across both sets. A categorical feature, called 'two-phase', representing the specific combination of phases involved, such as air-water, CO2, or gas-viscous liquid interactions was considered for stratification purposes. Given the overrepresentation of certain phase pairs, such as air-water, sample weights are applied to balance the dataset during model training. Specifically, a weight factor of 39.36 is applied to CO_2 samples for the void fraction prediction in the dimensional and dimensionless analysis. For flow pattern prediction in the dimensional and dimensionless analysis, weight factors of 13.42 for CO_2 and 15.4 for gas-viscous liquid samples are used. This is to ensure that each phase pair contributes equally to the model's learning process. These weight factors are determined by calculating the ratio of the number of samples in each phase pair category to the total number of samples. This process involves calculating the total number of samples in the training set, counting the instances of each phase pair (e.g., air-water, CO_2, and air-viscous liquid), and applying weight factors inversely proportional to the phase pair's frequency. For CO_2, the weight factor of 39.36 means

that each CO_2 sample is effectively treated as 39.36 samples during training. This approach ensures that the model is not biased toward the overrepresented phase pairs, such as air-water.

Finally, to standardize the input features and ensure uniformity across all variables, a Min-Max scaler is applied. This scaling method normalizes the data, bringing all features into a consistent range, which is essential for the convergence of machine learning algorithms. The 'two-phase' feature is also encoded to facilitate its integration into the machine learning model.

3.3.2. Model Selection and Development

A careful selection process was undertaken to identify the most suitable machine learning models and effectively predict the void fraction and flow pattern in vertical downward two-phase flow. Table 3-1 shows a list of the explored models.

Table 3-1 Machine Learning Models Explored

Models used for Void Fraction Prediction	Models used for Flow Pattern Prediction
Linear Regression	K-Nearest Neighbors (KNN)
K-Nearest Neighbors (KNN)	Decision Tree (DT)
Decision Tree (DT)	Random Forest (RF)
Random Forest (RF)	Gradient Boosting (GB)
Gradient Boosting (GB)	Cat Boost (CB)
Cat Boost (CB)	Light Gradient Boosting Machine (LGBM)
Light Gradient Boosting Machine (LGBM)	

To ensure robust model development, hyperparameter tuning was performed for each model, optimizing parameters to enhance predictive performance. Additionally, k-fold cross-validation was employed to evaluate the models' generalizability and reduce the risk of overfitting, ensuring that the models perform well on unseen data.

It is worth noting that the no-slip void fraction was used as a physical benchmark to provide context for the performances of the void fraction predictive models. This benchmark, derived from

the assumption that the two phases move at same velocity, offers a straightforward comparison point to evaluate a model's effectiveness in capturing the complexities of the actual flow.

The selection process was iterative, involving a detailed evaluation and comparison of each model's performance across different dimensions of the dataset. Throughout this process, CatBoost and LGBM emerged as the leading models for the preidtion of void fraction and flow pattern, respectively. These models demonstrate robust performances in both the dimensional and dimensionless analyses, successfully capturing the intricate relationships inherent in the data.

Figures 3.6 and 3.7 show the Feature importance plots for void fraction and flow pattern, respectively. They were created with dimensionless parameters as input features for the models. The feature importance plots for the CatBoost and LGBM models highlight the most influential dimensionless parameters for predicting void fraction and flow pattern, respectively. In the CatBoost model, which excelled in predicting void fraction, the no-slip void fraction emerges as the most significant feature, followed by the Weber number for gas and the Reynolds numbers for gas and liquid. This suggests that no-slip void fraction captures the fundamental void fraction behavior and plays a pivotal role in the CatBoost model's performance. Conversely, in the LGBM model, which was best for predicting flow patterns, the Reynolds number for gas stands out as the most critical parameter, followed closely by Reynolds number for liquid and no-slip void fraction. This reflects the dominant influence of inertial forces, captured by the Reynolds number, in defining flow pattern transitions.

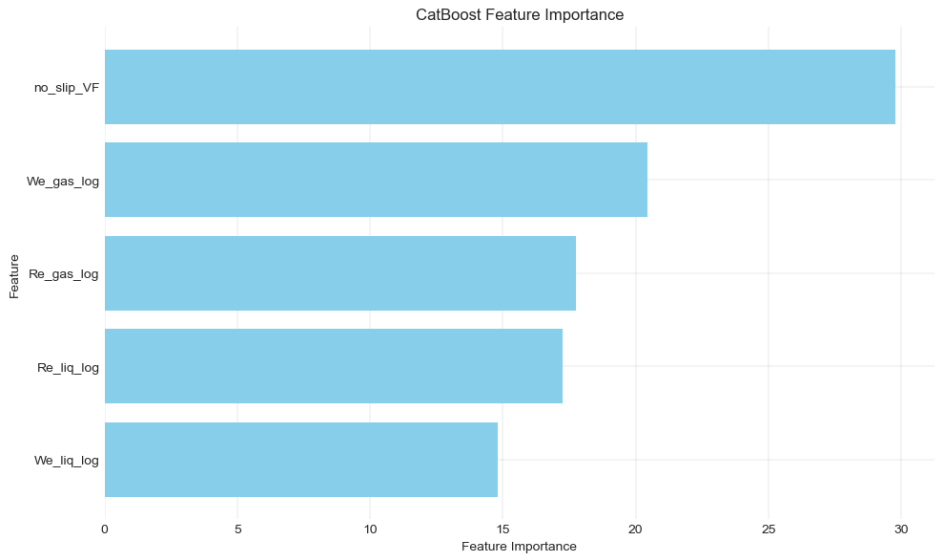


Figure 3.6. Feature Importance Plot for Void Fraction

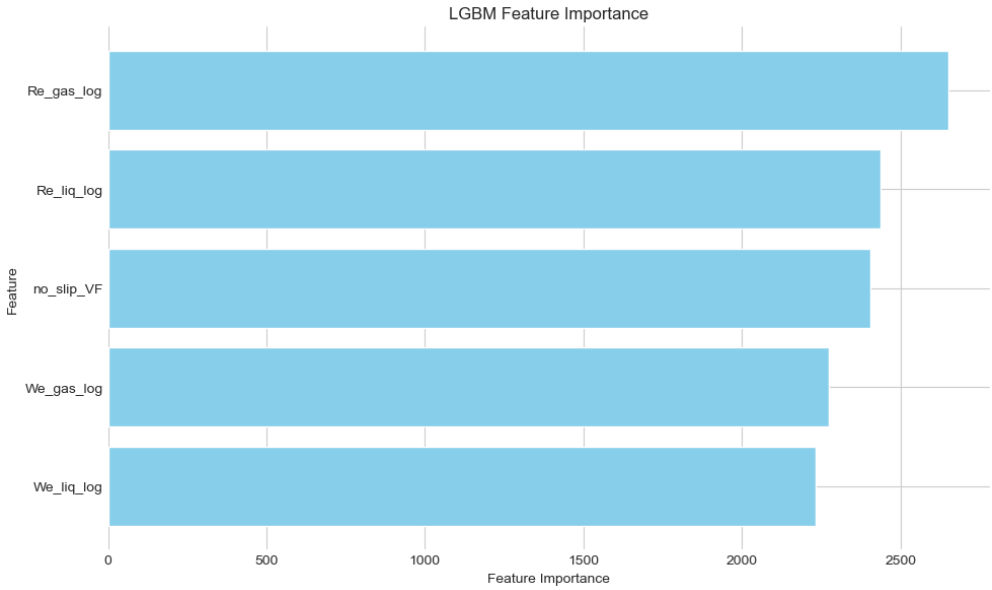


Figure 3.7. Feature Importance Plot for Flow Pattern

3.3.3. Model Evaluation

A rigorous evaluation process was conducted to ensure the accuracy and reliability of the predictive models developed in this study. The models tasked with predicting void fraction were evaluated using several key performance metrics, including Mean Squared Error (MSE), Root

Mean Squared Error (RMSE), and the Coefficient of Determination (R^2). These metrics provide a comprehensive assessment of a model's predictive capabilities.

MSE is employed to measure the average squared difference between the predicted values and the actual observed values as shown in Equation 3-1. A lower MSE indicates that the model's predictions are closely aligned with the actual data, reflecting a better overall fit.

$$MSE = \frac{1}{n}\sum_{i=1}^{n}(y_i - \breve{y}_i)^2 \qquad \text{Equation 3-1}$$

where is the y_i actual value, $\breve{y}_i$ is the predicted value and n is the total number of observations.

RMSE, as the square root of MSE as shown in Equation 3-2, offers insight into the magnitude of the prediction errors, with lower values indicating fewer and less severe deviations from the actual values. This metric is often preferred to MSE because it presents errors in the same units as the target variable, making it more interpretable.

$$RMSE = \sqrt{\frac{1}{n}\sum_{i=1}^{n}(y_i - \breve{y}_i)^2} \qquad \text{Equation 3-2}$$

R^2, or the Coefficient of Determination, measures the proportion of variance in the dependent variable that can be explained by the independent variables in the model, as shown in Equation 3-3. A higher R^2 value suggests that the model is effectively capturing the relationships within the data and can replicate observed outcomes.

$$R^2 = 1 - \frac{\sum_{i=1}^{n}(y_i - \breve{y}_i)^2}{\sum_{i=1}^{n}(y_i - \bar{y}_i)^2} \qquad \text{Equation 3-3}$$

where $\bar{y}_i$ is the mean of the actual values.

For the classification models, developed to predict flow patterns, evaluation was based on precision, recall, and the F1-score. Precision measures the accuracy of the model in terms of the proportion of correct positive predictions out of all positive predictions made, Equation 3-4.

$$Precision = \frac{True\ Positive\ (TP)}{True\ Positive\ (TP) + False\ Positive\ (FP)} \qquad \text{Equation 3-4}$$

Recall, also known as sensitivity, assesses the model's ability to identify all relevant instances of the target class, Equation 3-5.

$$Recall = \frac{True\ Positive\ (TP)}{True\ Positive\ (TP) + False\ Negative\ (FN)} \quad \text{Equation 3-5}$$

The F1-score is the harmonic mean of precision and recall, as shown in Equation 3-6. It provides a balanced evaluation, particularly useful in cases where class distributions are uneven.

$$F1 - score = 2 * \frac{Precision * Recall}{Precision + Recall} \quad \text{Equation 3-6}$$

Confusion matrices were also generated to further analyze the performances of the classification models. These matrices offered a visual representation of how well each model performed across different flow pattern classes, allowing for a detailed examination of both strengths and limitations. The confusion matrices highlight areas where the models excel and the areas where misclassifications are more frequent, providing valuable insights for further model refinement.

3.4. Overview of Model Results

This section provides an overview of modeling results based on the dataset obtained from the published studies. These results show the performance of various machine learning techniques. More details on the model performance can be found in Osuagwu and Karami (2024).

3.4.1. Overview of Void Fraction Result

Figures 3.8 and 3.9 show the RMSE of each model using dimensional and dimensionless parameters respectively, providing a quantitative measure of the prediction errors. The percentage lines represent the Pareto line. The Pareto line shows the cumulative percentage of RMSE reduction achieved as each model is added in sequence from left to right. The figures show that the models with the lower bars contribute most significantly to lowering the prediction error.

The no-slip model is used as a baseline. It has the highest error, with an RMSE of 19.5, due to the oversimplified assumptions of the model. Given the complex and non-linear nature of the data, the linear regression model has the second highest RMSE for both cases. Going down the bar and moving towards the ensemble models, the error gets further reduced, indicating more refined predictive capabilities.

A reverse trend is observed for Figure 3.10 and 3.11, showing the R^2 values for all the models for both cases. Going up the bar and moving towards the ensemble models, the coefficient of determination or R^2 increases, also indicating more refined predictive capabilities. The pareto line for the R^2 plot represents the cumulative impact of variance of each model. Models with lower percentages have more impact on increasing the R^2 value meaning they fit better to the actual prediction. The models with higher percentages have lesser impact on increasing the R^2 value.

The CatBoost (CB) model performs the best in both cases, with the lowest RMSE of 10.29 and highest R^2 of 85% when dimensional parameters are used, and lowest RMSE of 7.05 and highest R^2 of 93% when dimensionless parameters are used, indicating its strong ability to handle the complexities of the void fraction data in comparison to other models. The results when using dimensionless parameters are generally better compared to the usage of dimensionless parameters.

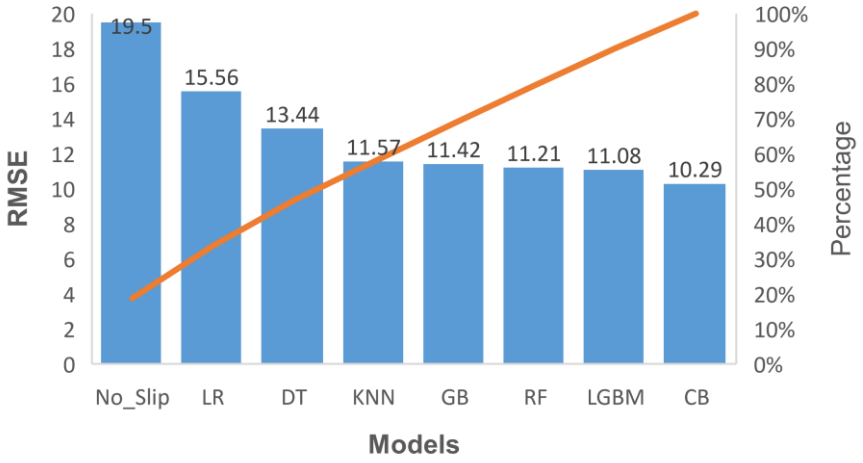


Figure 3.8. Void Fraction Prediction Errors of Various Models (Dimensional Parameters)

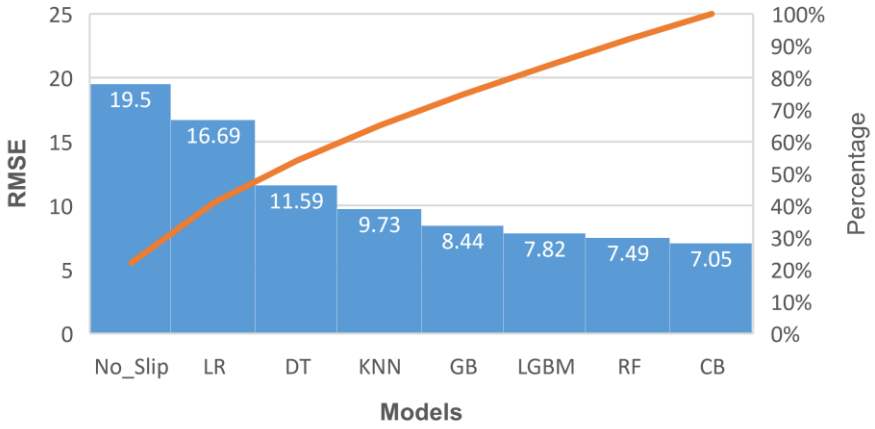


Figure 3.9. Void Fraction Prediction Errors of Various Models (Dimensionless Parameters)

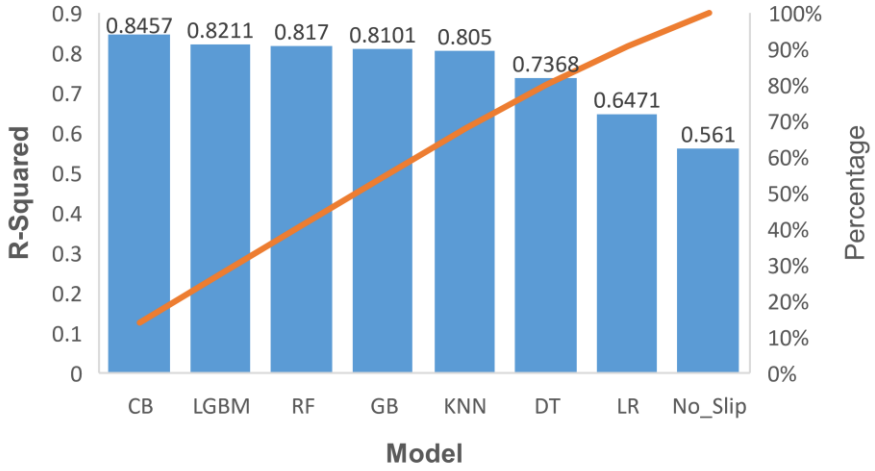


Figure 3.10. Coefficient of Determination (R^2) Results for Various Models (Dimensional Parameters)

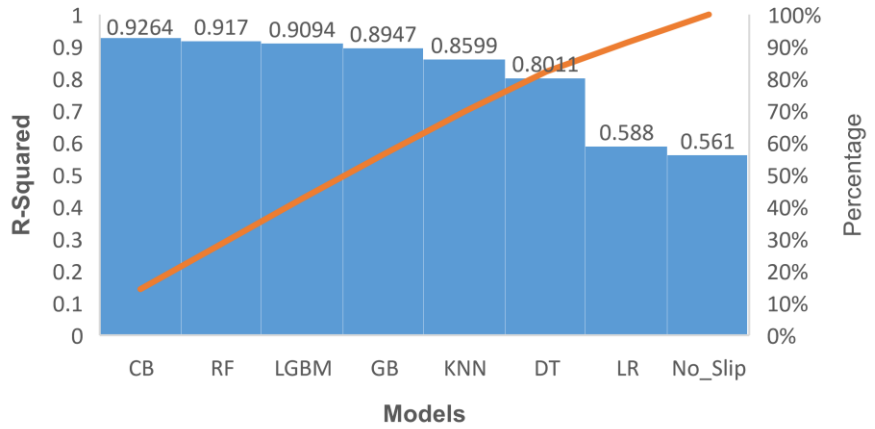


Figure 3.11. Coefficient of Determination (R^2) Results for Various Models (Dimensionless Parameters)

Moving further to access the generalizability of the models, Figures 3.12 and 3.13 show the stratified k-fold cross validation for CB model for both cases. The CB model built using the dimensional parameters provides more stability across cross-validation folds with consistent, but higher RMSE compared to the one built using the dimensionless parameters. This suggests the model using the dimensional parameters, Figures 3.12 generalizes better within the distribution seen in the training data even though it is not capturing the underlying relationships as much as the one using the dimensionless parameters.

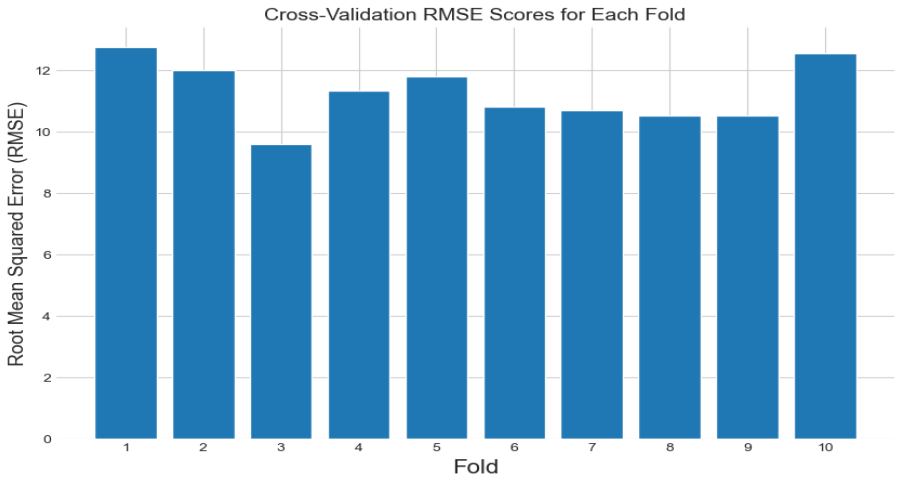


Figure 3.12. Cross Validation Result for CB Model (Dimensional Parameters)

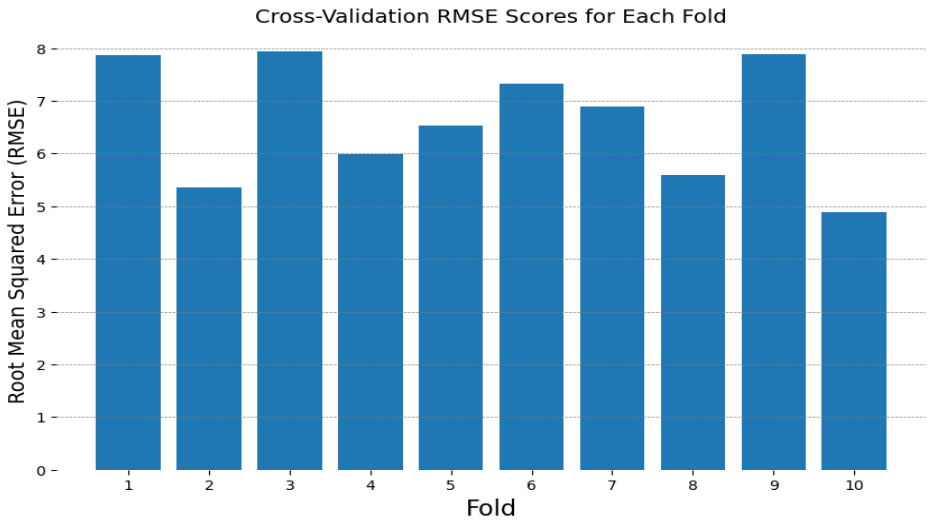


Figure 3.13. Cross Validation Result for CB Model (Dimensionless Parameters)

Figures 3.14 and 3.15 show the comparisons of the tested void fraction dataset with CB prediction for both cases. These regression plots show how well the predicted void fraction matches the actual void fraction. Figures 3.15 shows a better fit to the regression line.

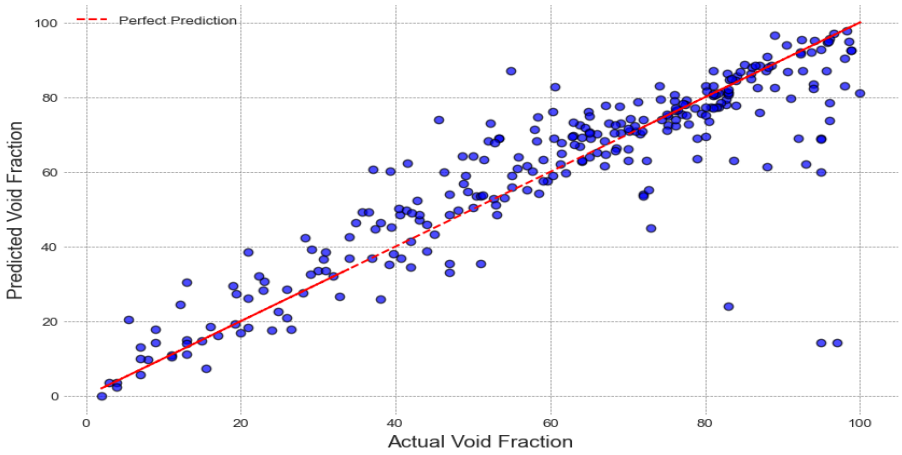


Figure 3.14. Actual Void Fraction vs Predicted Void Fraction by CB model (Dimensional Parameters)

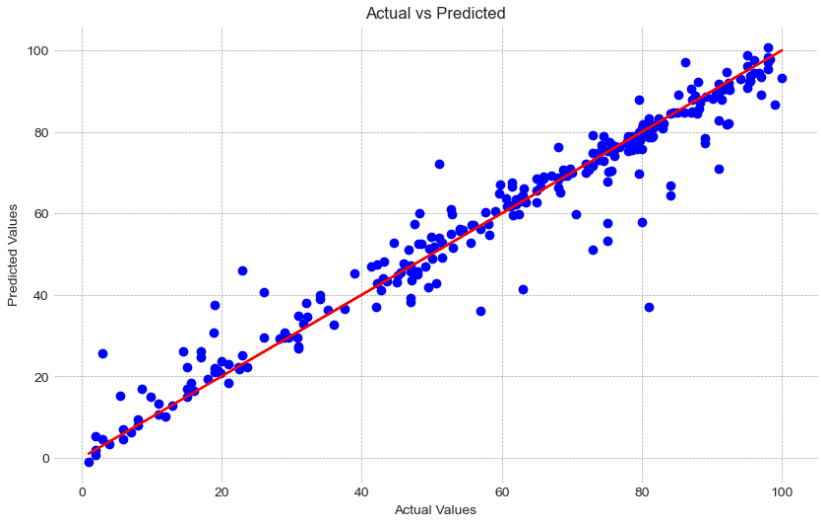


Figure 3.15. Actual Void Fraction vs Predicted Void Fraction by CB model (Dimensionless Parameters)

In summary, while the model using dimensionless parameters can capture the underlying relationships better by providing more accurate predictions with lower RMSE and better fit to the

regression line, the model built using the dimensional parameters offers better generalization across the folds.

3.4.2. Overview of Flow Pattern Result

Tables 3-1 and 3-2 summarizes the precision, recall, and F1-scores for flow pattern predictions of each model tested using both dimensional and dimensionless features respectively. Among all the models, LGBM stands out as the best-performing model in both cases, although the model performs better when the dimensionless parameters are used. This consistent performance indicates that LGBM is highly effective at predicting flow patterns based on literature data. CatBoost model is a close second with a F1-score of 0.81 and 0.87 respectively for both cases.

Table 3-1 Summary of Flow Pattern Results for Various Models Using Dimensional Parameters

Models	Precision	Recall	F1-Score
KNN	0.72	0.67	0.69
DT	0.76	0.75	0.76
RF	0.81	0.74	0.77
GB	0.77	0.77	0.77
LGBM	0.82	0.82	0.82
CB	0.81	0.81	0.81

Table 3-2 Summary of Flow Pattern Results for Various Models Using Dimensionless Parameters

Models	Precision	Recall	F1-Score
KNN	0.88	0.76	0.78
DT	0.79	0.79	0.79
RF	0.85	0.81	0.83
GB	0.83	0.83	0.83
LGBM	0.90	0.90	0.90
CB	0.87	0.87	0.87

Figures 3.16 and 3.17 show the confusion matrix for LGBM, the best-performing model for both dimensional and dimensionless parameter usage. It provides a deeper look into the model's classification accuracy across specific flow patterns. The model achieves excellent predictive

performance for most of the flow patterns, with only minor areas of confusion. The biggest source of confusion is between the slug and churn flow patterns, which is understandable considering the similarities between these flow patterns. The predictions when using dimensionless parameters are generally better compared to the usage of dimensionless parameters.

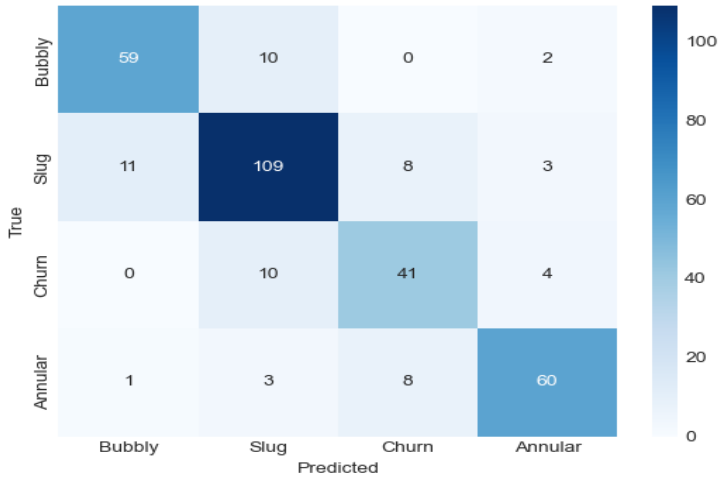


Figure 3.16. Confusion Matrix for LGBM Flow Pattern Prediction (Dimensional Parameters)

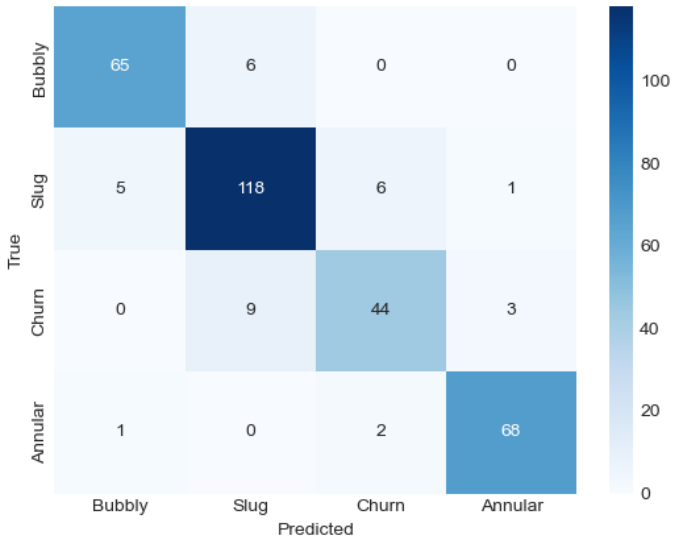


Figure 3.17. Confusion Matrix for LGBM Flow Pattern Prediction (Dimensionless Parameters)

A range of v_{Sg} and v_{SL} data points was chosen for development of a predicted flow pattern map using the LGBM model. Figure 3.18 shows that the model effectively distinguishes between

flow patterns based on velocity conditions. Slug flow tends to occur at low to medium values of v_{Sg}, for all v_{SL} values. As the v_{Sg} increases further, with increasing v_{SL}, churn flow is observed. Annular flow occurs at high v_{Sg} values, particularly at lower v_{SL}. At very high v_{SL}, annular flow does not exist within the tested range. Slight misclassifications can be observed, but generally, the model is able to predict the flow pattern trends with respect to the influence of both v_{SL} and v_{Sg}.

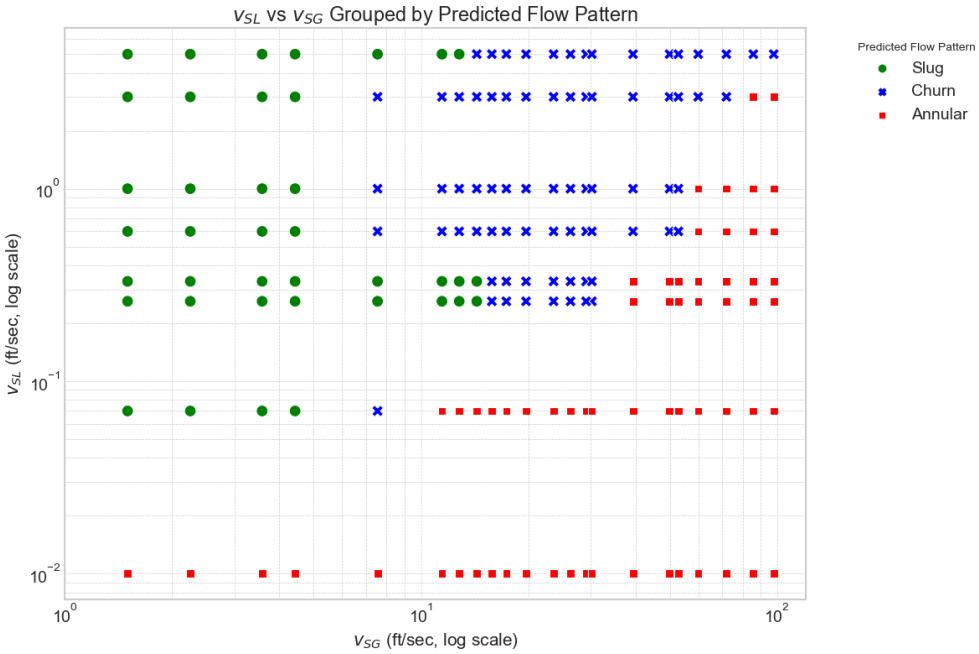


Figure 3.18. Predicted Flow Pattern Map

Chapter 4

EXPERIMENTAL METHODOLOGY

This chapter outlines the experimental approach taken in this study to investigate vertical downward two-phase flow. The experimental design is described in detail, including the design and configuration of the vertical flow loop, the procedure for running the experiments, the data acquisition system, preprocessing and analysis of the experimental data, and the test matrix.

4.1. Experimental Setup

The experimental facility setup used for this vertical downward two-phase flow study is located at the Well Construction Technology Center at the University of Oklahoma. The setup consists of a 25-ft long, 2-in. inner diameter (ID) vertical steel pipe flow loop, as shown in Figure 4.1. It is designed to simulate the flow conditions in a vertical tubular.

The facility is equipped with liquid and gas inlet lines, the vertical test section, and a return line to the liquid tank, enabling the circulation of the liquid phase and venting of the gas phase into the atmosphere. The gas inlet line includes a compressor, a set of safety valves, and a thermal flow meter. The liquid inlet line includes the tank, a pump, and a Coriolis flow meter. The test section is equipped with a camera, quick-closing valves for holdup measurement, pressure, temperature, and differential pressure transmitters. A comprehensive schematic of the facility can be seen in Figure 4.2.



Figure 4.1. Vertical Flow Loop Overview Image

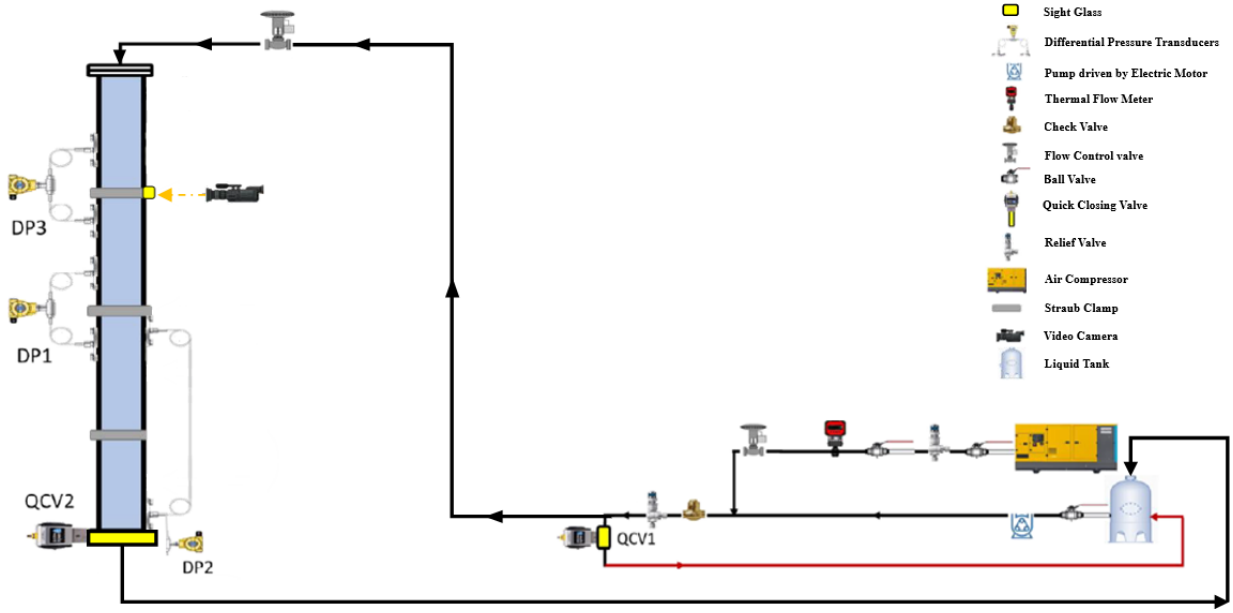


Figure 4.2. An Illustration of the Facility Schematic

The two-phase flow experiments were carried out with water as the liquid phase and air as the gas phase. The fluid properties can be seen in Table 4.1.

Table 4-1. Tested Fluid Properties

Fluid	Temperature (°F)	Density (kg/m^3)	Viscosity (N.s/m^2)	Surface Tension (N/m)
Air	80	1.225	1.8E-05	NA
Water	80	1000	0.001	0.0728

A specially constructed tee is placed at the base of the test section to ensure correct mixing of the fluids at the inlet, as shown in Figure 4.3. Recirculation is possible during the experiments because the liquid is returned to the tank through a return line after passing through the test section. The gas phase is vented to the atmosphere, considering safety and proper gas flow regulation.



Figure 4.3. Fluid Mixing at Tee

A progressive cavity pump is used for the liquid phase, driven by an electric motor, as shown in Figure 4.4. The pump transports the liquids from the storage tank into the test section.

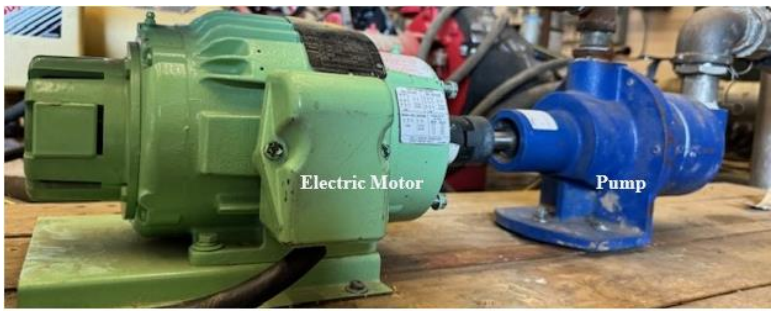


Figure 4.4. Pump Driven by an Electric Motor

The pump's flow rate is controlled through its motor's operational frequency. This frequency is precisely controlled by a variable frequency drive (VFD), shown in Figure 4.5. By varying the frequency of the motor, using LABVIEW software interfaced with the data acquisition system (DAQ), the VFD ensures that the liquid flow could be adjusted in real-time. This helps meet the desired experimental conditions and provide a high degree of control over the v_{SL} and liquid phase flow dynamics (Olubode et al., 2022).



Figure 4.5. Variable Frequency Drive

The gas phase is supplied by a rotary screw compressor, shown in Figure 4.6, capable of delivering air at rates up to 2718 m^3/h and pressures up to 800 kPa (100 psig). The air flow is regulated by a control valve, with the valve opening adjustments made through the LabVIEW. A thermal mass flow meter is used to measure the air flow rate.



Figure 4.6. Air Compressor

Pressure control in the system is maintained using two relief valves—one located at the inlet of the test section and the other positioned after the air flow meter. These valves ensure that the system operates below the facility's allowable pressure limit of 310 kPa (30 psig). As the liquid tank is open to the atmosphere, the outlet pressure remains fixed at atmospheric pressure throughout the experiments. The Straub clamps used in the facility serve to connect the pipe sections, contributing to the overall pipe length of 25 ft.

4.2. Measurement and Control Systems

A comprehensive analysis of two-phase flow behavior requires precise measurements of various parameters, including gas and liquid flow rates, pressure gradient, and liquid holdup. In addition, video recordings are used to capture the flow behavior visually. The following instruments were used for data acquisition and control during the experiments:

4.2.1. Pressure measurements

The pressure drop across the test section is measured using differential pressure (DP) transducers, configured in a wet-leg setup. Figure 4.7 shows a picture of one of these sensors. The DPs are strategically positioned to measure pressure gradients across specific sections by comparing the pressures at their two end taps. To ensure accurate measurements, the tap lines on both ends are regularly purged using a constant-density fluid, specifically water. This prevents false readings that could arise from compressible fluids, such as air, entering the DP tap lines.

It is critical to maintain zero readings on the DP sensors when the system is not in use. If deviations occur, the lines must be purged to remove any trapped air. In this wet-leg configuration, the DP transducers are located below the high and low-pressure ports. This helps keep the lines

filled with water and maintain zero readings during non-test periods, minimizing the need for frequent purging and ensuring more reliable measurements.

This experimental setup has three differential pressure transducers (DP1, DP2, and DP3) used to provide detailed pressure measurements along the test section. DP1 has a range of 0–40 kPa (0-160 inches of water), covering 121.5 in. (10.125 ft) length of the test section. DP2 has a range of 0–50 kPa (0-200 inches of water), covering 168 in. (14 ft) length of the test section. DP3 has a range of 0–10 kPa (0-40 inches of water), covering 39 in. (3.25 ft) length of the test section. In this study, however, only the differential pressure readings from DP2 were considered, this is because DP1 and DP3 were not properly configured and as such were not purged properly.



Figure 4.7. Differential Pressure Sensor

4.2.2. Gas and liquid flow control

The gas flow is provided into the test section by a rotary screw compressor. The air flow was regulated using a thermal mass flow meter, calibrated for flow rates ranging from 0 to 550 kg/hr (0 to 1200 lb/hr), along with a control valve. The flow meter generates signal outputs between 4 and 20 mA, converted to a voltage range of 0-10 V using a resistor. These signals are transmitted to a data acquisition (DAQ) system for real-time monitoring and control.

The liquid phase is supplied using a pump driven by an electric motor. The pump, connected to a 679 L water tank, can deliver a maximum flow rate of 23gpm, ensuring reliable liquid delivery. The liquid flow rate is controlled using the LABVIEW software, which adjusts the motor's speed via a variable frequency drive (VFD). The VFD regulates the motor, which in turn powers the pump to deliver the liquid from the oil tank.

4.2.3. Quick-closing valves (QCVs)

Quick-closing valves (QCVs), shown in Figure 4.8, are strategically positioned in the setup to measure the liquid holdup. One QCV, located at the base of the test section, remains open during testing to allow fluid flow. It closes immediately after each test to trap the liquids and measure the liquid holdup. Another QCV, positioned near the fluid mixing tee, operates in the reverse manner. It only opens when the first QCV closes, to release the fluids and prevent pressure buildup. These QCVs are controlled by pneumatic actuators, which respond to 0 or 10-volt electrical signals from the DAQ system, enabling quick opening and closing within fractions of a second. It is important to note that the QCVs operate in tandem. The opening of one valve triggers the automatic closure of the other, ensuring seamless control of fluid flow. This synchronized operation can only be interrupted if an override is manually initiated.



Figure 4.8. A Picture of the Quick-Closing Valve

4.2.4. Data acquisition and control

An OMEGA multi-function I/O DAQ system, shown in Figure 4.9, is used to integrate the signals from all the instruments involved in the experimental setup. A close-up picture of the power supply for the VFD is also shown in the figure. The DAQ system includes various input and output ports to receive signals for the measured data and send signals to control the valves and VFD.

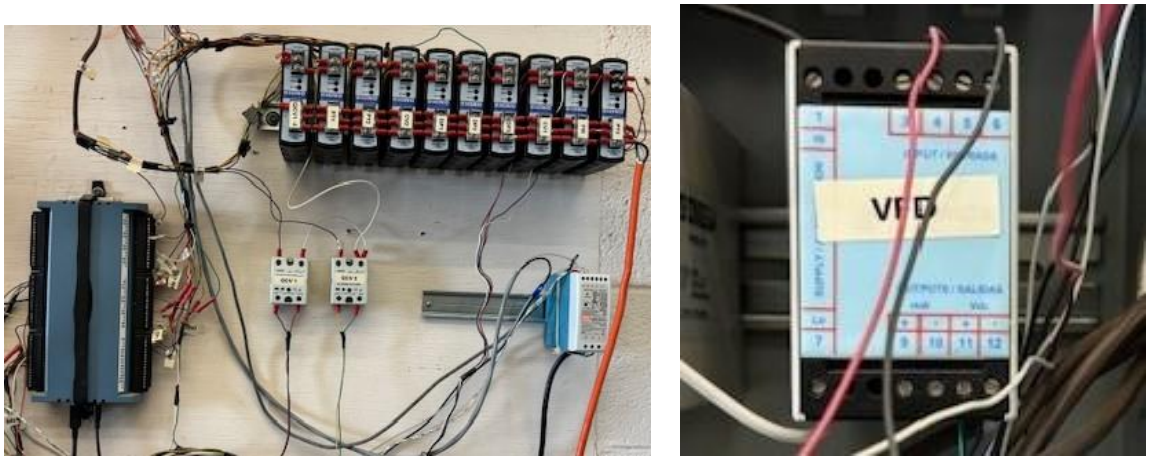


Figure 4.9. Data Acquisition System

The system is controlled using a custom-built LabVIEW program to configure and execute the necessary data acquisition tasks. A screenshot of the front-end of the program is shown in Figure 4.10. The program regulates the liquid and gas flow rates using Proportional-Integral-Derivative (PID) algorithms (Alsanea, 2022). The DAQ system also provides real-time feedback through control charts and stores the collected data in comma-separated values (.csv) files. These files then get used for further processing and data analysis after each test. Figure 4.11 shows the backend of the LabVIEW program.

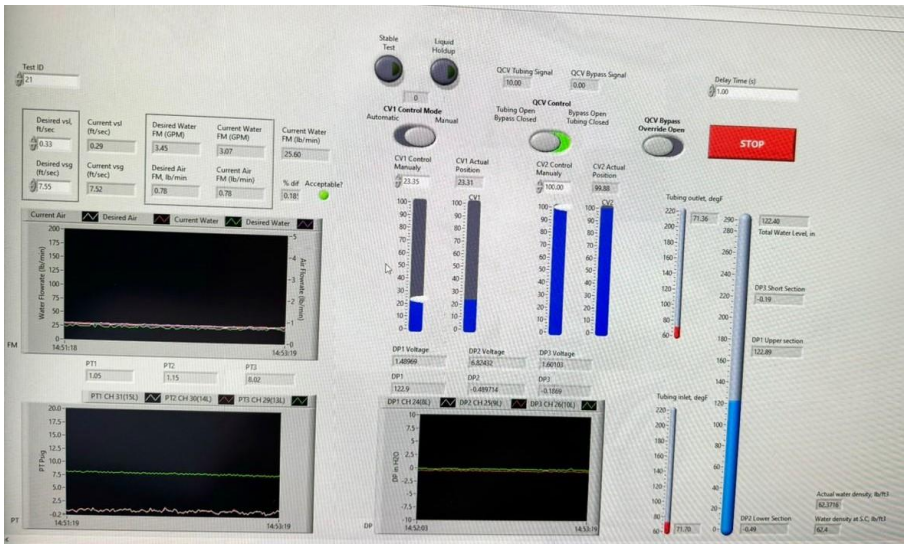


Figure 4.10. LabVIEW Program during a Test

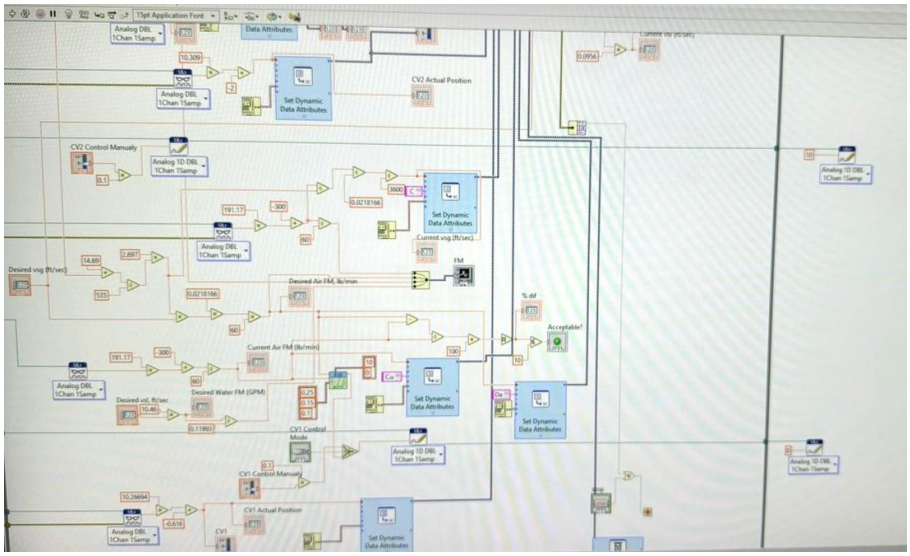


Figure 4.11. LabVIEW Block Diagram

4.2.5. Video recording

A GoPro Hero 9 Black camera is employed to capture real-time video footage of the flow behavior during the experiments through a sight glass. Figure 4.12 shows the camera and the sight glass in the test section. It is positioned at a height of 20 ft from the inlet of the test section.



Figure 4.12. Sight Glass, Video Section

4.2.6. Test Procedure

The following experimental procedure was carefully designed to ensure the safe, repeatable, and accurate execution of vertical downward two-phase flow tests. Each step must be followed meticulously to prepare, conduct, and conclude the tests.

- **Powering the Instruments:** Begin by turning on the power supply for all the instruments and devices involved in the experiment.
- **InstaCal Setup:** Open InstaCal, a program used to manage and interface with LabVIEW, ensuring that the DAQ system can read the data effectively.
- **LabVIEW Initialization:** Launch the LabVIEW program and check the initial readings of the differential pressure transducers (DPs). The readings should ideally be close to zero. If any of the DPs show values above zero, the DP lines would need to be purged to ensure accurate measurements.

- **Air Compressor Setup:** Turn on the air compressor and connect the air hose. Before running the compressor, ensure that the oil and fuel levels are adequate to avoid interruptions during testing.
- **Water Flow Meter Activation:** Turn on the water flow meter to start monitoring and controlling the liquid flow rate.
- **Variable Frequency Drive (VFD) Activation:** Power on the Variable Frequency Drive (VFD) by clicking the "Run" option on the system. It will control the speed of the pump during the experiment.
- **Camera Mounting:** Mount the GoPro camera in the designated location for video recording of the flow patterns in the test section. Ensure that it is positioned correctly for optimal visual data collection.
- **Test Execution:**
    - On the LabVIEW program, input the test index and set the desired superficial liquid and gas velocities.
    - Open the quick closing valve (QCV) at the bottom of the test section and adjust the air flow rate in LabVIEW using the control valve (CV) controller in manual or automatic setting, until the actual v_{Sg} aligns with the desired v_{Sg}.
    - Similarly, adjust the liquid flow rate using the pump control interface in LabVIEW until the actual v_{SL} matches the desired v_{SL}.
    - Allow the system to stabilize for about three minutes before proceeding with data recording to ensure steady-state conditions.
- **Data Collection and Liquid Holdup Measurement:** Once the test stability is confirmed, start recording the data for about three minutes. After completing the test, close the QCV

at the bottom of the test section and wait one minute for the liquid to accumulate. Measure the liquid holdup using DP2 and document the number.

- **Test Repetition:** Repeat the test execution and data collection steps for the required number of tests. Adjust the flow conditions, including v_{SL} and v_{Sg}, for each set of experimental conditions as needed.
- **System Shutdown:** After all tests are completed, begin the shutdown process:
    - Set the test index, v_{SL}, and v_{Sg} values to zero. After setting the desired v_{Sg} value to zero, wait until the actual v_{Sg} reaches zero, and then stop the software.
    - While waiting for the actual v_{Sg} to reach zero, gradually reduce the liquid flow rate using the pump control in LabVIEW until it reaches zero, then stop the software.
    - Close LabVIEW and InstaCal. Verify the acquired data to ensure their accuracy.
- **Compressor Shutdown:** Unload the air compressor and close the air supply valve. Turn off the air compressor, vent air lines and disconnect the air hose. Switch off the compressor from the internal controls to conserve battery power.
- **Camera Dismounting:** Carefully dismount the camera used for video recording, ensuring it is properly stored after use. This concludes the experiment.

4.3. Data Analysis

The data analysis for this chapter involves processing and analyzing the extensive dataset collected during the vertical downward two-phase flow experiments. Given the high frequency of data recording (one second interval) and the number of tests conducted (over 140 tests, including repeated tests), an automated approach was essential to handle the volume of data efficiently. The

Python programming language (version 3.10.12) was used to streamline the data preprocessing, validation, and analysis steps. The key stages in this process are outlined below:

- Data Acquisition: At the conclusion of each test, raw data files are generated in comma-separated values (.csv) format, containing readings from pressure transducers and flow meters. These readings include tests in unstable conditions marked by '0' and tests in stable conditions marked by '1'. Liquid holdup measurements are manually added to these files. In most cases, tests are repeated to ensure accuracy and consistency in the data. These raw files are retrieved and prepared for processing.
- Data Validation: Each '.csv' file is validated to ensure it corresponds to the correct experiment. This step is crucial in eliminating any data inconsistencies, such as files containing incomplete records or errors during data collection. Afterwards, the files are cleaned using Python to filter out and remove the test data marked by '0', signifying unstable tests. This leaves only test data acquired in stable conditions, marked by '1'.
- Data Integration: Once validated and cleaned, individual '.csv' files are merged into a single comprehensive data frame. This unified structure allows for easier management of the dataset, ensuring that all data points are consolidated for subsequent processing.
- Column Revision: Additional columns are computed and incorporated into the data frame to enhance the analysis. These newly added columns include calculations for converting liquid holdup and pressure gradient into the desired units. This improves consistency and accuracy in subsequent analyses.
- Data Inspection: To ensure data quality, visual inspection methods are employed. Plots are generated to visually examine the data for any anomalies or irregularities that could

compromise the integrity of the analysis. Outliers or suspicious data points are flagged and investigated further.

- Statistical Analysis: Key statistical measures such as mean values, standard deviations, and coefficients of variation are calculated for each test to capture the data variability across different flow patterns. In addition, the uncertainty associated with each measurement is assessed based on the specifications and tolerances of the instruments used in the experiments.
- Pre-Processed Data Finalization: After performing the necessary calculations and analyses, a final data frame is generated to serve as the foundation for advanced data exploration and visualization in the subsequent stages of analysis.

As previously mentioned, the tests are carefully monitored to ensure stable data acquisition and the highest quality of results. Fluctuations in the air flow rate are considered, given the critical role of this parameter in determining flow patterns and void fractions. An output signal of 4–20 mA is received from the air flow meter, converted to a 0-10 voltage value using a resistor. The computer receives the voltage data from the DAQ card, and the LabView program transforms them to mass flow rate values within 0-550 kg/hr (0–1200 lb/hr). The equation of state is used to get the air density using the pressure at the bottom of the test section and a temperature of 24 °C (75 °F). Equation 4-1 provides the air density calculation assuming ideal gas. Equation 4-2 illustrates how the air velocity is then computed using the determined air density.

$$\rho_A = \frac{P}{R_{air}T} \qquad \text{Equation 4-1}$$

$$v_{sg} = \frac{\dot{m}}{\rho_A A} \qquad \text{Equation 4-2}$$

The measured v_{sg} is then utilized to compute the relative error with respect to the target v_{sg} (Alsanea, 2022). If the error is less than 10%, LabView displays a green indicator, signifying a consistent flow rate. Figure 4.13 shows the error margins between the target and measured v_{sg}. values for the tests of this study. The stable flow with less than 10% error must persist for at least the final three minutes of the test.



Figure 4.13. Error Margin between Target and Measured v_{sg}

Pressure data corresponding to the stable flow region are considered for the pressure gradient analysis. The pressure gradients from the differential pressure transducer (DP2) are calculated by dividing the DP readings by the corresponding distances.

Liquid holdup (H_L) represents the proportion of the pipe volume occupied by the liquid phase. At the end of each test, the liquid level (h_L) is measured using the DP2 reading of the liquid accumulation. The total length of the test section (h_{total}) is 300 inches (25 feet). Since the diameter of the test section remains constant, the liquid holdup is calculated using Equation 4-3, which is the ratio of the liquid height to the total height of the test section (Mateus Rubiano, 2023).

$$H_L = \frac{h_L}{H_{total}}$$ Equation 4-3

4.4. Test Matrix

The experiments are conducted using water as the liquid phase and air as the gas phase. To investigate the impact of liquid rate on flow behavior, five superficial liquid velocities are tested. A broad range of superficial gas velocities (v_{Sg}) is also examined, spanning from annular to slug flow pattern. For each test, the actual average superficial gas velocity is recorded during the stable period, which may slightly differ from the target value due to experimental variability. The test matrix, detailing the experimental conditions, is presented in Table 4-2. In most cases, experiments are repeated under identical conditions to ensure the consistency of results, with the reported values reflecting the averages from these repeated trials.

Table 4-2. Test Matrix

Fluid	Water and Air
v_{SL} (ft/s)	0.07, 0.26, 0.33, 0.6, 1
v_{Sg} (ft/s)	3.58, 4.43, 7.55, 11.45, 12.80, 14.34, 15.81, 17.36, 19.72, 23.56, 26.28, 29.07, 30.18, 39.37, 49.87

Chapter 5

RESULTS AND DISCUSSION

In this chapter, the results of the experimental analysis on vertical downward two-phase flow are discussed in detail. The experiments captured key parameters, including superficial liquid and gas velocities, void fraction, pressure gradient, and flow pattern. These parameters are critical in understanding the complex behavior of multiphase flow in vertical tubular systems.

The void fraction and pressure gradient values measured from the experimental setup are compared against the predictions from several well-established physical models, such as OLGA, TUFFP, Ansari, and Gregory, providing a comprehensive model evaluation. Additionally, the CatBoost and LGBM models are used to predict void fraction and flow pattern, and the predictions are compared with the experimental data.

This comparative analysis provides insight into the performance of the data-based and conventional physical models in capturing the dynamics of vertical downward two-phase flow. This chapter aims to draw meaningful conclusions from the experimental results, identifying key patterns and discrepancies in the prediction of flow behavior.

5.1. Experimental Results

5.1.1. Flow Observations

The analysis of flow pattern plays a crucial role in understanding the transition between different patterns and their physical significance in any multiphase flow study. The presented

images correspond to various flow patterns, each showcasing a distinct interaction between the liquid and gas phases.

Figure 5.1a, at a v_{Sg} of 3.58 ft/s, corresponds to the intermittent or slug flow pattern. The slug flow pattern consists of a mixture of gas bubbles and liquid intermittently flowing. This forms distinct slugs of liquid separated by pockets of gas. Given the low gas velocity, it does not carry as much liquid, as such the sight glass appears clear. Figure 5.1d reveals a slug of liquid with entrained gas bubbles. In this case, the slug formation is more pronounced, showing a clear liquid mass with intermittent gas inclusions. The slugs are observed to occur at average six-second intervals, displaying a relatively regular periodic nature.

Slug flow transitions to churn follow at higher gas velocities. The churn flow is a chaotic, highly turbulent regime that occurs as gas velocity increases and the regularity of slug formation breaks down. Figure 5.1b and c show the image of the churn flow in a clear phase at a v_{Sg} of 14.34 and 30.18ft/s, respectively. The interaction between the gas and liquid can be seen at the top of the pipe. The chaotic nature can be observed in Figure 5.1e and f, as turbulence comes in, occurring at intervals averaging four seconds, indicative of increased gas velocity driving more frequent flow disruptions. Annular flow is not observed within the showed ranges.



a) v_{Sg} = 3.58 ft/sec ***b) v_{Sg} = 14.34 ft/sec*** ***c) v_{Sg} = 30.18 ft/sec***



d) v_{Sg} = 3.58 ft/sec *e) v_{Sg} = 14.34 ft/sec* *f) v_{Sg} = 30.18 ft/sec*

Figure 5.1. Vertical Downward Two-phase Flow Behavior at v_{SL} = 0.26 ft/sec

Figure 5.2 shows similar screenshots, but with a v_{SL} of 0.07 m/s. It offers insights into how lower liquid velocities influence the flow patterns observed within a vertical downward multiphase flow setup. The liquid slugs in Figure 5.2a appear lighter compared to Figure 5.1b with a v_{SL} of 0.26 ft/sec, showing a reduced volume of liquid in the flow and more entrapment of the gas bubbles in the liquid. A lower frequency is observed for slug formation at the v_{SL} of 0.07 m/s, with approximate intervals of 10 seconds. The reduced liquid mass allows the gas to dominate the flow for longer periods, delaying the formation of slugs.

Figure 5.2b and c depicts annular flow at a gas velocity of 14.34 and 30.18 ft/s, respectively, contrasting with Figure 5.1e and f, where churn flows are observed at the same respective gas velocity but with a higher v_{SL} of 0.26 ft/s. Here, the flow is characterized by a distinct liquid film along the pipe walls, with a dominant central gas core. This transition to annular flow at a lower v_{SL} is expected, as the reduced liquid volume promotes the formation of a continuous gas core, pushing the liquid toward the pipe walls.



a) v_{Sg} = 3.58 ft/sec *b) v_{Sg} = 14.34 ft/sec* *c) v_{Sg} = 30.18 ft/sec*

Figure 5.2. Vertical Downward Two-phase Flow Behavior at v_{SL} = 0.07 ft/s

Figure 5.3 shows the flow observations at a higher liquid rate, with a v_{SL} of 1 ft/s. The increased v_{SL} significantly influences the behavior of all the flow regimes. In comparison to Figure 5.1, Figure 5.3a shows a higher frequency of slug occurrence, averaging approximately 2 seconds per interval. Figure 5.3b and c shows the churn flow becoming more chaotic with increased liquid turbulence. This highlights the role of v_{SL} in determining flow behavior, with higher velocities leading to more liquid dominance in two-phase flow patterns. The larger presence of liquid at v_{SL} = 1 ft/s contrasts with the more gas-dominant structures observed in the earlier images, where v_{SL} values are lower.



a) v_{Sg} = 3.58 ft/sec *b) v_{Sg} = 14.34 ft/sec* *c) v_{Sg} = 30.18 ft/sec*

Figure 5.3. Vertical Downward Two-phase Flow Behavior at v_{SL} = 1 ft/s

5.1.2. Void Fraction and Flow Pattern Analysis

In this section, the relationships between the void fraction, v_{Sg}, v_{SL}, and flow pattern (annular, churn, and slug) are analyzed. In addition, this section extends the analysis using non-dimensional parameters, specifically, the gas-oil ratio (GOR) and the no-slip void fraction to provide scale-independent insights into flow behavior and slippage effects.

The plot of void fraction vs. v_{Sg}, grouped by v_{SL} and flow pattern, shown in Figure 5.4, presents a comprehensive overview of how changes in v_{Sg} and v_{SL} influence the void fraction and flow pattern for downward two-phase flow. From Figure 5.4, the relationship between void fraction and v_{Sg} is not significant across all v_{SL} values and flow patterns. This is in contrast with what has been reported in the literature for upward two-phase flow. At lower to intermediate v_{Sg}, the void fraction exhibits considerable variation across different flow patterns, particularly for higher v_{SL} values. This suggests a more pronounced effect of liquid rate on void fraction of downward flow. This is especially clear in slug and churn flow conditions, where the interaction between the liquid and gas phases is more complex. The variations are minimal and can be attributed to the measurement uncertainties. These uncertainties are larger for slug flow because of the large variations in void fraction as the slugs pass through the test section. At the lowest v_{SL} of 0.07 ft/sec, the void fraction is consistently above 97.5% across all v_{Sg} values with little variations. This indicates that the liquid is flowing through the pipe quickly regardless of the v_{Sg} value. This region is mainly annular flow dominated.

The figure reveals how the liquid rate influences gas-liquid distribution. An increasing v_{SL} consistently decreases the void fraction in the pipe. At the lower v_{SL} values, the void fractions are typically higher, indicating a more gas-dominated flow. As v_{SL} increases, the void fraction begins

to decrease. This is because more liquid is present in the pipe, pushing the gas out of the pipe, thereby decreasing the void fraction. As the liquid phase becomes more prominent, slug and churn flow patterns become more prevalent, for instance annular flow is not observed within the experimented range at high v_{SL} values.

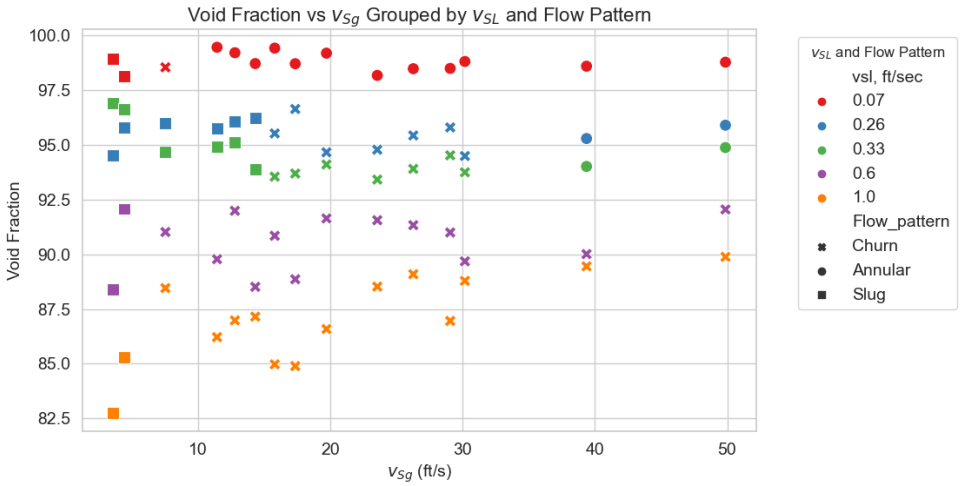


Figure 5.4. Void Fraction Experimental Analysis

A correlation can be observed between flow pattern and void fraction. In general, annular flow exhibits the highest void fraction because of gas dominance in the region. Churn and slug flows exhibit lower void fractions due to the presence of intermittent liquid slugs or churn regions, which increase the liquid holdup. The plot provides valuable insight into the complex interplay between superficial velocities, void fraction, and flow patterns, contributing to a deeper understanding of vertical downward two-phase flow dynamics.

Figure 5.5 shows the plot of void fraction vs. GLR, grouped by flow pattern. It shows that void fraction increases with increasing GLR. Low GLR is characterized by liquid dominated flow patterns (slug and churn) and the void fraction is relatively lower. As the GLR increases, the void fraction increases, due to increased presence of gas. Further increase in the GLR is characterized by higher void fraction and annular flow pattern. The GLR term is used to remove dependency on

the physical dimensions of the system. This makes the analysis broadly applicable to different systems and scales. The formular for GLR is shown in Equation 5-1.

$$GLR = \frac{v_{Sg}}{v_{SL}} \qquad \text{Equation 5-1}$$

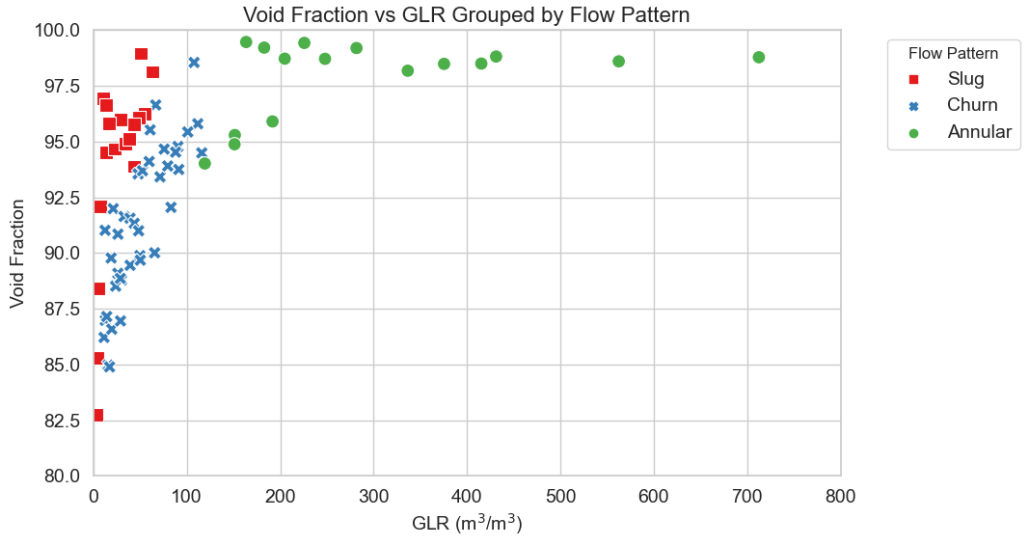


Figure 5.5. Void Fraction vs GLR

Figure 5.6 shows the plot of void fraction vs. no-slip void faction (α_{NS}), grouped by flow pattern. It shows the correlation between void fraction and no-slip void fraction in vertical downward two-phase flow. The red dashed line (slippage line) represents the ideal no-slip condition, where the void fraction becomes equal to the no-slip value. Figure 5.6 shows scenarios where the no-slip void fraction is less than or greater than the void fraction. When the gas phase travels downward slower than the liquid, the void fraction becomes larger than the no-slip value. This is due to gravity effects causing the denser liquid to accelerate more than the gas. It is commonly observed in slug flow. The smaller void fraction than the no-slip value occurs when the gas phase travels faster than the liquid. This is common in churn and annular flow. The formular for no-slip void fraction is shown in Equation 5-2.

$$\alpha_{NS}(\%) = 100 \times \left(\frac{v_{Sg}}{v_{Sg}+v_{SL}}\right) \qquad \text{Equation 5-2}$$

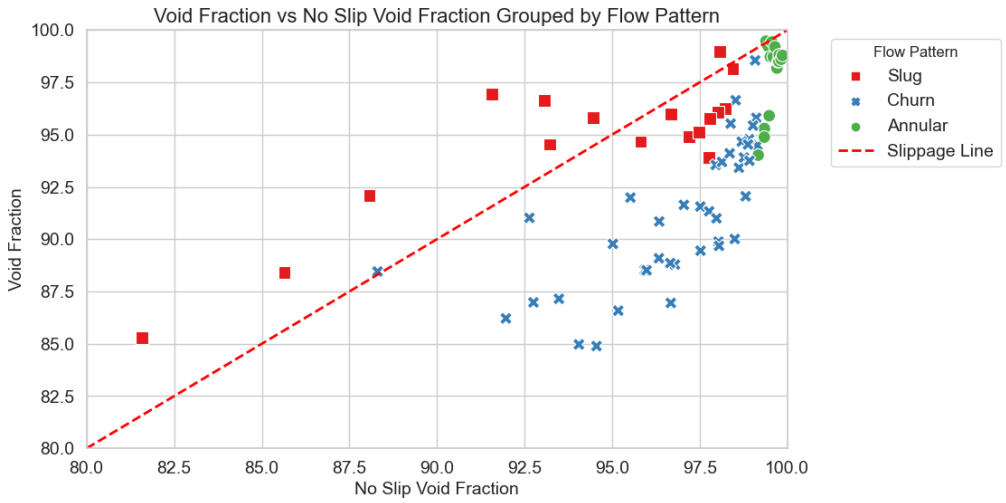


Figure 5.6. void fraction vs. no-slip void faction

5.1.3. Pressure Gradient and Flow Pattern Analysis

In vertical downward two-phase flow, the pressure gradient can vary between positive and negative values due to the balance between gravitational forces, which drive the flow downward, and frictional forces, which resist it. When gravitational forces dominate, the gradient can be positive, but as the gas rate (v_{Sg}) increases, frictional forces become more significant, often leading to a negative pressure gradient.

Figure 5.7 shows the relationships between the superficial gas velocity (v_{Sg}), superficial liquid velocity (v_{SL}), and flow pattern (annular, churn, or slug) with the pressure gradient of downward two-phase flow. There is a general decrease in pressure gradient as v_{Sg} and v_{SL} increase. However, each flow pattern has different characteristics in terms of phase distribution and interfacial area, affecting both the frictional and gravitational components.

At low v_{Sg} values of slug and churn flow region, the flow is dominated by gravitational forces rather than gas momentum. In the slug region, the pressure gradient does not vary much across the v_{SL} values, however higher v_{SL} show higher pressure gradient compared to lower v_{SL} values. As the flow transitions to churn region, the decrease in pressure gradient with increasing

v_{Sg} becomes more visible. The influence of v_{SL} on the pressure gradient becomes clearer in churn flow. This is because the increased gas velocity starts to dominate the flow behavior, and the frictional losses become more significant. The increasing frictional forces begin to overcome gravitational forces, leading to a more pronounced decrease in pressure gradient. In the annular region, higher v_{SL} values result in even greater decrease in pressure gradient, because of the increased interfacial friction.

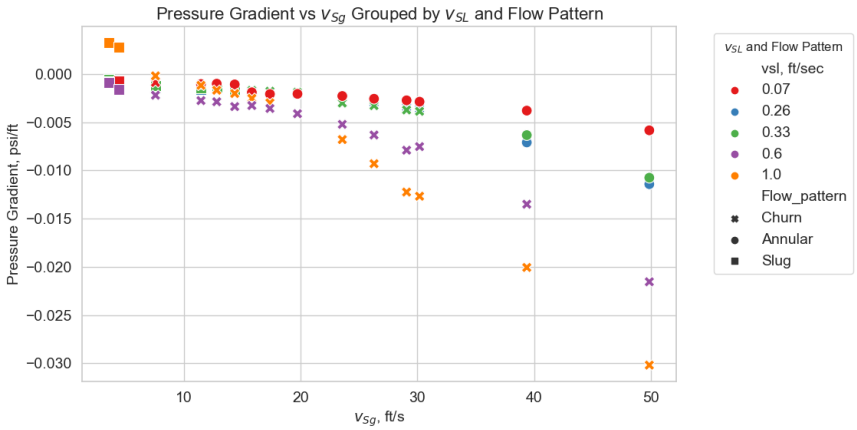


Figure 5.7. Pressure Gradient Experimental Analysis

In summary, the trend suggests that at lower gas velocities, the contribution of the friction to the overall pressure gradient is minimal. The flow appears to be more gravity-dominated in this region, as the downward flow of the liquid phase is balanced by the gravitational forces. The shift toward more negative pressure gradients at higher v_{Sg} values signifies an increase in friction. This is indicated by the steeper pressure gradient curves, due to higher momentum exchange between phases and, consequently, higher pressure losses. This decrease is more pronounced at the transition from churn to annular flow. The high velocities introduce more shear stress and turbulence, leading to increased frictional pressure losses. Hence, the flow transitions to being more friction-dominated, as shown in Figure 5.8.

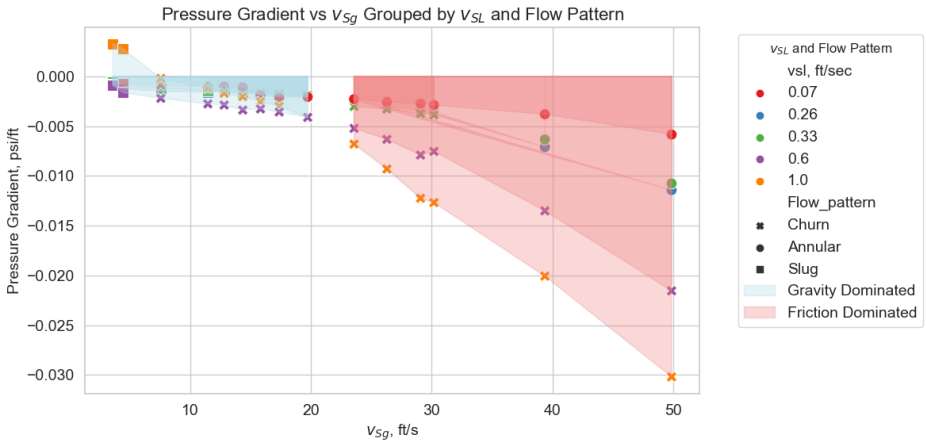


Figure 5.8. Pressure Gradient Region Separation

5.1.4. Test Repeatability

Figures 5.9 and 5.10 present the initial and repeated void-fraction and pressure gradient results with a superficial liquid velocity of 0.26 ft/s. There are instances where the measurements differ after repeating the tests, specifically in the churn region. This can be attributed to the chaotic nature of churn flow. However, the differences are negligible in the other regions. For these cases with measurement difference, the average value of the two tests was used for analysis.

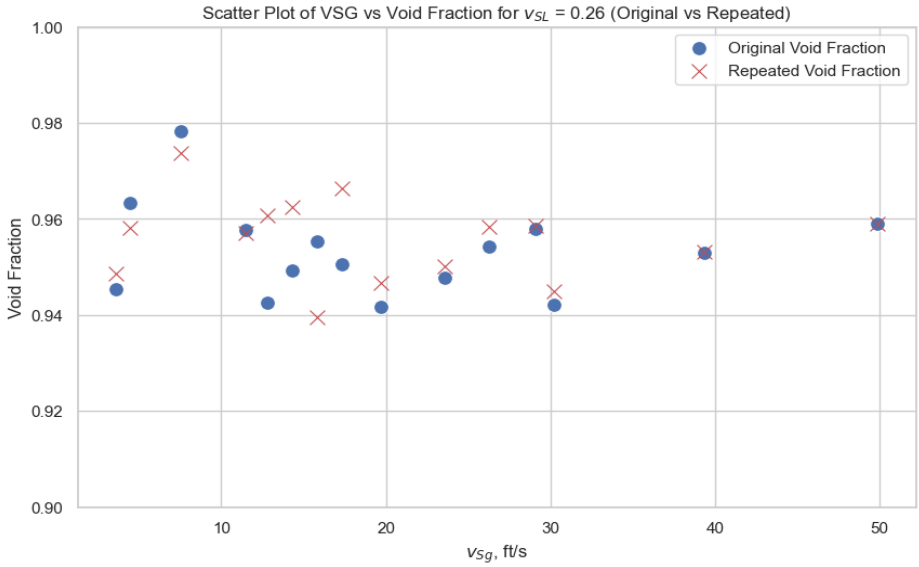


Figure 5.9. Void Fraction Repeatability Plot

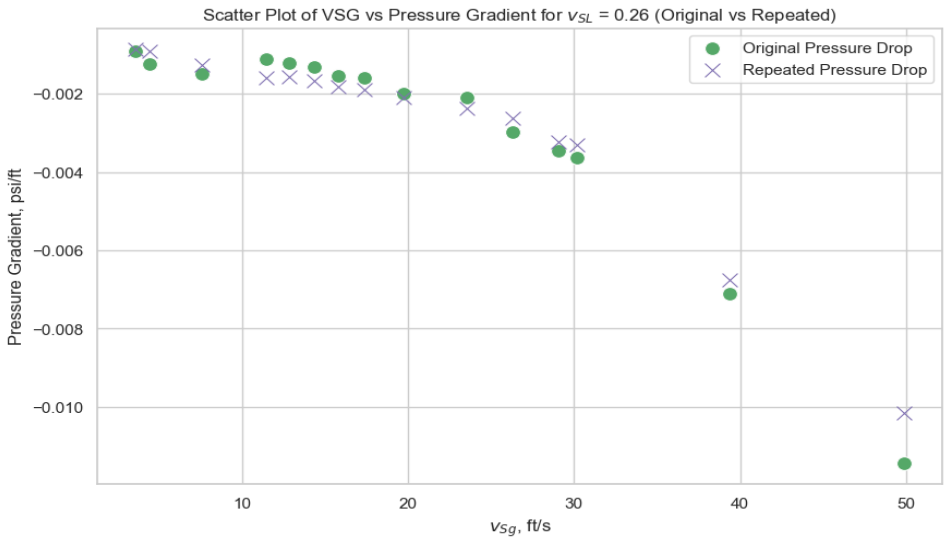


Figure 5.10. Pressure Gradient Repeatability Plot

5.2. Physical Model Evaluation

This section presents a detailed comparison of the void fraction and pressure gradient predictions derived from four established physical models with the experimental results obtained in this study. The models of OLGA, Ansari, Gregory, and TUFFP are used for this analysis. Each of these models has been widely employed in the prediction of the multiphase flow behavior. The objective is to evaluate their performances in vertical downward gas-liquid flows. PIPESIM, a standard oil and gas industry software, was used to generate model predictions.

While experimental results offer direct insights into the flow system under the tested experimented conditions, physical models provide theoretical or empirical predictions based on their respective assumptions and computational frameworks. The aim of comparing the performance of these models against experimental data is to assess their accuracy and applicability for liquid-gas downward flow. The evaluation is presented in two sections, first for the void fraction, and then for the pressure gradient predictions.

5.2.1. Void Fraction Prediction

5.2.1.1. Void Fraction Prediction based on OLGA

OLGA is a dynamic multiphase flow simulator widely used in the oil and gas industry for predicting flow behavior in pipelines and wellbores. It incorporates the effects of friction, gravity, and fluid properties and is capable of modeling complex flow conditions, including slugs, waves, and hydrodynamic instabilities in pipelines. It solves a set of coupled mass, momentum, and energy balance equations to simulate transient multiphase flows, accounting for gas, liquid, and solid phases (Bendiksen et al. 1991). It uses a two-fluid model approach, as follows:

- Solving separate continuity equations for gas and liquid phases.
- Considering slippage between phases, using closure relations for interfacial friction.
- Accounting for different flow patterns and transitions between them.

The OLGA model generally shows a trend of increasing void fraction with increasing gas velocity as shown in Figure 5.11. In comparison to the experimental results, the OLGA void fraction results show good agreement across some of the v_{SL} values. However, OLGA generally underpredicts the void fraction at lower v_{SL} values. While OLGA maintains a uniform upward trend in void fraction with increasing v_{Sg}, the experimental values exhibit more variation, particularly in the intermediate slug and churn flow patterns. This disparity indicates that OLGA's predictions may not fully capture the complex flow dynamics, such as interfacial waves and slugs, particularly at lower liquid rates for downward flow.

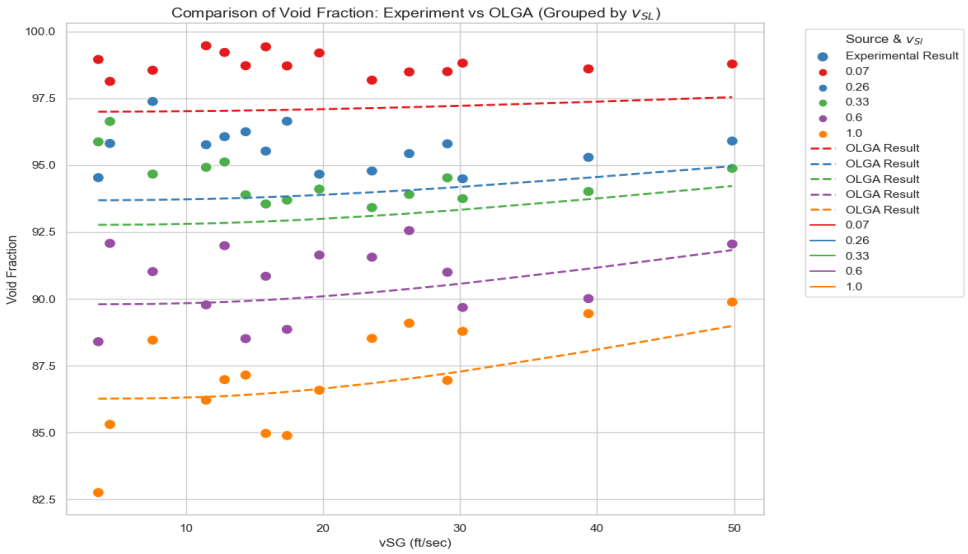


Figure 5.11. Experimental Results vs. Olga Predictions (Void Fraction)

5.2.1.2. Void Fraction Prediction based on Gregory's Model

Gregory model, often referenced alongside the Neotec-Gregory correlation, is an empirical model for multiphase flow systems. It was originally developed for horizontal flow, identifies a flow pattern on the basis of the given design parameters (fluids, flow rates, pipe characteristics, etc.) then applies the correlation best suited for the flow pattern to predict the expected liquid holdup and pressure drop (Gregory et al., 1975). It was later adapted for vertical flow.

There is a notable difference in comparison of void fraction between the experimental results and Gregory predictions, particularly at lower v_{Sg} values, as shown in Figure 5.12. In this region, the model underpredicts the void fraction, suggesting that the Gregory model does not fully capture the slug and churn flow dynamics in downward flow. However, from the intermediate to higher v_{Sg} regions, the model performs better, especially for lower v_{SL} values of 0.07 and 0.26 ft/s. In this range, the model captures the impact of higher v_{Sg} on void fraction. Overall, the Gregory model exhibits a general tendency to underpredict void fractions across the range of v_{SL} values. This suggests that while the Gregory model provides a reasonable trend, it may not accurately capture the downward gas-liquid interactions.

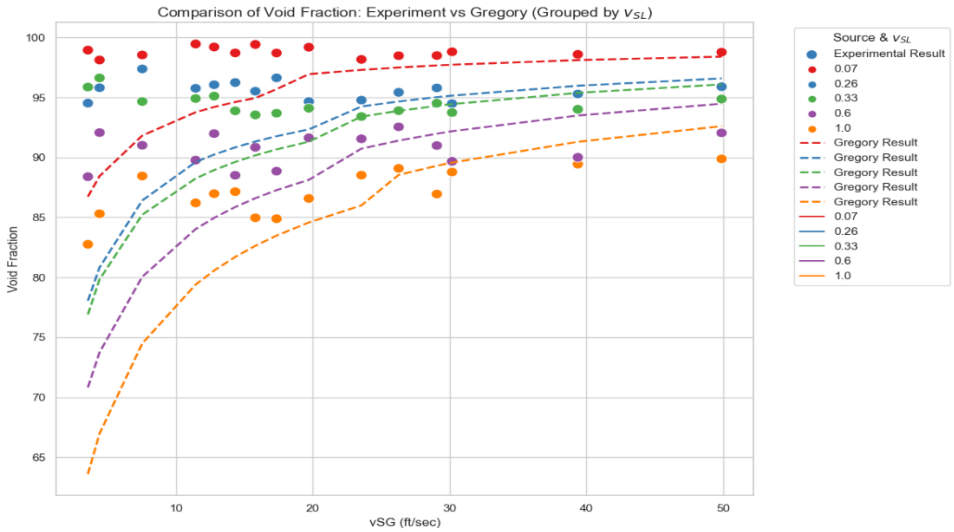


Figure 5.12. Experimental vs Gregory (Void Fraction)

5.2.1.3. Void Fraction Predictions based on Ansari's Model

The Ansari model is a mechanistic model designed to predict multiphase flow behavior in vertical wells (Ansari et al., 1994). It uses separate momentum balance equations for each flow pattern to predict the void fraction. The model was originally developed for upward flow, but its principles can be adapted for downward flow, with appropriate modifications to account for the change in flow direction.

As shown in Figure 5.13, Ansari's model aligns with experimental observations only within the slug region. It shows a better fit with the experimental observations at the lowest v_{SL}, 0.07 ft/s, compared to other v_{SL} values. As the v_{SL} increases, the model tends to overpredict the void fraction, particularly at high gas rates of annular flow. Based on the plot, it's suggested to use Ansari only for slug flow in downward vertical pipes.

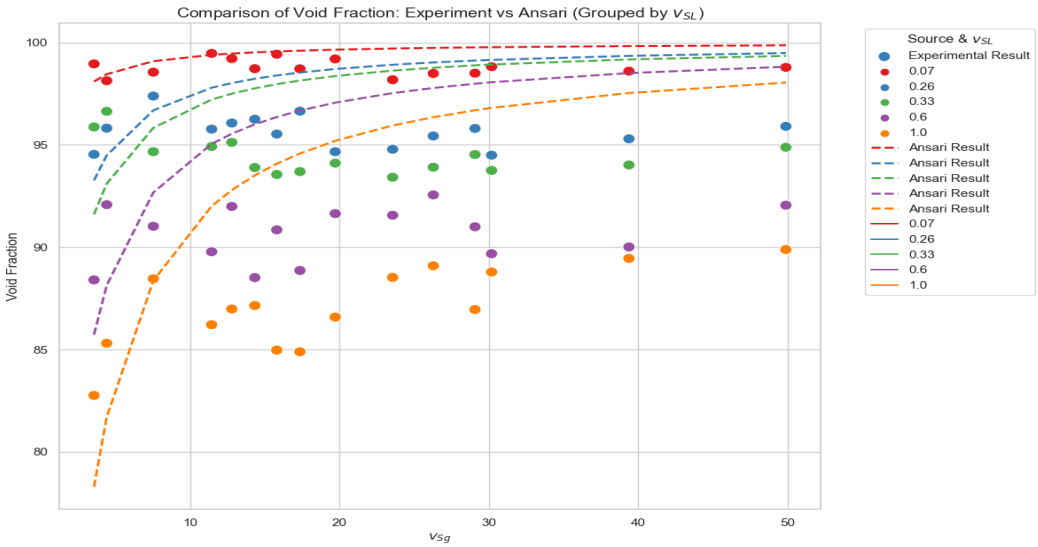


Figure 5.13. Experimental vs Ansari (Void Fraction)

5.2.1.4. Void Fraction Predictions based on TUFFP Unified Model

This model was developed at the Tulsa University Fluid Flow Projects (TUFFP) by (Zhang et al. 2003). It is based on mechanistic and empirical correlations for two-phase flow in pipes. It is designed to predict flow pattern, liquid holdup, and pressure gradient for multiphase flow in pipes with all inclination angles. TUFFP's unified model assumes intermittent flow in the pipe and predicts the transition to other flow patterns based on the ratio of the film length to the slug body length. The model uses experimental data and a set of mechanistic equations to describe the interaction between the phases.

The general trends of the TUFFP model predictions for our experimental data are shown in Figure 5.14. There are some discrepancies between the model predictions and the experimental data. At higher v_{SL} values, the model captures the downward flow dynamics better, showing the gradual increase of void fraction with increasing v_{Sg}. At lower v_{SL} values, however, the model underpredicts the void fraction. The discrepancy is not as much for higher v_{SL} tests, showing a better model alignment with the data.

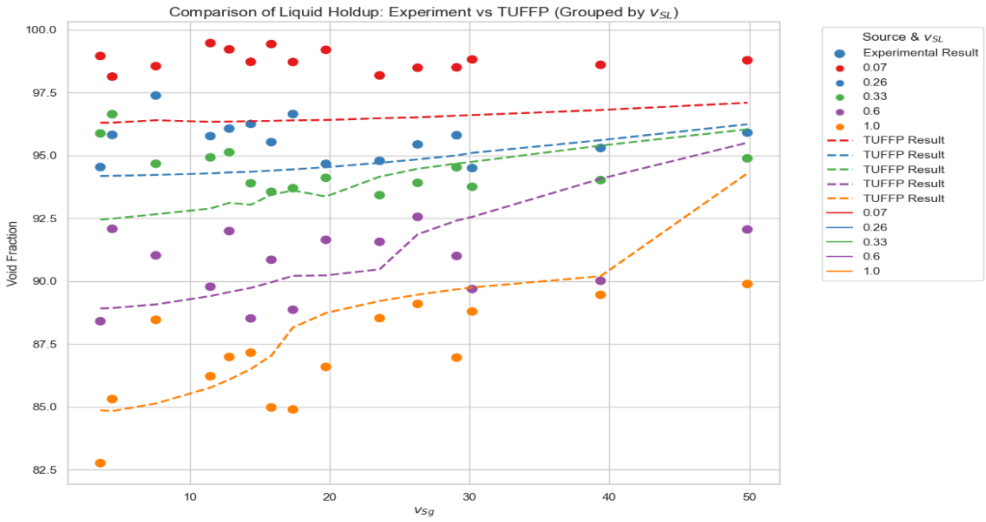


Figure 5.14. Experimental vs TUFFP (Void Fraction)

5.2.1.5. Summary of Physical Model Void Fraction Predictions

In summary, all the models exhibit some form of overprediction or underprediction. However, OLGA captures the trends of the experiment better than the other models, despite a significant underprediction at the low v_{SL} value of 0.07 ft/sec. Also, TUFFP performance is relatively good, particularly for higher liquid rates. TUFFP aligns well with experimental observations in the churn flow. Gregory model aligns better with the experiments in the annular flow pattern, while Ansari's model aligns with the experiments in the slug flow pattern.

5.2.2. Pressure Gradient Predictions

5.2.2.1. Pressure Gradient Predictions based on OLGA

OLGA calculates pressure gradients by using flow pattern-dependent correlations for wall and interfacial friction factors. The model incorporates the effects of pipe inclination, fluid properties, and flow rates. From Figure 5.15, the OLGA's pressure gradient predictions follow a similar trend as the experimental results across the test matrix. It accurately captures the trend of decreasing pressure gradient with increasing v_{Sg}. Some over-predictions are observed in the

gravity-dominated area, with v_{Sg} values below 20 ft/s. In the friction-dominated region, there are some overpredictions at the higher v_{SL} values. This can be attributed to overestimation of interfacial friction.

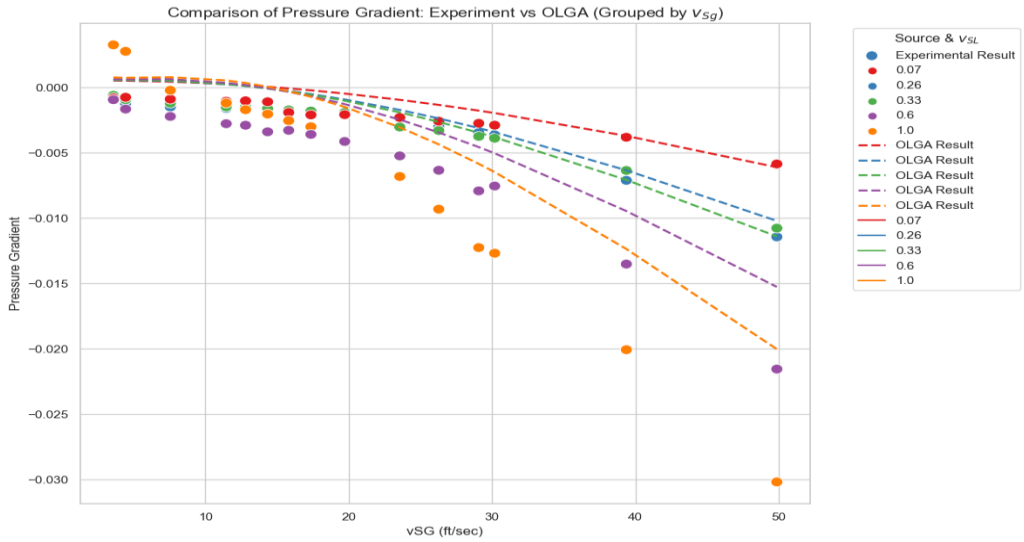


Figure 5.15. Experimental vs OLGA (Pressure Gradient)

5.2.2.2. Pressure Gradient Prediction based on Gregory

As shown in Figure 5.16, Gregory's model follows the trend of experimental observations with the pressure gradients decreasing with increasing v_{Sg}. However, it significantly underpredicts the friction effect on pressure gradient. The experiments show little to no decrease in pressure gradient as v_{SL} decreases at lower v_{Sg}. Instead, the decrease in pressure gradient becomes noticeable as v_{Sg} increases due to friction. The reverse is the case for Gregory's model, as it overemphasizes the impact of v_{SL} at low v_{Sg}.

The Gregory model also significantly overpredicts the pressure gradient at the gravity dominated region, the overprediction is much lower in the frictional region. The inaccuracy of the model in the gravity-dominated flow conditions compared to friction-dominated conditions might be because it was originally developed for horizontal flow and may not accurately account for the complex interplay between gravitational and frictional forces in vertical downward flow.

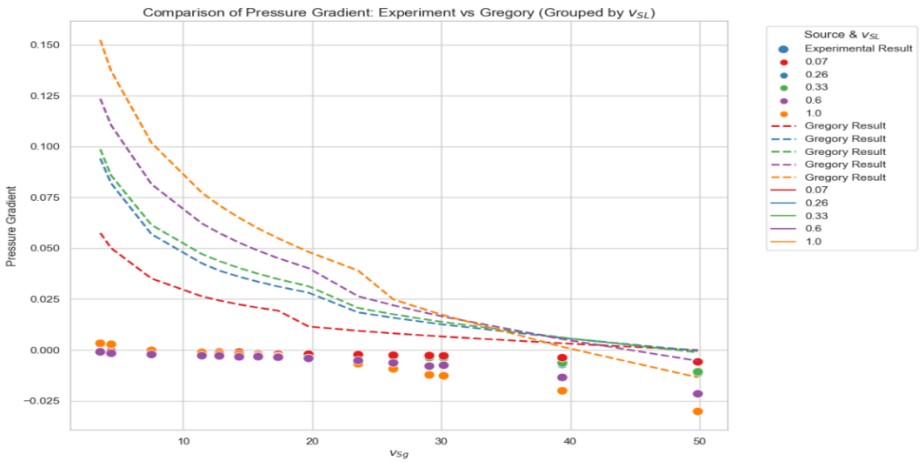


Figure 5.16. Experimental vs Gregory (Pressure Gradient)

5.2.2.3. Pressure Gradient Prediction based on Ansari

Ansari model considers frictional, gravitational, and acceleration components in pressure gradient prediction. The predictions are similar to Gregory in terms of significantly overpredicting the pressure gradient at lower v_{Sg} ranges as shown in Figure 5.17. This can be due to the overestimation of liquid holdup, and hence the gravitational pressure gradient at lower v_{Sg} ranges. However, Ansari perfectly fits the experimental observations at the friction-dominated higher v_{Sg} region. As the v_{Sg} increases, the pressure gradient decreases, similar to the experimental results. Again, this can be attributed to a better void fraction estimation by Ansari in annular flow range.

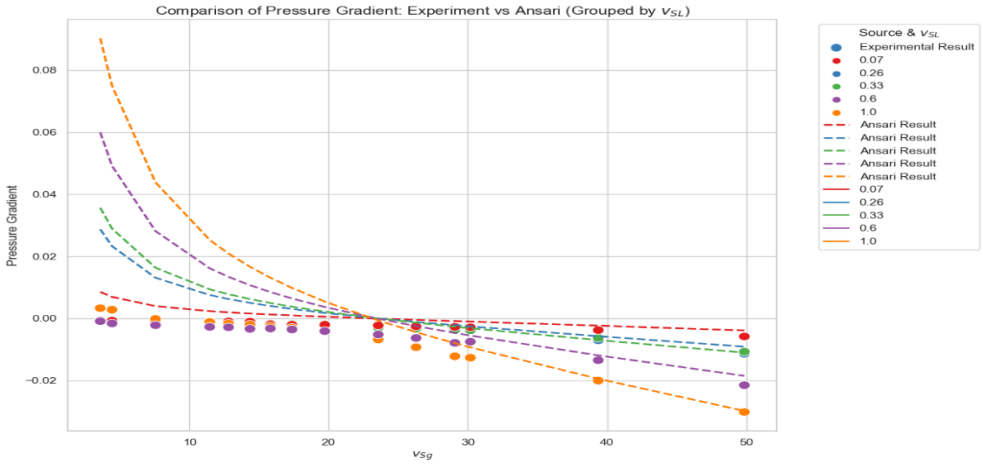


Figure 5.17. Experimental vs Ansari (Pressure Gradient)

5.2.2.4. *Pressure Gradient Prediction based on TUFFP*

From Figure 5.18, the TUFFP model aligns with the experimental observations in the prediction of decreasing pressure gradient as v_{Sg} increases. Although with little overprediction, the model seems to be performing well in the lower v_{Sg} region. The model underpredicts the pressure gradient for the higher v_{SL} values as the v_{Sg} increases. This is because the model overestimates the impact of liquid velocity on pressure gradient in this region, due to the overestimation of interfacial friction. The downward liquid-gas annular flow includes complex interfacial waves, where the liquid film pushes the gas core downward. The model seems to have some errors in prediction of this annular flow.

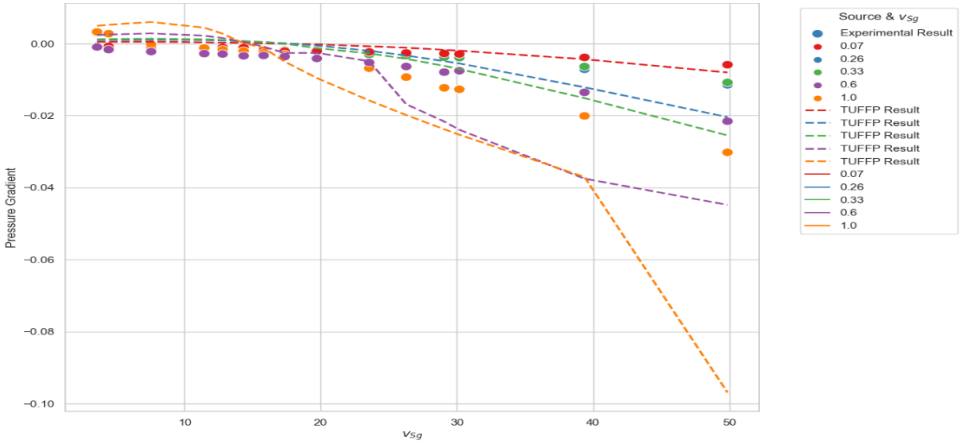


Figure 5.18. Experimental vs TUFFP (Pressure Gradient)

5.2.2.5. *Summary of Physical Models for Pressure Gradient*

In summary, the OLGA model performs better than other models in predicting the trends of the experimental result. It shows some overprediction at lower v_{Sg}, across all v_{SL} values, and also, at high v_{Sg} and high v_{SL}. TUFFP performs in a similar manner, however, it shows more significant overprediction at the high v_{Sg} range and for high v_{SL} tests. Gregory and Ansari models perform similarly at the lower v_{Sg} region, showing significant overprediction, but Ansari performs better at higher v_{Sg} region.

5.3. Machine Learning Model Evaluation

This section primarily presents the predictions from the machine learning models on void fraction and flow pattern in comparison with the experimental results. The model development based on a comprehensive liquid-gas downward flow dataset from the literature is described in Chapter 3. It was shown that CatBoost (CB) has the best performance in void fraction prediction compared to a few other machine learning techniques. In addition, LGBM performs the best in predicting the downward flow pattern. This is why further analysis is limited to these two models to predict the experimental data.

The training foundation of the CatBoost and LGBM models involved a robust dataset with various downward flow conditions and resulting observations. It provided the models with the capability to generalize across a range of two-phase flow scenarios. The models are further fine-tuned through transfer learning to better align with the specific conditions of the experiment.

Transfer learning, a machine learning technique, allows a model pre-trained on a large dataset to be fine-tuned for a more specific task or dataset with minimal data. In this context, the pre-trained CatBoost and LGBM models are used as a foundation and then fine-tuned using a some portion of the experimental data to adjust their predictions. The fine-tuning process proved to be beneficial, enhancing the model performances on the experimental data.

In addition, the section extends to presenting the predictions from the machine learning models on pressure gradient, built solely on the experimental data.

5.3.1. Void Fraction Prediction Based on CatBoost Model

The model generally follows the trends, staying within the range of experimental observations as seen in Figure 5.19. However, the model tends to underpredict the void fraction,

particularly for the lower v_{Sg} regions. It fits the data better in the churn and annular flow region, especially at the lower v_{SL} values.

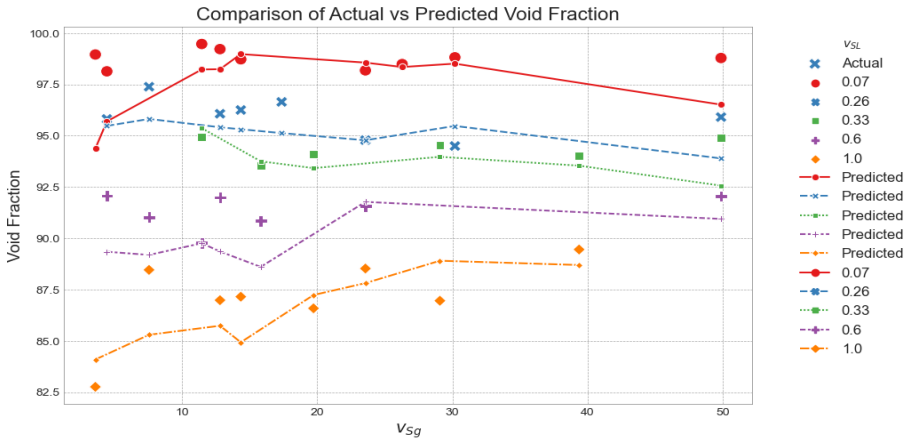


Figure 5.19. Experimental vs CatBoost (Void Fraction)

5.3.2. Flow Pattern Prediction based on LGBM Model

Figure 5.20 shows the confusion matrix results of the LGBM model for flow pattern prediction, compared to the experimental data. The model performs well overall in identifying the flow patterns across all the flow conditions. However, there is a slight misclassification of churn as annular flow regime. This could be due to the uncertainties involved in flow pattern recognition, especially for the transition of churn and annular flows.

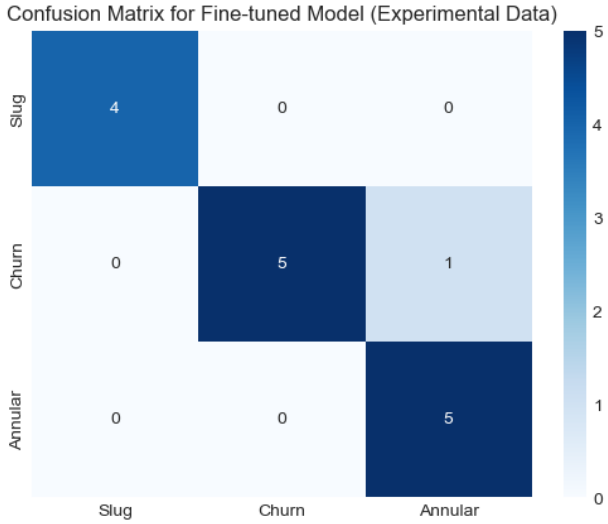


Figure 5.20. Experimental vs LGBM (Flow Pattern)

The machine learning models developed and fine-tuned have shown excellent performance when applied to this study's experimental data. They demonstrate strong predictive capabilities for both void fraction and flow pattern classification, with minor mispredictions.

5.3.3. Pressure Gradient Prediction

Table 5-2 summarizes the predictive performance of the machine learning models for pressure gradient prediction based on the experimental data, evaluated using RMSE and R^2 scores. Gradient boosting (GB) is the best model for predicting the pressure gradient, as evidenced by its superior RMSE and R^2 values. It is closely matched by the light gradient boost machine (LGBM), offering a competitive alternative. CatBoost (CB) also performs well. The tree-based models (DT and RF) provide strong predictions, but are outperformed by gradient boosting methods. Linear regression is unsuitable for this dataset, as it fails to capture the underlying complexity of the data.

Table 5-1. Overview of Models Performance

Models	RMSE	R2
LR	0.0536	0.419
KNN	0.0036	0.744
DT	0.0023	0.893
RF	0.0021	0.911
GB	**0.0012**	**0.968**
CB	0.0016	0.949
LGBM	0.0013	0.967

Figure 5.21 illustrates the comparison between the actual and predicted pressure gradient values for the testing dataset using the gradient boost (GB) model. The red line represents the ideal case of perfect match with the actual values. Most of the predicted points are closely aligned with the red line, with a few slight deviations, indicating that the model has high predictive accuracy.

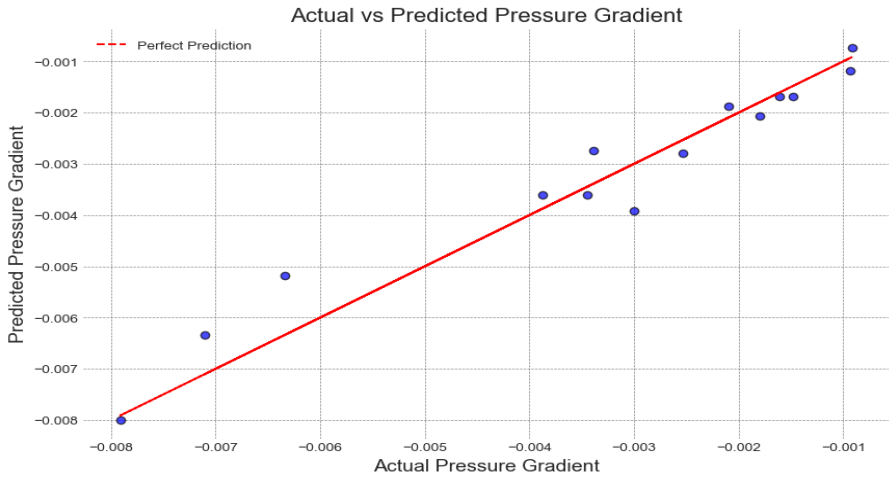


Figure 5.21. Actual vs Predicted Pressure Gradient

5.4. Relative Error Comparison Across All Models

Relative error is a key metric used to assess the performances of models by measuring the deviation of predicted values from the experimentally measured values. It provides insight into the magnitude and direction of errors, helping to compare the accuracies of different models. This formula normalizes the error by expressing it as a percentage of the actual (measured) value, which makes it easier to compare errors across different scales and conditions. The formula used to calculate the relative error in this analysis is seen in Equation 5-1.

$$Relative\ Error = \frac{Predicted\ Value - Measured\ Value}{Measured\ Value} * 100 \qquad \text{Equation 5-3}$$

5.4.1. Void Fraction Relative Error

The relative error comparison between models—OLGA, Neotec Gregory, Baker Ansari, TUFFP, and CatBoost—is visualized in Figure 5.22. The goal is to assess how these models perform in predicting the void fraction for different v_{SL} and v_{Sg} values.

CatBoost: This machine learning model demonstrates relatively consistent performance with moderate errors at lower and higher v_{Sg} values and low errors for intermediate v_{Sg} values,

across all v_{SL} values. This shows that it can effectively capture the experimental void fraction, particularly at intermediate gas rates of churn flow.

OLGA: The OLGA model shows relatively low errors at higher v_{Sg} regions and moderate errors in lower and intermediate v_{Sg} regions, across all v_{SL} values. This indicates its robustness in certain flow conditions.

Neotec Gregory: This model displays the highest relative error (underprediction), particularly for lower and mid-range v_{Sg} values, suggesting that it struggles to accurately predict void fractions in downward slug and churn flows. It consistently produces higher error bars, making it less reliable.

Ansari: While Ansari's model performs moderately well at lower v_{Sg}, its relative error increases (overprediction) at intermediate and higher v_{Sg} values. The relative error also increases with increasing v_{SL}, showing more variance at these points.

TUFFP: This model shows similar behavior to OLGA, with low relative errors across all v_{Sg} values.

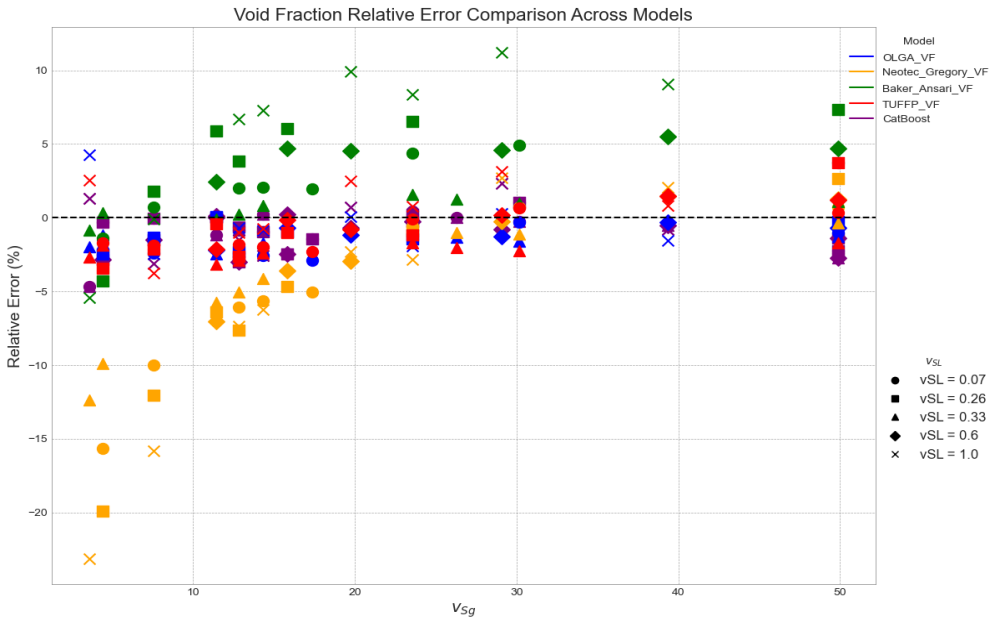


Figure 5.22. Void Fraction Relative Error Comparison

The CatBoost model demonstrates competitive performance in the void fraction prediction when compared to OLGA and TUFFP. A clearer analysis of the relative errors of these three models can be seen in Figures 5.23, 5.24, and 5.25. The TUFFP model captures the experimental patterns better, but the CatBoost and OLGA models seem to have lower relative errors compared to it. CatBoost performs better than the OLGA model for the intermediate v_{Sg} ranges, but OLGA performs slightly better at higher v_{Sg} ranges. Overall, all the models have consistently low error distributions and the ability to handle various flow conditions. This suggests that they can successfully capture the complex physics of vertical downward two-phase flow.

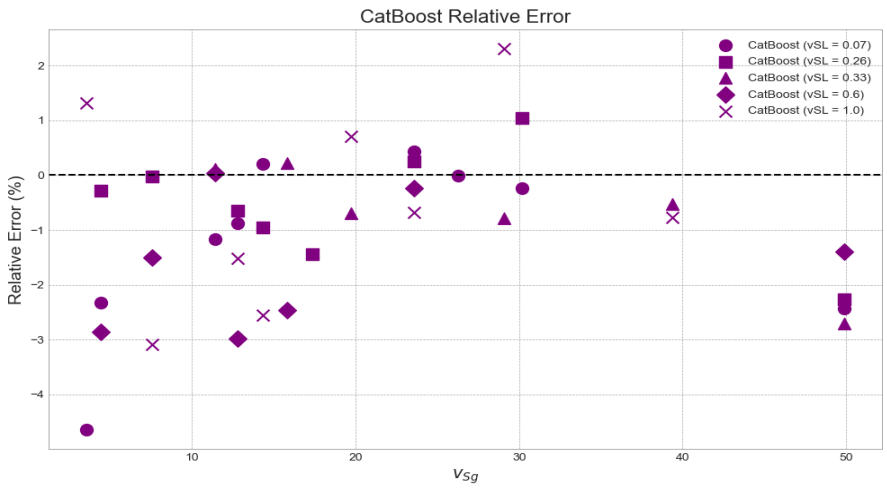


Figure 5.23. Void Fraction Relative Error Comparison (CatBoost)

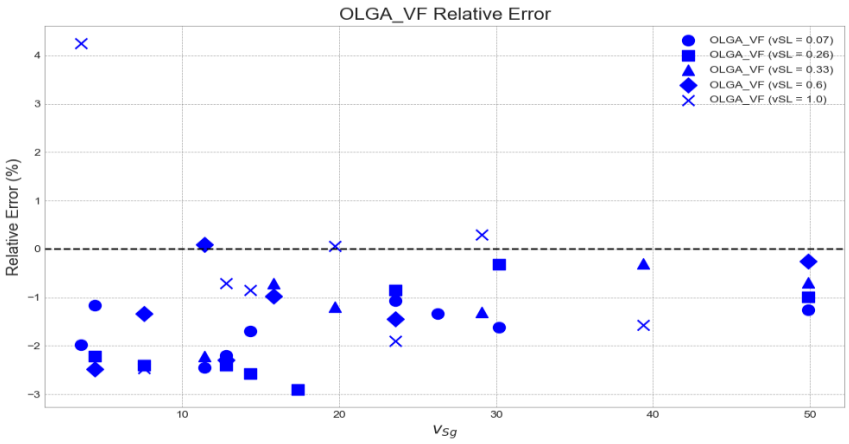


Figure 5.24. Void Fraction Relative Error Comparison (OLGA)

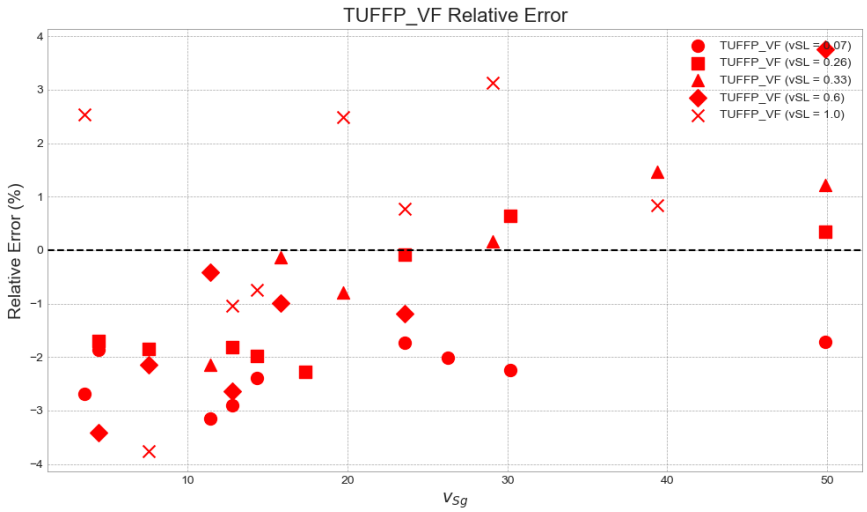


Figure 5.25. Void Fraction Relative Error Comparison (TUFFP)

Three statistical parameters are considered based on the relative error to further evaluate the best performing models: average percent error (ε_1), absolute average percent error (ε_2), and percent standard deviation (ε_3). A summary of the results is shown in Table 5-2.

Average Percent Error (ε_1): This parameter measures the average signed difference between the actual and predicted values. It helps assess whether a model tends to overestimate or underestimate. A small value close to zero indicates that the model's predictions are neither biased towards overestimation nor underestimation. In this analysis, CatBoost, OLGA, and TUFFP have low average percent errors, indicating relatively balanced predictions.

$$\varepsilon_1 = \frac{1}{n}\left(\sum_{i=1}^{n} e_{R,i}\right) \qquad \text{Equation 5-4}$$

where $e_{R,i}$ is the relative error percentage.

Absolute Average Percent Error (ε_2): This metric takes the absolute value of the percent error, meaning it disregards the direction of the error and focuses on its magnitude. It provides an overall measure of the model's accuracy. Lower values of ε_2 indicate better accuracy. Based on

this metric, CatBoost (-1.28%) and OLGA (-1.49%) perform the best, followed closely by TUFFP (-1.77%).

$$\varepsilon_2 = \frac{1}{n}\left(\sum_{i=1}^{n} |e_{R,i}|\right) \qquad \text{Equation 5-5}$$

Percent Standard Deviation (ε_3): This metric measures the variability of the model's errors. A lower value indicates a more consistent performance, meaning the model's predictions are closer to the actual values across all data points. CatBoost (1.43%), OLGA (1.2%), and TUFFP (1.87%) show low variability, making them more reliable in terms of prediction consistency.

$$\varepsilon_3 = \sum_{i=1}^{n} \sqrt{\frac{(e_{R,i}-\varepsilon_1)^2}{n-1}} \qquad \text{Equation 5-6}$$

The Absolute Average Percent Error (ε_2) is the most important metric when evaluating model performances because it directly reflects the magnitude of prediction errors. Based on this metric, CatBoost emerges as the most accurate model, followed closely by OLGA. Both models also show good consistency with low Percent Standard Deviation (ε_3), making them the most reliable for predicting void fraction. On the other hand, Gregory and Ansari perform less reliably, with larger errors and greater variability.

Table 5-2 Void Fraction Error Summary Table

Model	Average percent error, ε_1 (%)	Absolute average percent error, ε_2 (%)	Percent standard deviation, ε_3 (%)
CatBoost	-0.91	1.28	1.43
OLGA	-1.24	1.49	1.2
Gregory	-5.12	5.73	6.18
Ansari	3.27	3.91	3.68
TUFFP	-0.85	1.77	1.87

5.4.2. Pressure Gradient Relative Error

Figure 5.26 compares the relative pressure gradient prediction errors for the tested physical models—OLGA, Neotec Gregory, Baker Ansari, and TUFFP. The relative errors are calculated based on the data and model predictions for negative pressure gradient or pressure drop.

Neotec Gregory shows the highest relative errors, particularly at lower v_{Sg} values (below 20 ft/s), where the error reaches above 15,000%. The large error bars reflect significant variability in the predictions made by this model, especially for lower v_{Sg} values. TUFFP and OLGA consistently show the smallest relative errors across all v_{Sg} ranges. This suggests that they provide the most accurate prediction of pressure gradients compared to the other models, with smaller variability. Due to a lack of downward flow pressure gradient data in the literature, the machine learning models were not trained to predict the pressure gradient of downward liquid-gas flow.

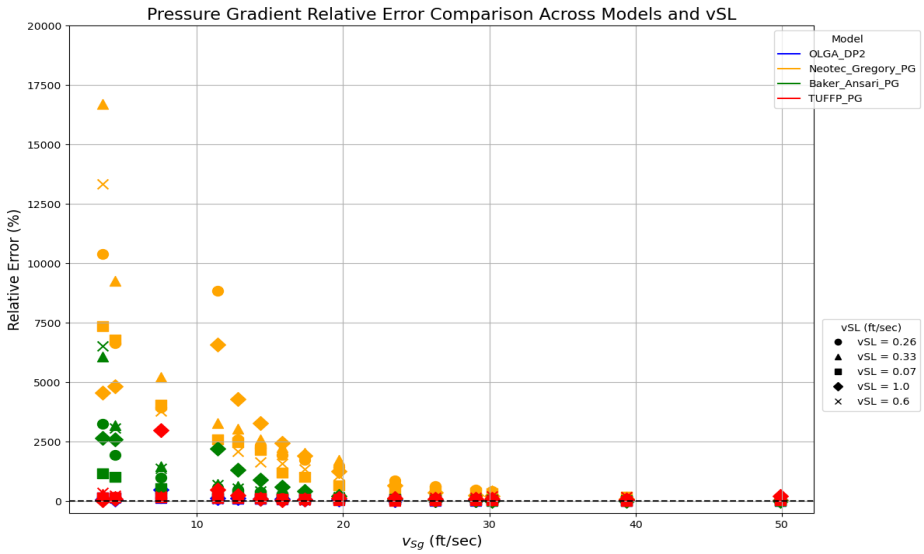


Figure 5.26. Pressure Gradient Relative Error Comparison for the Physical Models

Figure 5.27 shows a clearer view for the two better performing models, OLGA and TUFFP Unified, to have a better comparison of the two. the OLGA model shows lower relative errors compared to the TUFFP model. The relative errors seem consistent across the v_{Sg} values for both models.

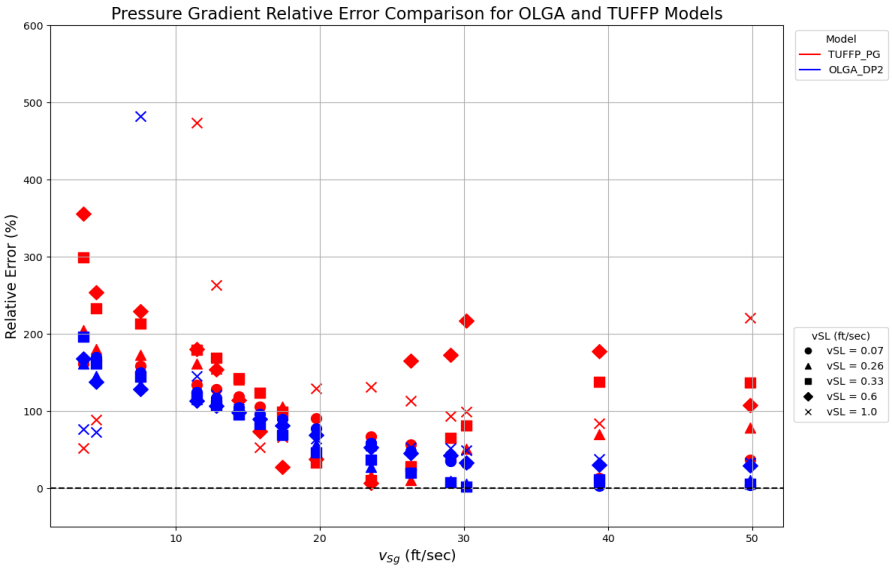


Figure 5.27. Pressure Gradient Relative Error Comparison (OLGA and TUFFP)

Figures 5.28, 5.29, and 5.30 show clearer views of the pressure gradient prediction relative errors for tests with a low v_{SL} value of 0.07 ft/s, a medium v_{SL} value of 0.33 ft/s, and a high v_{SL} value of 1 ft/s, respectively. For the lower v_{SL} tests, prediction errors consistently decrease as the v_{Sg} increases and flow pattern changes to churn and annular flow. The plots look similar for v_{SL} of 0.07 and 0.33 ft/sec, but the behavior changes for the v_{SL} of 1.0 ft/sec especially in the slug region. The TUFFP model mostly overpredicts the pressure gradient for lower v_{Sg} cases, but it underpredicts the pressure gradient at v_{SL} of 1.0 ft/sec. In conclusion, OLGA generally provides a slightly better and more consistent performance for predicting the pressure gradient.

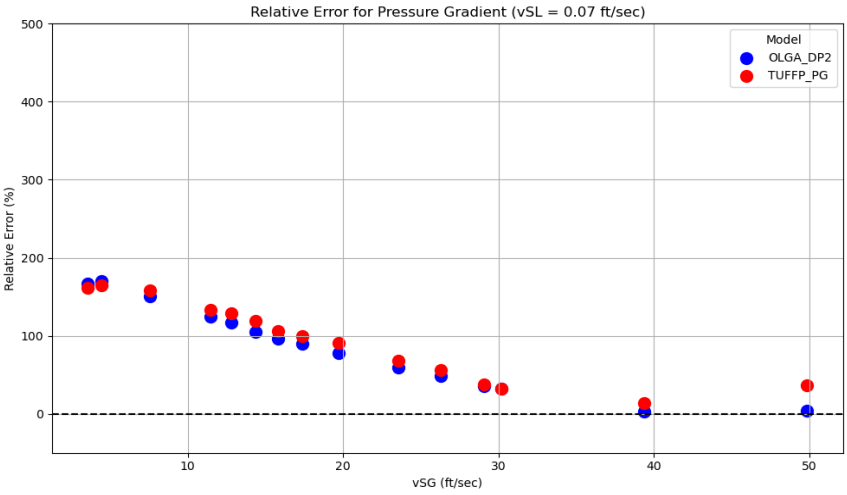


Figure 5.28. Pressure Gradient Relative Error Comparison (OLGA and TUFFP, v_{SL} = 0.07ft/sec)

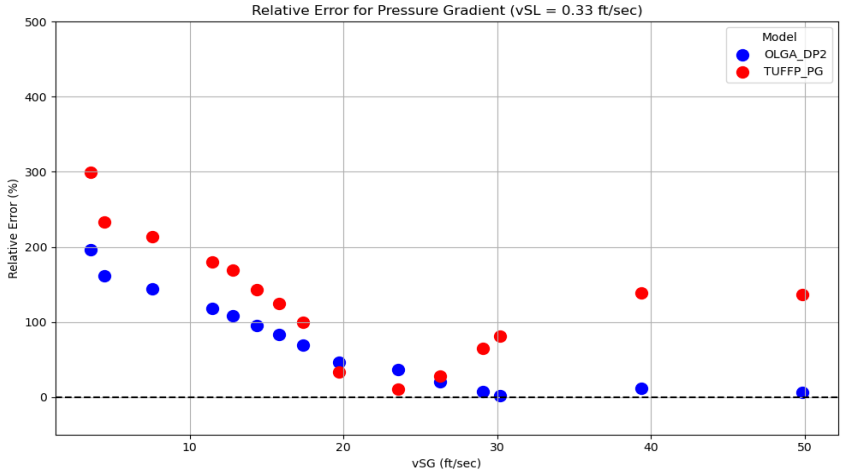


Figure 5.29. Pressure Gradient Relative Error Comparison (OLGA and TUFFP, v_{SL} = 0.33 ft/sec)

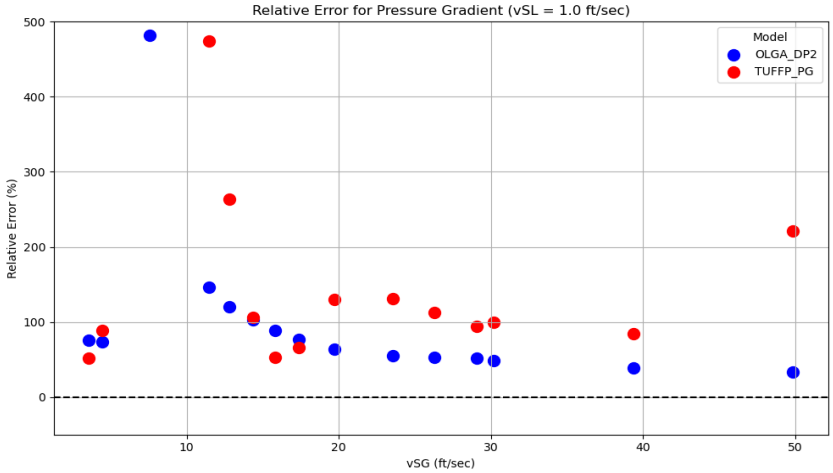


Figure 5.30. Pressure Gradient Relative Error Comparison (OLGA and TUFFP, v_{SL} = 1.0 ft/sec)

The same statistical parameters used for the void fraction evaluation were used again to evaluate the pressure gradient predictions. The results for the ε_1, ε_2, and ε_3 metrics are summarized in Table 5-3. OLGA stands out as the most reliable model for predicting pressure gradient based on experimental conditions, with the lowest average and absolute errors, and the smallest standard deviation. Gregory and Ansari models show the largest errors, struggling to capture the dynamics of downward liquid-gas flow.

Table 5-3 Pressure Gradient Error Analysis Summary Table

Model	Average percent error, ε_1 (%)	Absolute average percent error, ε_2 (%)	Percent standard deviation, ε_3 (%)
OLGA	82.49	82.49	67.95
Gregory	3168.74	3168.74	6251.69
Ansari	972.40	972.40	2668.20
TUFFP	162.61	162.61	341.85

5.5. Summary of Result

In this chapter, the experimental results were comprehensively analyzed for vertical downward two-phase flow, focusing on void fraction, pressure gradient, and flow patterns. The results were evaluated through a detailed comparison with various physical models and machine learning predictions, using statistical metrics to quantify model performances.

The void fraction, a critical parameter in multiphase flow analysis, was measured experimentally across slug, churn, and annular flow patterns at various liquid and gas rates. As the v_{Sg} increases, the flow transitions from slug to churn. At higher v_{Sg} values, the flow evolves into an annular pattern, where a gas core dominates and liquid forms a thin film along the pipe walls. There is a general increase in void fraction as v_{Sg} increases. However, the experiments show large variations. As v_{SL} increases, void fraction tends to decrease due to the increasing presence of liquid.

These observations were compared against the predictions made by CatBoost and four physical models: OLGA, TUFFP, Gregory, and Ansari. The void fraction results from these models were visualized and compared using statistical evaluation parameters based on the relative error. While CatBoost, OLGA, and TUFFP outperform the other models with smaller average errors and more consistent predictions, Catboost slightly outperforms both. Also, the LGBM data-based model demonstrates high accuracy in classifying flow patterns.

The pressure gradient was also experimentally measured under varying flow conditions. Higher v_{Sg} and v_{SL} result in lower pressure gradients due to increased friction. The measured pressure gradients were compared with the physical models, revealing significant differences in model accuracy. The OLGA model generally performs well across a range of velocities. It tends to overestimate the pressure gradients at lower v_{Sg} and higher v_{SL} values, but the performance gets better at higher v_{Sg} and lower v_{SL}. Gregory and Ansari show significant overpredictions at low v_{Sg}. Gregory also shows a slight overprediction at high v_{Sg}, while Ansari fits the experimental results. TUFFP's predictions, while reasonable at lower velocities, tend to underestimate the pressure gradient at higher v_{Sg} values.

Chapter 6

CONCLUSIONS AND RECOMMENDATIONS

This thesis investigates vertical downward two-phase flow characteristics, focusing on void fraction, pressure gradient, and flow pattern. The study evaluates both traditional physical models and advanced machine learning techniques in predicting experimental observations.

6.1. Conclusions on Downward Flow Data-Based Modeling

A comprehensive dataset was collected from 11 published works on vertical downward two-phase flow. Data points, v_{Sg}, v_{SL}, void fraction, and flow pattern were gathered to build a robust training set. Dimensionless features like Reynolds and Weber numbers of both liquid and gas phases were utilized, along with several machine learning models.

- Relationships of v_{Sg}, v_{SL}, flow pattern, and void fraction analyzed. As v_{Sg} increases and v_{SL} decreases, the void fraction increases, and the flow pattern changes from bubbly to slug, churn, and then annular flow.
- CatBoost and LGBM were highlighted for their superior accuracy in predicting void fraction and flow pattern, respectively.

6.2. Conclusions on Experimental Observations

This study's experimental data provide essential insights on downward flow dynamics. Some of the main experimental observations are:

- Void fraction increases non-uniformly with rising superficial gas velocity (v_{Sg}) across most superficial liquid velocities (v_{SL}). However, at very low v_{SL}, void fraction shows minimal increases with increased v_{Sg}.
- Increased v_{SL} generally reduces void fraction, indicating higher liquid presence in the pipe and the promotion of slug and churn flow, compared to annular flow.
- Pressure gradient is positive at low v_{Sg} values, due to the gravitational gain in downward flow. However, as v_{Sg} increases, the pressure gradient decreases and becomes negative across all v_{SL} values due to the added friction.
- Flow patterns transition from slug to churn to annular flow with rising v_{Sg}. Higher v_{SL} values extend slug and churn flow patterns, delaying annular flow onset.

6.3. Conclusions on Model Performances

All models display instances of over- and under-prediction, with challenges in transition regions and extreme conditions.

6.3.1. Void Fraction Prediction

- TUFFP and OLGA models closely align with experimental trends, outperforming other physical models.
- CatBoost demonstrates the best performance with an absolute average percent error of 1.28%, slightly better than OLGA's 1.49%.
- Gregory and Ansari models show larger discrepancies, with average errors of 5.73% and 3.91%, respectively, indicating limitations in capturing experimental conditions.

6.3.2. Pressure Gradient Prediction

- All models capture the trend of decreasing pressure gradient with increasing v_{SG}, though with varying accuracy.
- OLGA model has the best accuracy, with an average percent error of 82.5%.
- Gregory model shows the highest error, at 3168.7%, indicating limitations in downward flow prediction.

6.3.3. Flow Pattern Observation and Prediction

- Flow pattern transitions are influenced by interactions between v_{SG} and v_{SL}.
- The LGBM model shows high accuracy in classifying flow patterns, with minimal misclassification, especially between churn and annular flow.

6.3.4. Potential of Machine Learning in Two-Phase Flow Modeling

- Machine learning models effectively predict void fraction and classify flow patterns, highlighting their value in enhancing traditional physical models.
- Their ability to capture complex relationships without simplifying assumptions marks a promising advancement in multiphase flow prediction.
- Improved predictive accuracy benefits industries managing vertical downward two-phase flows, such as oil and gas, geothermal, and nuclear cooling, supporting optimized design, operational efficiency, and improved safety outcomes.

6.4. Recommendations

Given the findings of this thesis, several recommendations are proposed to enhance the understanding and prediction of vertical downward multiphase flow.

- Extend the range of experimental conditions to include different fluid combinations, such as gas-oil, and CO_2. This helps in yielding more generalized conclusions.

- Investigate the effects of pipe diameter and inclination angle on vertical downward two-phase flow behavior in similar flow conditions.
- Extend the experimental range to cover higher pressure and temperature conditions relevant to industrial applications.
- Investigate hybrid approaches to use machine learning models like CatBoost in conjunction with traditional models like OLGA to optimize flow predictions and enhance operational efficiency.
- Implement high-speed imaging and tomography techniques to gain deeper insights into flow structures and transitions.
- Investigate the application of advanced deep learning algorithms, particularly Convolutional Neural Networks (CNNs) for improved prediction accuracy of two-phase flow.
- Investigate the use of computational fluid dynamics (CFD) simulations to complement experimental studies and validate simplified models.

NOMENCLATURE

Symbol	Meaning	Units
CB	CatBoost	--
CCUS	Carbon Capture Utilization and Storage	--
CFD	Computational Fluid Dynamics	--
CNN	Convolutional Neural Networks	--
CPDF	Cumulative Probability Density Function	--
CSV	Comma Separated Values	--
CV	Control Valve	--
DAQ	Data Acquisition	--
DP	Differential Pressure	inH_2O
DT	Decision Tree	--
GB	Gradient Boost	--
GLR	Gas Liquid Ratio	--
ID	Inner Diameter	--
KNN	K-Nearest Neighbors	--
LOCA	Loss Coolant Accident	--
LGBM	Light Gradient Boost Model	--
LWR	Light Water Reactors	--
ML	Machine Learning	--
MSE	Mean Square Error	--
PDF	Probability Density Function	--
PNN	Probabilistic Neural Network	--
QCV	Quick Closing Valve	--
R^2	Coefficient of Determination	--
Re	Reynold Number	--
RF	Random Forest	--
RMSE	Root Mean Square Error	--

RNN	Recurrent Neural Networks	--
SONN	Self-Organized Neural Network	--
SVM	Support Vector Machine	--
v_{SL}	Superficial Liquid Velocity	ft/sec
v_{Sg}	Superficial Gas Velocity	ft/sec
VFD	Variable Frequency Drive	--
We	Webber Number	--

REFERENCE

Alsanea, M. (2022). Effects of restrictions and liquid properties on liquid loading in natural gas wells. https://shareok.org/handle/11244/336894

Ansari, A. M., Sylvester, N. D., Sarica, C., Shoham, O., & Brill, J. P. (1994). A comprehensive mechanistic model for upward two-phase flow in wellbores. SPE Production & Facilities, 9(02), 143–151. https://doi.org/10.2118/20630-PA

Autee, A., Srinivasa Rao, S., Puli, R., & Shrivastava, R. (2015). An experimental study on two-phase pressure drop in small diameter horizontal, downward inclined, and vertical tubes. *Thermal Science*, *19*(5), 1791–1804. https://doi.org/10.2298/TSCI130118081A

Awad, M. M. (2012). *Two-Phase Flow*. https://doi.org/10.5772/76201

Barnea, D., Shoham, O., & Taitel, Y. (1982). Flow pattern transition for vertical downward twophase flow. *Chemical Engineering Science*, *37*, 741–744. https://www.sciencedirect.com/science/article/pii/0009250982850331

Bar-Neir, G. (2014). Multiphase Flow. In *Potto.org*. https://potto.org/fluidMech/phase.php

Bhagwat, S. M., & Ghajar, A. J. (2012). *experimental investigation and performance evaluation of isothermal frictional twophase pressure drop correlations in vertical downward gas-liquid two phase flow*. https://asmedigitalcollection.asme.org/HT/proceedings-abstract/HT2012/44786/337/245167

Bhagwat, S. M., & Ghajar, A. J. (2012). Similarities and differences in the flow patterns and void fraction in vertical upward and downward two phase flow. *Experimental Thermal and Fluid Science*, *39*, 213–227. https://doi.org/10.1016/j.expthermflusci.2012.01.026

Bendlksen, K. H., Malnes, D., Moe, R., & Nuland, S. (1991). The dynamic two-fluid model olga: theory and application. *SPE Production Engineering*, *6*(02), 171–180. https://doi.org/10.2118/19451-PA

Bouyahiaoui, H., Azzi, A., Saidj, F., & Zeghloul, A. (2008). Flow patterns of a vertically downward two phase flow. International Journal of Heat and Mass Transfer, 51, 3442–3459. https://cmm2017.sciencesconf.org/129161/Azzi_CMM2017.pdf

Bouyahiaoui, H., Azzi, A., Zeghloul, A., Hasan, A., & Berrouk, A. S. (2018). Experimental investigation of a vertically downward two-phase air-water slug flow. *Journal of Petroleum Science and Engineering*, *162*, 12–21. https://doi.org/10.1016/j.petrol.2017.12.028

Chalgeri, V. S., & Jeong, J. H. (2019). Flow patterns of vertically upward and downward air-water two-phase flow in a narrow rectangular channel. *International Journal of Heat and Mass Transfer*, *128*, 934–953. https://doi.org/10.1016/j.ijheatmasstransfer.2018.09.047

Cheng, L., Ribatski, G., & Thome, J. R. (2008). Two-phase flow patterns and flow-pattern maps: Fundamentals and applications. In *Applied Mechanics Reviews* (Vol. 61, Issues 1–6, pp. 0508021–05080228). https://doi.org/10.1115/1.2955990

Chisholm, D. (1967). A theoretical basis for the lockhart-martinelli correlation for two-phase flow. *International Journal of Heat and Mass Transfer*, *10*(12), 1767–1778. https://www.sciencedirect.com/science/article/pii/0017931067900476

Chisholm, D. (1973). *Heat Mass Trans/er* (Vol. 16). Pergamon Press.

Chawla, N., Bowyer, K., Hall, L. O., & Kegelmeyer, W. P. (2002). SMOTE: synthetic minority over-sampling technique. *ArXiv*, *abs/1106.1813*. https://api.semanticscholar.org/CorpusID:1554582

Cioncolini, A. (2023). Liquid entrainment in annular gas-liquid two-phase flow: A critical assessment of experimental data and prediction methods. In *Physics of Fluids* (Vol. 35, Issue 11). American Institute of Physics Inc. https://doi.org/10.1063/5.0174027

Collignon, M., Mazzini, A., Schmid, D. W., & Lupi, M. (2018). Modelling fluid flow in active clastic piercements: Challenges and approaches. In *Marine and Petroleum Geology* (Vol. 90, pp. 157–172). Elsevier Ltd. https://doi.org/10.1016/j.marpetgeo.2017.09.033

Golan, L. P., & Stenning, A. H. (1969). *Two-phase vertical flow maps*.

Gosline, J. E. (1936). Experiments on the vertical flow of gas-liquid mixtures in glass pipes. *Transactions of the Society of Petroleum Engineers of the American Institute of Mining, Metallurgical, and Petroleum Engineers, Inc.*, *118*(01), 56–70. https://doi.org/10.2118/936056-g

Gregory, G. A., Mandhane, J. M., & Aziz, K. (1975). Some design considerations for two-phase flow in pipes. Journal of Canadian Petroleum Technology, 14(01). https://doi.org/10.2118/75-01-07

Hammer, M., Deng, H., Liu, L., Langsholt, M., & Munkejord, S. T. (2021). Upward and downward two-phase flow of CO2 in a pipe: Comparison between experimental data and model predictions. *International Journal of Multiphase Flow*, *138*. https://doi.org/10.1016/j.ijmultiphaseflow.2021.103590

Han, S., Kashfipour, M. A., Ramezani, M., & Abolhasani, M. (2020). Accelerating gas-liquid chemical reactions in flow. *Chemical Communications*, *56*(73), 10593–10606. https://doi.org/10.1039/d0cc03511d

Ishii, M. (1977). *One-dimensional drift-flux model and constitutive equations for relative motion between phases in various two-phase flow regimes*. https://www.sciencedirect.com/science/article/pii/S0017931003003223

Ishii, M., Paranjape, S. S., Kim, S., & Sun, X. (2004). Interfacial structures and interfacial area transport in downward two-phase bubbly flow. *International Journal of Multiphase Flow*, *30*(7-8 SPEC. ISS.), 779–801. https://doi.org/10.1016/j.ijmultiphaseflow.2004.04.009

Kan, Z., & Liu, X. (2021). The study on void fraction prediction of gas-liquid two phase flow based on convolutional neural network. *Journal of Physics: Conference Series*, *2121*(1). https://doi.org/10.1088/1742-6596/2121/1/012029

Kanin, E., Vainshtein, A., Osiptsov, A., & Burnaev, E. (2018). The method of calculation the pressure gradient in multiphase flow in the pipe segment based on the machine learning algorithms. *IOP Conference Series: Earth and Environmental Science*, *193*(1). https://doi.org/10.1088/1755-1315/193/1/012028

Kawaji, M. (2017). Fundamental equations for two-phase flow in tubes. In *Handbook of Thermal Science and Engineering* (pp. 1–58). Springer International Publishing. https://doi.org/10.1007/978-3-319-32003-8_46-1

Kendoush, A. A., & Ai-Khatab, S. A. W. (1994). *Experiments on flow characterization in vertical downward two-phase flow*. https://www.sciencedirect.com/science/article/pii/0894177794900051

Kohanpur, A. H., Rahromostaqim, M., Valocchi, A. J., & Sahimi, M. (2020). Two-phase flow of CO2-brine in a heterogeneous sandstone: Characterization of the rock and comparison of the lattice-Boltzmann, pore-network, and direct numerical simulation methods. *Advances in Water Resources*, *135*. https://doi.org/10.1016/j.advwatres.2019.103469

Kremleva, E., Fantoft, R., & Mikelsen, R. (2010). *SPE Russian Oil & Gas Technical Conference and Exhibition*. https://www.researchgate.net/publication/241789365_Inline_Technology_-_New_Solutions_for_Gas-Liquid_Separation

Lee, J. Y., Ishii, M., & Kim, N. S. (2008). Instantaneous and objective flow regime identification method for the vertical upward and downward co-current two-phase flow. *International Journal of Heat and Mass Transfer*, *51*(13–14), 3442–3459. https://doi.org/10.1016/j.ijheatmasstransfer.2007.10.037

Li, H., Zhang, W., Hu, L., Zhu, B., & Wang, F. (2023). Studies on flow characteristics of gas–liquid multiphase pumps applied in petroleum transportation engineering—A Review. In *Energies* (Vol. 16, Issue 17). Multidisciplinary Digital Publishing Institute (MDPI). https://doi.org/10.3390/en16176292

Li, X., Li, L., Wang, W., Zhao, H., & Zhao, J. (2022). Machine learning techniques applied to identify the two-phase flow pattern in porous media based on signal analysis. *Applied Sciences (Switzerland)*, *12*(17). https://doi.org/10.3390/app12178575

Li, Z., Wang, G., Yousaf, M., Yang, X., & Ishii, M. (2018). Flow structure and flow regime transitions of downward two-phase flow in large diameter pipes. *International Journal of Heat and Mass Transfer*, *118*, 812–822. https://doi.org/10.1016/j.ijheatmasstransfer.2017.11.037

Lokanathan, M., & Hibiki, T. (2016). Flow regime, void fraction and interfacial area transport and characteristics of co-current downward two-phase flow. In *Nuclear Engineering and Design* (Vol. 307, pp. 39–63). Elsevier Ltd. https://doi.org/10.1016/j.nucengdes.2016.05.042

Madhumitha, R., Shriram, S. B., & Venkatesan, M. (2023). Flow transitions during laminar stratified two-phase flow in mini channels. *Chemical Papers/Chemické Zvesti*, *77*(11), 7121–7129. https://doi.org/10.1007/s11696-023-03003-y

Martin, C. S. (1976). Vertically downward two-phase slug flow. Journal of Fluids Engineering, 98. https://doi.org/10.1115/1.3448466

Mateus Rubiano, C. A. (2023). Study on the effects of tubular restrictions on liquid lifting in natural gas wells. https://shareok.org/handle/11244/340048

Montoya, G., Lucas, D., Baglietto, E., & Liao, Y. (2016). A review on mechanisms and models for the churn-turbulent flow regime. In *Chemical Engineering Science* (Vol. 141, pp. 86–103). Elsevier Ltd. https://doi.org/10.1016/j.ces.2015.09.011

Ojeda, L. C. O. (2023). Application of machine learning and dimensional analysis to evaluate the performances of various downhole centrifugal separator types. D011S999R006. https://doi.org/10.2118/217484-STU

Olubode, M. O., Iradukunda, P., Karami, H., Podio, T., & McCoy, J. N. (2022). Experimental analysis of centrifugal downhole separators in boosting artificial lift performance. Journal of Natural Gas Science and Engineering, 99, 104408. https://doi.org/10.1016/j.jngse.2022.104408

Potdar, K., Pardawala, T., Pai, C. (2017) A comparative study of categorical variable encoding techniques for neural network classifiers. International Journal of Computer Applications, 175. https://doi.org/10.5120/ijca2017915495

Qian, J., Li, X., Wu, Z., Jin, Z., & Sunden, B. (2019). A comprehensive review on liquid–liquid two-phase flow in microchannel: flow pattern and mass transfer. *Microfluidics and Nanofluidics*, *23*(10). https://doi.org/10.1007/s10404-019-2280-4

Qiao, S., Li, J., Ren, J., & Kim, S. (2023). Experimental investigation on effects of flow orientation on interfacial structure of air–water two-phase flow. *Coatings*, *13*(1). https://doi.org/10.3390/coatings13010005

Qiao, S., Mena, D., & Kim, S. (2017). Inlet effects on vertical-downward air–water two-phase flow. *Nuclear Engineering and Design*, *312*, 375–388. https://doi.org/10.1016/j.nucengdes.2016.04.033

Radman, S., Fiorina, C., & Pautz, A. (2021). Development of a novel two-phase flow solver for nuclear reactor analysis: algorithms, verification and implementation in openfoam. *Nuclear Engineering and Design*, *379*. https://doi.org/10.1016/j.nucengdes.2021.111178

Roshani, M., Phan, G. T. T., Jammal Muhammad Ali, P., Hossein Roshani, G., Hanus, R., Duong, T., Corniani, E., Nazemi, E., & Mostafa Kalmoun, E. (2021). Evaluation of flow pattern recognition and void fraction measurement in two phase flow independent of oil pipeline's scale layer thickness. *Alexandria Engineering Journal*, *60*(1). https://doi.org/10.1016/j.aej.2020.11.043

Schmid, D., Verlaat, B., Petagna, P., Revellin, R., & Schiffmann, J. (2022). Flow pattern observations and flow pattern map for adiabatic two-phase flow of carbon dioxide in vertical upward and downward direction. *Experimental Thermal and Fluid Science*, *131*. https://doi.org/10.1016/j.expthermflusci.2021.110526

Serra, P. L. S., Masotti, P. H. F., Rocha, M. S., de Andrade, D. A., Torres, W. M., & de Mesquita, R. N. (2020a). Two-phase flow void fraction estimation based on bubble image segmentation using Randomized Hough Transform with Neural Network (RHTN). *Progress in Nuclear Energy*, *118*. https://doi.org/10.1016/j.pnucene.2019.103133

Serra, P. L. S., Masotti, P. H. F., Rocha, M. S., de Andrade, D. A., Torres, W. M., & de Mesquita, R. N. (2020b). Two-phase flow void fraction estimation based on bubble image segmentation using Randomized Hough Transform with Neural Network (RHTN). *Progress in Nuclear Energy*, *118*. https://doi.org/10.1016/j.pnucene.2019.103133

Schmid, D., Verlaat, B., Petagna, P., Revellin, R., & Schiffmann, J. (2022). Flow pattern observations and flow pattern map for adiabatic two-phase flow of carbon dioxide in vertical upward and downward direction. Experimental Thermal and Fluid Science, 131, 110526. https://doi.org/10.1016/j.expthermflusci.2021.110526

Shi, S., Wang, Y., Qi, Z., Yan, W., & Zhou, F. (2021). Experimental investigation and new void-fraction calculation method for gas–liquid two-phase flows in vertical downward pipe. *Experimental Thermal and Fluid Science*, *121*. https://doi.org/10.1016/j.expthermflusci.2020.110252

Szalinski, L., Abdulkareem, L. A., Da Silva, M. J., Thiele, S., Beyer, M., Lucas, D., Hernandez Perez, V., Hampel, U., & Azzopardi, B. J. (2010). Comparative study of gas-oil and gas-water two-phase flow in a vertical pipe. *Chemical Engineering Science*, *65*(12), 3836–3848. https://doi.org/10.1016/j.ces.2010.03.024

Tengesdal, J., State, P. U., & Kaya, A. (1999). *Flow-Pattern Transition and Hydrodynamic Modeling of Churn Flow*. https://www.researchgate.net/publication/348231882_Flow-Pattern_Transition_and_Hydrodynamic_Modeling_of_Churn_Flow

Troniewski, L., & Selsak, W. (1987). Brief communication flow patterns in two-phase downflow of gas and very viscous liquid. In *Int. J. Muldphase Flow* (Vol. 13, Issue 2). https://www.sciencedirect.com/science/article/pii/0301932287900334

Usama Kadri. (2009). *Long liquid slugs in stratified gas/liquid flow in horizontal and slightly inclined pipes*. Delft University of Technology. https://repository.tudelft.nl/record/uuid:9fadabd6-aae7-4e05-8aba-685d658941ab

Usui, K., & Sato, K. (1989). Vertically Downward Two-Phase Flow, (I) Void Distribution and Average Void Fraction. In *Journal of Nuclear Science and Technology*. https://www.tandfonline.com/doi/pdf/10.1080/18811248.1989.9734366

Voinov, N. A., Frolov, A. S., Bogatkova, A. V., Zemtsov, D. A., & Zhukova, O. P. (2023). Method for intensive gas–liquid dispersion in a Stirred Tank. *ChemEngineering*, *7*(2). https://doi.org/10.3390/chemengineering7020030

Wang, G., Li, Z., Yousaf, M., Yang, X., & Ishii, M. (2018). Experimental study on vertical downward air-water two-phase flow in a large diameter pipe. *International Journal of Heat and Mass Transfer, 118*, 919–930. https://doi.org/10.1016/j.ijheatmasstransfer.2017.11.065

Xue, Y., Li, H., Hao, C., & Yao, C. (2016). Investigation on the void fraction of gas–liquid two-phase flows in vertically-downward pipes. *International Communications in Heat and Mass Transfer, 77*, 1–8. https://doi.org/10.1016/j.icheatmasstransfer.2016.06.009

Yamaguchi, K., & Yamazaki, Y. (1984). Combinated flow pattern map for cocurrent and countercurrent air-water flows in vertical tube. *Journal of Nuclear Science and Technology*, *21*(5), 321–327. https://doi.org/10.1080/18811248.1984.9731053

Yang, Z., Shan, J., Gou, J., Ishii, M. (2018). SGTR analysis on CPR1000 with a passive safety system. Nuclear Engineering and Design, 332. https://doi.org/10.1016/j.nucengdes.2018.03.009

Yao, C., Li, H., Xue, Y., Liu, X., & Hao, C. (2018). Investigation on the frictional pressure drop of gas liquid two-phase flows in vertical downward tubes. *International Communications in*

Heat and Mass Transfer, *91*, 138–149. https://doi.org/10.1016/j.icheatmasstransfer.2017.11.015

Zhang, H.-Q., Wang, Q., Sarica, C., & Brill, J. (2003). Unified model for gas-liquid pipe flow via slug dynamics: part 1—model development. Journal of Energy Resources Technology-Transactions of The Asme - J Energy Resource Technolgy, 125. https://doi.org/10.1115/1.1615246

Zhao, Y., Bi, Q., & Hu, R. (2013). Recognition and measurement in the flow pattern and void fraction of gas-liquid two-phase flow in vertical upward pipes using the gamma densitometer. *Applied Thermal Engineering*, *60*(1–2), 398–410. https://doi.org/10.1016/j.applthermaleng.2013.07.006

Zhong, W., Qiao, S., Hao, S., Li, X., & Tan, S. (2021, August 4). Vertical-downward two-phase flow regime identification by probabilistic neural network (pnn) and nonlinear support vector machine (svm). ICONE28. https://doi.org/10.1115/ICONE28-65467

Zhou, C., Xie, B., Chen, J., Fan, Y., & Zhang, J. (2023). An efficient and safe platform based on the tube-in-tube reactor for implementing gas-liquid processes in flow. In *Green Chemical Engineering* (Vol. 4, Issue 3, pp. 251–263). KeAi Communications Co. https://doi.org/10.1016/j.gce.2022.12.001

APPENDIX A. Experimental Error Analysis

In this section, a comprehensive error analysis is presented to quantify the uncertainties associated with void fraction and pressure gradient measurements. All experimental measurements are subject to uncertainties arising from random and systematic errors. The random errors are due to inherent variability in repeated measurements, while systematic errors are caused by limitations in measurement instruments. The random errors are determined using repeated experiments with statistical methods as shown in the equations below. The systematic errors of the sensors are shown in Table A-1 based on the specifications of the measuring instruments (from Alsanea 2022). The combination of these errors provides a more robust understanding of the confidence in the reported values, ensuring the validity of the experimental findings and their implications for flow characterization.

Table A-1 Measuring Equipment Uncertainty

Measured Parameter	**Measuring Equipment**	**Systematic Uncertainty**
Pressure Drop	Differential Pressure Sensors	± 0.000031 – 0.00016 psi/ft
Liquid Holdup	Differential Pressure Sensors	± 0.00087 – 0.0044 inches of water

The following equations were used in calculating the random errors (uncertainty) in the experiment. Equation A-1 was used to compute the mean of repeated measurements. Equation A-2 was used to compute the standard deviation. Then, Equation A-3 was used to compute random uncertainty. In addition, Equation A-4 was used to compute the total uncertainty, including both random and systematic values.

$$\overline{\mathbf{x}} = \frac{\sum_{\mathbf{i=1}}^{\mathbf{n}} \mathbf{x_i}}{\mathbf{n}} \qquad \text{Equation A-1}$$

$$\sigma = \sqrt{\frac{\sum_{i=1}^{n}(x_i - \overline{x})^2}{n-1}} \qquad \text{Equation A-2}$$

$$U_{random} = \frac{\sigma}{\sqrt{n}} \qquad \text{Equation A-3}$$

$$U_{total} = \sqrt{U_{random}^2 + U_{systematic}^2} \qquad \text{Equation A-4}$$

where n is the number of measurements and x_i is the value of the i^{th} data point.

Figures A.1 and A.2 shows the experimental error plots for void fraction and pressure gradient respectively. Figure A.1 shows higher errors at low v_{Sg} and an increase in the error as v_{SL} increases. At the lowest v_{SL}, no error is observed. Figure A.2 shows little to no error at lower v_{SL} and increased error at higher v_{SL}. This analysis shows that the errors are influenced by the presence of liquid. No error plot was made for v_{SL} of 0.6 ft/sec because the experiment was not repeated.



Figure A.1. Void Fraction Experimental Error Plot

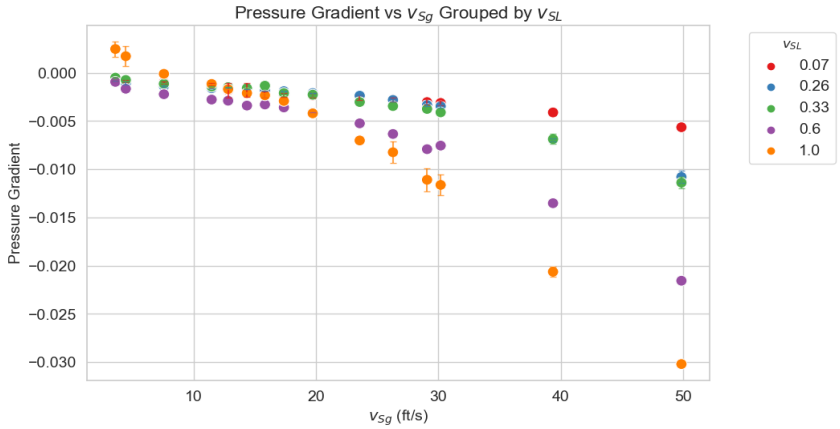


Figure A.2. Pressure Gradient Experimental Error Plot